
# CARBON MONOXIDE CLEAN-UP OF REFORMATE GAS BY PREFERENTIAL OXIDATION

**Dissertation**

In partial fulfilment of the requirements for the degree of

Masters of Science in Chemical Engineering

**Prepared by**:

Sibongile Muziki

**Prepared for**:

Prof Jack Fletcher

Dr Roald Brosius

**December 2015**

## Declaration

I know the meaning of plagiarism and declare that all the work in the document, save for that which is properly acknowledged, is my own

Signed by candidate

Signature Removed

Date 14/12/15

Sibongile Muziki

## Synopsis

The increase in demand for clean energy has led to the growth in the research of fuel cells utilising hydrogen as a fuel. One common field of research is the production of hydrogen ($H_2$) for use in a fuel cell. Different types of fuel cells have been developed and polymer electrolyte membrane fuel cells (PEMFC's) have been reported to exhibit high efficiency, rapid start-up and high power density.

Fuel processors provide an on-board hydrogen source of $H_2$ for the PEMFC via the reforming of a hydrocarbon such as liquefied petroleum gas (LPG) or natural gas. At the low operation temperature of the PEMFC (60 – 100 °C), the Pt catalyst in the anode is easily poisoned by carbon monoxide (CO). Therefore, the CO concentration in the $H_2$ stream to the PEMFC needs to be less than 10 ppm. The hydrocarbon source goes through a reforming step to form syngas. This step is then followed by a water-gas shift (WGS) reaction step. The purpose of the WGS step is to increase the concentration of $H_2$, as well as to decrease the CO concentration. The WGS alone cannot decrease the CO concentration to <10 ppm hence a further CO clean-up step is required. Different methods of CO clean-up have been proposed. This study focuses on the preferential oxidation (PrOx) of CO in a $H_2$ rich stream as a final clean-up step. In particular the aim is to develop highly active and highly selective platinum group metal (PGM) based catalysts for PrOx for fuel processor applications.

Ruthenium (Ru) catalysts supported on alumina were found to be the most active catalysts compared to the other PGM metals supported on alumina. However, Ru catalysts can also hydrogenate CO and carbon dioxide ($CO_2$) to form methane ($CH_4$). The hydrogenation of CO to $CH_4$ results in the undesirable consumption of $H_2$. However if the $CH_4$ formed is low, CO methanation can be beneficial because it lowers the CO concentration. $CO_2$ hydrogenation results in further $H_2$ consumption. Thus methanation should be minimised when using Ru catalysts.

In this study, two Ru catalysts were prepared in order to test the following hypothesis: "The Ru catalyst prepared using pH adjustment is more active than the incipient wetness impregnation prepared catalyst because the pH adjustment method increases dispersion and hence PrOx activity". The first catalyst was prepared by a wetness impregnation method at high pH in order to enhance strong electrostatic adsorption during impregnation. The second catalyst was prepared by a normal incipient wetness impregnation. Initial results showed that the presence of small amounts of $O_2$ during catalyst reduction led to the

sintering of Ru particles and hence decreased CO conversion and $CO_2$ selectivity. Thereafter the system was purged with $N_2$ in order to flush out $O_2$ before the catalyst was reduced. The results obtained showed that the Ru catalyst prepared at a high pH showed higher CO conversions at a space velocity of 120 000 ml/(h $g_{cat}$) at an $O_2$/CO ratio of 1 for the temperature range of 103 – 180 °C. The lowest exit CO concentrations were 35 ppm and 89 ppm on the Ru catalyst prepared at a high pH and via incipient wetness impregnation respectively both at 150 °C. The activity of the Ru_high pH catalyst was higher despite exhibiting a lower dispersion compared to the Ru_IWI catalyst. This however was not enough to disprove the original proposed hypothesis because the Ru_high pH and Ru_IWI catalysts were supported on $Al_2O_3$ supports with different surface areas. Thus further analysis needs to be done to test the effect of pH adjustment on the dispersion and hence activity of $Al_2O_3$ supported Ru catalysts. The detection of trace amounts of Na on the Ru_high pH catalyst led to the recommendation that the investigation of promotional effects of alkali metals needs to be investigated further to understand their effects on increasing PrOx activity. The highest $CO_2$ selectivity obtained at the highest CO conversion was ~50 % which was in line with literature results for Ru on alumina catalysts.

In literature, the sieving effect of zeolites is used to enhance selectivity. A Pt-Fe/mordenite catalyst in literature showed 100 % $CO_2$ selectivity at 100 % CO conversion with an $O_2$/CO ratio of 0.5. Based on this a Pt-Fe/mordenite catalyst was prepared in this study using solid state ion exchange to deposit Fe and competitive ion exchange to deposit Pt. This method was proposed in order to try and improve the preparation method reported in literature. The synthesised catalyst did not perform as well as the Pt-Fe/Mordenite reported in literature. A maximum CO conversion of 99 % with 47 % $CO_2$ selectivity at 180 °C, 120 000 ml/(h $g_{cat}$) and $O_2$/CO ratio of 1 was achieved. It was concluded that more research and experiments would need to be done in order to determine whether the catalyst preparation method for Pt-Fe/Mordenite described in literature can be improved.

## Acknowledgements

I would like to thank Prof. Jack Flethcher and Dr Roald Brosius for their support. I would also like to extend my gratitude to the fuel processing team (Stephen Roberts, Niels Lüchters, Walter Böhringer ) for their support and helpful feedback. Working with you guys was truly a pleasure.

To Waldo Koortz and Yi Zhou thank you for your assistance with the laboratory equipment. Zaheera Ahmend and Ntandoyenkosi Hlabangana, your dedication and strong work ethic encouraged me and challenged me to push myself further. Thank you ladies very much. I would also like to extend my gratitude to Zulfa le Riche from the analysis lab and Innocent Shuro from the Electron Microscope Unit for their support in the analysis of my catalyst samples.

I would also like to thank HySA/Catalysis for funding my project.

To all my friends, your encouraging messages throughout the highs and lows of my MSc journey are greatly appreciated. Many thanks to my family for their support. Most importantly, I am grateful to my mother for all her inspiring talks to motivate me and also for all her prayers. Your strength is something I greatly admire and hope to achieve one day. I dedicate this thesis to you.

Last but not least I would like to thank GOD for without him none of this would have been possible. *Mwari makatendeka*, *ndimi Mwari vanogona.*

# Table of Contents

## List of Figures

## List of Tables

## Glossary

| | |
|---|---|
| Inert support | does not take part in the reaction mechanism |
| Active support | the support takes part in the reaction mechanism |
| Microporous | pores <2 nm |
| Mesoporous | pores between 2 - 50 nm |
| Macroporous | pores > 50 nm |
| Promoted | a catalyst with an added alkali metal |
| Non promoted | a noble metal catalyst |
| Residence time | the time by the reactants in the catalyst bed |
| Zeolite | a porous crystalline structure composed of aluminium silicon and oxygen |

## Nomenclature

| Abbreviation | Meaning |
|---|---|
| GC | Gas chromatograph |
| GHSV | Gas hourly space velocity |
| HTS | High temperature shift |
| HySA | Hydrogen South Africa |
| ICP-OES | Inductively coupled plasma optical emission spectrometry |
| kJ/mol | Kilojoules per mole |
| LPG | Liquified petroleum gas |
| LTS | Low temperature shift |
| MFC | Mass flow controller |
| MFI | A type of ZSM-5 zeolite |
| MS5 | Molsieve 5A column |
| PEMFC | Polymer electrolyte membrane fuel cell |
| PGM | Platinum group metal |
| PrOx | Preferential oxidaton |
| PZC | Point of zero charge |
| rWGS | Reverse water gas shift |
| SCCM | standard cubic centimetres per minute (273 K, 1 atm) |
| $S_{CO2}$ | CO2 selectivity |
| SMETH | Selective methanation |
| SV | Space velocity [ml/(h $g_{cat}$)] |
| T | Temperature [°C] |

| | |
|---|---|
| TCD | Thermal conductivtiy detector |
| TEM | Transmission electron microscopy |
| TOF | Turnover frequency [$s^{-1}$] |
| ToS | Time on stream |
| WGS | water gas shift |
| $X_{CO}$ | CO conversion |
| $X_{O2}$ | O2 conversion |
| XRD | X-ray diffraction |
| ΔH | Heat of reaction [kJ/mol] |

# 1. Introduction

The increase in demand for clean energy has led to the growth of the research of hydrogen as a fuel. In particular are fuel processors which provide an on-board hydrogen source for polymer electrolyte membrane fuel cells (PEMFC). PEMFC's produce electricity from hydrogen ($H_2$) and oxygen ($O_2$) forming water and heat in the process. The PEMFC with a fuel processor can then be used for power generation in remote areas. Hydrogen South Africa (HySA) aims to develop a fuel processor which uses platinum group metal (PGM) based catalysts in order to utilise the abundant PGM reserves in South Africa. Hence research for the best PGM-based catalysts for fuel processor applications is underway.

Steam reforming is used to produce $H_2$ on site for the PEMFC in order to eliminate the risks associated with storing $H_2$ onsite. Other by-products from the steam reforming process include water ($H_2O$), carbon dioxide ($CO_2$), carbon monoxide (CO) and in some cases methane ($CH_4$). Since the Pt catalyst in the anode of the PEMFC is easily poisoned by CO at low temperatures (<100 °C) the CO concentration in the feed needs to be less than 10 ppm. The water-gas shift (WGS) process after steam reforming reduces the CO concentration but not to less than 10 ppm since the reaction is thermodynamically limited. Thus a further CO removal step is required. Some of the CO removal techniques include Pd-membrane separation, pressure swing adsorption, catalytic methanation and preferential oxidation (PrOx) of CO in a stream with excess $H_2$. From the various investigations performed on these processes, PrOx seems to be the most promising for fuel processors. Research for PrOx is focused on developing highly active catalysts which also exhibit a high selectivity for $CO_2$ to prevent $H_2$ oxidation. This study focused on preparing and optimising a PGM catalyst for PrOx.

The prepared catalysts were characterised in order to determine the physical characteristics of the catalyst. In addition, activity tests (for CO conversion and $CO_2$ selectivity) to determine an operation window were performed and a commercial catalyst was also tested. To determine the operation window the following variables were tested to observe their effect on CO conversion and $CO_2$ selectivity;

- Oxygen to carbon monoxide ($O_2$/CO) ratio
- Space velocity (SV)

- Operation temperature

Some very important criteria for the PrOx catalyst are;

- High CO conversion in order to reduce the CO concentration to the required concentration (<10 ppm)
- High $CO_2$ selectivity in order to minimise $H_2$ oxidation
- Wide operation temperature window since the CO clean up conditions can be affected by fluctuations in the upstream process
- Preserve performance despite fluctuations in space velocities and feed composition from the upstream processes
- Low $O_2$/CO ratio to achieve a high thermal efficiency in the fuel processor

# 2. Literature review

A drive towards the use of alternative energy sources in order to reduce greenhouse gas emissions has led to an increase in fuel cell research. For South Africa in particular research in fuel cells is driven by the need to utilize the abundant platinum resources and also to provide power to remote areas. Hydrogen South Africa (HySA) is a project by the South African government which aims to launch South Africa as one of the top countries exporting competitive products into the global hydrogen and fuel cell markets. HySA aims to achieve this buy utilizing the abundant platinum group metal (PGM) resources available in South Africa in the development of the fuel cell systems.

## 2.1. Fuel Cells

A fuel cell is an electrochemical energy conversion device which converts $H_2$ and $O_2$ into $H_2O$, producing electricity. There are various types of fuel cells (Figure 2-1) that have been developed.

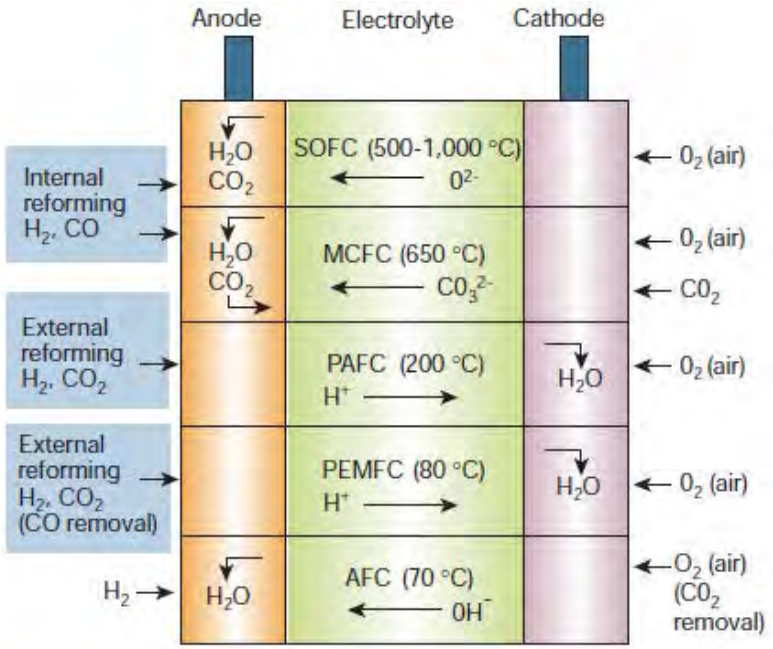


**Figure 2-1: Types of fuel cells taken from (Steele & Heinzel, 2001)**

The PEMFC has been very attractive for application in the motor as well as the residential power generation industry. This is because of its high efficiency, rapid start-up and high power density (Ashraf et al.,2014) and (Song, 2002). The reactions that take place in a PEMFC are as follows:

Anode : $H_2 \rightarrow 2H^+ + 2e^-$ reaction 1

Cathode: $2H^+ + 0.5O_2 + 2e^- \rightarrow H_2O$ reaction 2

Overall: $H_2 + 0.5O_2 \rightarrow H_2O$ reaction 3

Hydrogen is oxidised on the Pt electrode to produce protons and electrons. The protons are then transported across the membrane and the electrons travel through an external circuit generating electricity. The protons and the electrons then react with $O_2$ at the cathode to form water. A PEMFC typically operates at around 80$^o$C (Joensen et al., 2002).

Since the PEMFC uses $H_2$ as a fuel, there needs to be a process that generates $H_2$. The required $H_2$ can be supplied to the PEMFC from an on-board $H_2$ storage vessel or generated on-site. $H_2$ storage on site for PEMFC's proves to be a challenge in terms of size, cost and weight based on the required quantity and density (Ghenciu, 2002). The main advantages of on-site $H_2$ production include: easier fuel supply, safer and cheaper if reforming is the $H_2$ production method (López et al., 2008).

The required purity for the $H_2$ stream in PEMFC's is a CO concentration <10 ppm to prevent poisoning the platinum (Pt) anode catalyst (Watanabe et al., 2003). Lower CO concentrations increase the efficiency of the fuel cell (Joensen et al., 2002) since CO strongly adsorbs onto the Pt catalyst at temperatures below 150 $^o$C, thus blocking the active sites from $H_2$ which results in a decrease in the cell voltage (Figure 2-2).

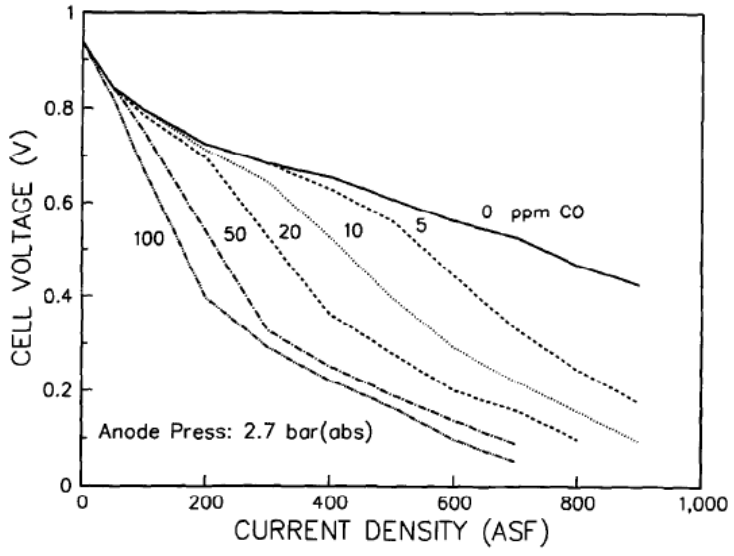


**Figure 2-2: Effect of CO concentration on the performance of the PEMFC taken from (Amphlett et al., 1996)**

The system that produces $H_2$ through reforming of a hydrocarbon and lowers the CO concentration to the desired level is known as a fuel processor.

## 2.2. Fuel processing system

A fuel processor converts a type of hydrocarbon to a $H_2$ rich stream which is then flows to the PEMFC to generate power. Currently there is an increase in the development of fuel processing systems for transportation and stationary applications (Echigo et al., 2003). Figure 2-3 shows the main steps in a general fuel processor.

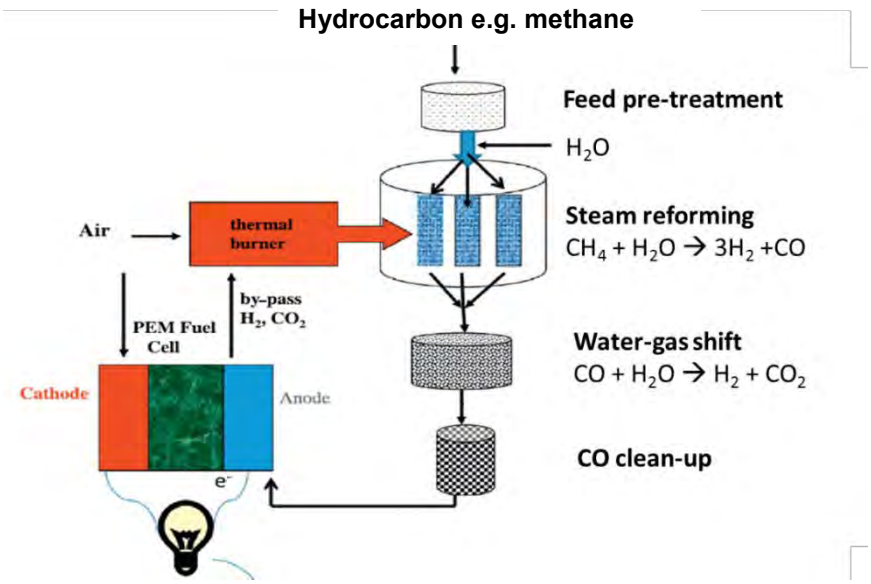


**Figure 2-3: Fuel processor schematic, taken from (Farrauto, 2014)**

The hydrocarbon first undergoes a feed pre-treatment step to remove any impurities that may poison the reforming catalyst. The reforming step is followed by the water-gas shift step then finally a CO clean-up step. In addition to the steps in Figure 2-3, a fuel processor also contains a heat integration system in order to improve the energy efficiency of the process. The requirements for a fuel processor are; quick start-up, simple construction and operation, dynamic response, low cost and high fuel conversion (Recupero et al., 2005).

### 2.2.1. Hydrogen production

The main routes of $H_2$ formation are through steam reforming (SR), partial oxidation (PO) and autothermal reforming (ATR) of hydrocarbons (Choudhary & Goodman, 2002). ATR is a combination of oxidation and steam reforming in one step. The exothermic PO reaction provides heat to drive the endothermic SR reaction (Ghenciu, 2002). This results in high $H_2$

concentrations with a reduced heat transfer and size limitation (Ghenciu, 2002). The general reactions are as follows:

$C_nH_m + nH_2O \rightarrow nCO + (n+0.5m)H_2$ *SR* (Trimm, 1999) reaction 4

$C_nH_m + 0.5n\ O_2 \rightarrow nCO + (0.5m)H_2$ *PO* (Opoku-Gyamfi et al., 1998) reaction 5

$C_nH_m + aO_2 + (n-2a)H2O \rightarrow nCO + (0.5m+n-2a)H_2$ *ATR* (de Souza et al., 2014) reaction 6

Ashraf et al.,(2014) compared the performance of a fuel processing unit using ATR and SR. The results of this study are summarised in the Table 2-1.

**Table 2-1: Effects of ATR and SR on the performance of a fuel processing system, taken from (Ashraf et al.,2014).**

| Parameter | ATR | SR |
|---|---|---|
| - Water rate to NI-WGS | - Lower: **pros** | - Higher: **cons** |
| - Air global requirement | - Higher: **cons** | - Lower: **pros** |
| - $H_2$ specific production HSP | - Little higher: **pros** | - Little lower: **cons** |
| - $H_2$ concentration in syngas | - Lower: **cons** | - Higher (≈ 30%): **pros** |
| - $N_2$ in the final syngas when coupled with CO-SMET | - Present (average 23.8%): **cons** | - Absent: **pros** |
| - $N_2$ in the final syngas when coupled with CO-PROX | - Present (average 25.3%): **cons** | - Present (≈4%): **tolerable** |
| - Electric power consumption | - Higher: **cons** | - Lower: **pros** |
| - FPU gross efficiency | - Higher: **pros** | - Lower: **cons** |
| - FPU net efficiency | - Higher: **pros** | - Lower (but with a gap about halved respect the gross one): **cons** |

Both ATR and SR have their respective advantages and disadvantages. For this project, the steam reforming of methane ($CH_4$) will be considered as a $H_2$ production method. This is considered to be the most energy efficient method of $H_2$ production (Ashray et al., 2014). The steam reforming of $CH_4$ occurs according to the following reaction:

$CH_4 + H_2O \leftrightarrow CO + 3H_2 \quad \Delta H^\circ_{298} = 198\ kJ/mol\ CH_4$ reaction 7

Methane steam reforming (reaction 7) is a reversible reaction, hence reaction conditions need to favour the forward reaction in order to increase $CH_4$ conversion. These conditions are shown in Figure 2-4.

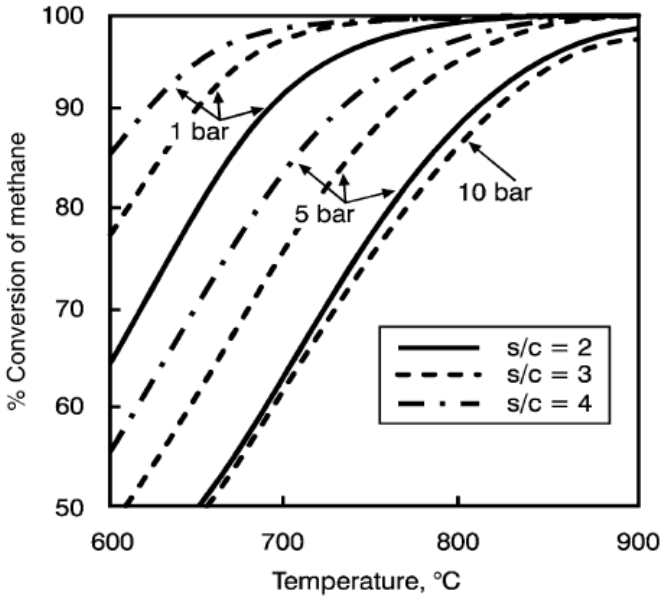


**Figure 2-4: Effect of temperature, steam/carbon ratio and pressure on the equilibrium $CH_4$ conversion taken from (Joensen et al., 2002)**

The best operating conditions for $CH_4$ steam reforming are at high temperature, low pressure and high steam to carbon ratio. High temperatures are favoured because the forward reaction is an endothermic reaction. Increasing the S/C ratio shifts the equilibrium to the right according to Le Chatelier's principle thus increasing $CH_4$ conversion. The same principle applies to lowering the pressure; the equilibrium will shift to the right, increasing $CH_4$ conversion.

### 2.2.2. Water gas shift

The water gas shift (WGS) step follows the reforming step according to the following reaction:

$CO + H_2O \rightarrow CO_2 + H_2$ $\Delta H_{rxn} = -41.1$ kJ/mol CO reaction 8

This process increases the $H_2$ concentration and also lowers the CO concentration to approximately 0.5 – 1 %. However, at this concentration the CO will poison the anode of the PEMFC. Consequently, the CO concentration needs to be reduced further to below 10 ppm. WGS alone cannot reduce the CO concentration to lower than 10 ppm at realistic operating conditions for the WGS reaction because the reaction is thermodynamically limited (Shekhawat et al., 2011) (Figure 2-5).

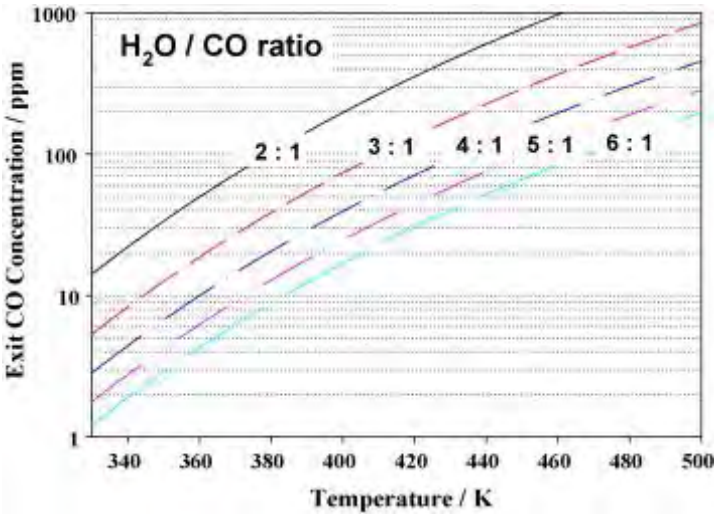


**Figure 2-5: Calculated CO exit gas concentrations as a function of temperature and initial $H_2O$/CO feed ratio taken from (Park et al., 2009a).**

In order to achieve a CO concentration of less than 10 ppm using water gas shift alone, lower temperatures would be required. However the catalysts for water gas shift reactions show low catalytic activity at low temperatures (Park et al., 2009b). As a result there needs to be another CO clean-up step.

### 2.2.3. CO clean-up

Some of the CO removal techniques include Pd-membrane separation, selective methanation (SMETH) of CO and preferential oxidation (PrOx) of CO in a stream with excess $H_2$ (Korotkikh & Farrauto, 2000). The disadvantage of Pd-membrane separation is the high pressure required for the reaction (Yan et al., 2004). High pressures are highly undesirable for fuel processor applications due to safety concerns. HySA plans to focus on the use of PrOx or SMETH as the final CO clean-up step.

#### 2.2.3.1. Selective methanation

The goal in SMETH is to hydrogenate CO to $CH_4$. However, there is a possibility of $CO_2$ hydrogenation to $CH_4$. Hence a highly active as well as selective catalyst to CO methanation is required for this process. One main disadvantage of SMETH is that the process consumes a significant amount of $H_2$ according to the following reaction:

$CO + 3H_2 \rightarrow CH_4 + H_2O$ $\Delta H = -206.2$ kJ/mol reaction 9

Furthermore, if the catalyst is not 100 % selective to CO methanation, then more $H_2$ is lost during $CO_2$ methanation according to the following reaction:

$CO_2 + 4H_2 \rightarrow CH_4 + 2H_2O$ $\Delta H = -165$ kJ/mol reaction 10

A decrease in the $H_2$ concentration is undesirable because it results in a decrease in the total efficiency of the fuel cell (Huang et al., 2007).

#### 2.2.3.2. Preferential Oxidation

Preferential oxidation (PrOx) is the oxidation of CO to $CO_2$ in the presence of oxygen according to the following reaction:

$CO + 0.5O_2 \rightarrow CO_2$ $\Delta H = -283$ kJ/mol reaction 11

However a side reaction also occurs in which $H_2$ is consumed according to the following reaction:

$H_2 + 0.5O_2 \rightarrow H_2O$ $\Delta H = -242$ kJ/mol reaction 12

Catalysis research for PrOx focuses on developing highly active and selective catalysts resistant to high concentrations of $H_2O$ and $CO_2$ and should work well for temperatures between 80 – 200 $^oC$ since the PrOx step is after the LTS reactor (200 $^oC$) and before the PEMFC (80 $^oC$) (Liu et al., 2012).

The methanation of CO and $CO_2$ as well as the rWGS could also take place under these conditions according to the following reactions.

$CO + 3H_2 \rightarrow CH_4 + H_2O$ $\Delta H = 206$ kJ/mol reaction 13

$CO_2 + 4H_2 \rightarrow CH_4 + 2H_2O$ $\Delta H = -165$ kJ/mol reaction 14

$CO_2 + H_2 \rightarrow CO + H_2O$ $\Delta H = 41.1$ kJ/mol reaction 15

The methanation of CO results in the decrease in CO concentration. However, these methanation reactions lead to a decrease in $H_2$ concentration which is undesirable. In addition the methanation of $CO_2$ could result in a runway reaction due to the possibility of a self-catalytic reaction by its own exothermal heat of reaction (Echigo et al., 2003). Therefore the CO and $CO_2$ methanation should be minimised. The rWGS reaction is also undesirable since it increases the outlet CO concentration. This reaction can be encountered at low space velocity and temperatures above 150 °C (Kim et al., 2009b). The CO conversion ($X_{CO}$) and $CO_2$ selectivity $S_{CO2}$ are defined as follows;

$$X_{CO} = \frac{n_{CO,in} - n_{CO,out}}{n_{CO,in}} * 100 \quad \text{equation 1}$$

$$S_{CO_2} = \frac{n_{CO_2,formed}}{2*(n_{O_2,in} - n_{O_2,out})} * 100 \quad \text{equation 2}$$

A disadvantage of PrOx for fuel processors is the challenge of providing and maintaining the required $O_2$ (from air) level to the reactor since the $O_2$/CO ratio plays a significant role in the outlet CO concentration. If the air flow becomes too low then the amount of CO going to the anode increases, which would result in poisoning the anode. If the flow of air increases then $H_2$ oxidation is increased which results in a decreased PEMFC power output. However, smaller amounts of $H_2$ are consumed in PrOx compared to SMETH (Park et al., 2009b). Another advantage of PrOx versus SMETH is that PrOx allows for higher space velocities thus reducing the reactor size (Mishra & Prasad, 2011). Ashraf et al., (2014) summarised the advantages and disadvantages of PrOx and SMETH as follows:

**Table 2-2: Comparison of PrOx and SMETH reactor systems, taken from (Ashraf et al., 2014)**

| Parameter | CO-PROX reactor | CO-SMET reactor |
|---|---|---|
| - $H_2$ ratio HR in the final syngas | - Higher (≈3%): **pros** | - Lower: **cons** |
| - $H_2$ concentration in the syngas | - Lower: **cons** | - Higher (2–4%): **pros** |
| - $H_2$ specific production HSP | - Higher (4–5.3%, depending on reformer type): **pros** | - Lower: **cons** |
| - $H_2$ consumption | - Lower (about 50%): **pros** | - Higher: **cons** |
| - Heat released rate | - Higher (3 times more): **pros** | - Lower (2/3 less): **cons** |
| - Reactor working temperature | - Lower: **cons** | - Higher: **pros** |
| - Thermodynamic value of the released heat rate | - Lower (since at lower temperature): **cons** | - Higher (since at higher temperature): **pros** |
| - Gross/net energy efficiencies | - Lower: **cons** | - Higher (very feebly): **pros** |
| - $N_2$ in the final syngas when coupled with SR | - Present (≈4%): **tolerable** | - Absent: **pros** |
| - $N_2$ in the final syngas when coupled with ATR | - Present (25.3% on average): **cons** | - Present (23.8% on average): **cons** |
| - $CH_4$ in the final syngas | - Absent: **pros** | - Present (≈1%): **cons** |

From the various investigations performed on these processes, PrOx process seems to be the most promising for fuel processors (Liu et al., 2012), (Shen et al., 2012) and (Ghenciu, 2002). In terms of selectivity, for PrOx to perform better than SMETH a selectivity of 25 % at maximum CO conversion is required. This was determined by assuming a SMETH process that is 100 % selective to CO methanation and achieves 100 % CO conversion. This represents a consumption of 3 moles of $H_2$ per mol of CO (reaction 13). A consumption of 3 moles of $H_2$ per mol of CO in PrOx is equivalent to 1.5 moles of $O_2$ in $H_2$ oxidation and 0.5 moles of $O_2$ for complete CO oxidation (using the reaction stoichiometry in reactions 11 and 12). This represents a total of 2 moles of $O_2$ which represents a selectivity of 25 % (using equation 2).

This study focuses on PrOx as a CO clean-up method.

## 2.3. Catalysts for PrOx

The catalyst for PrOx needs to be highly active and selective at temperatures between the WGS reactor (250 – 300 °C) and the PEMFC (70 – 80 °C) in order to simplify the heat integration system (Recupero et al., 2005). Several different types of catalysts have been studied for PrOx. These can be categorised as base metal oxide (e.g CuO, $Co_3O_4$) catalysts and noble metal catalysts (e.g Au, Pt, Ru). The temperature ranges and conversion of these metals as catalysts are shown in Figure 2-6.

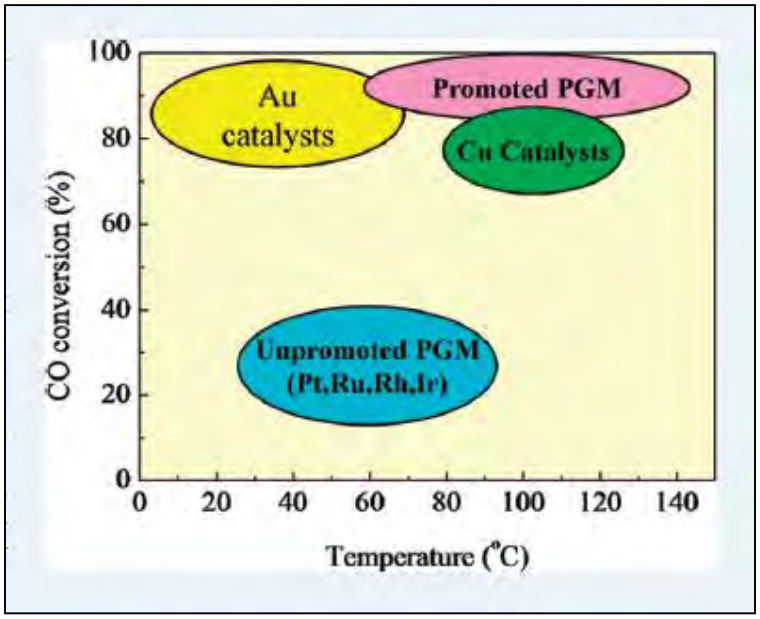


**Figure 2-6: Comparison of catalyst operating temperatures and CO conversion adapted from (Liu et al., 2012)**

As seen from Figure 2-6 Au catalysts have a high conversion outside the required temperature range for PEMFC (80 – 200 °C). In addition, it has been found that the Au catalysts do not reduce the CO concentration to less than 10 ppm at higher temperatures due to the increase in $H_2$ oxidation at increased temperatures (Denkwitz et al., 2009). Cu catalysts are active at temperatures above 100 °C but it has been found that they have very poor resistance towards $CO_2$ and $H_2O$ (Snytnikov et al., 2008). One such base metal oxide catalyst that has been widely studied is CuO-$CeO_2$ which has shown high activity and selectivity for CO oxidation. However it has been shown that they have poor stability in the presence of $H_2O$ (Ko et al., 2006). As a result PGM catalysts are considered to be promising for PrOx. Unprompted PGM metals have been shown to achieve high CO concentration at temperatures higher than those shown in Figure 2-6.

### 2.3.1. Platinum group metal catalysts for PrOx

Liu et al., (2012) proposed the following mechanisms for platinum group metals (PGM) catalysts:

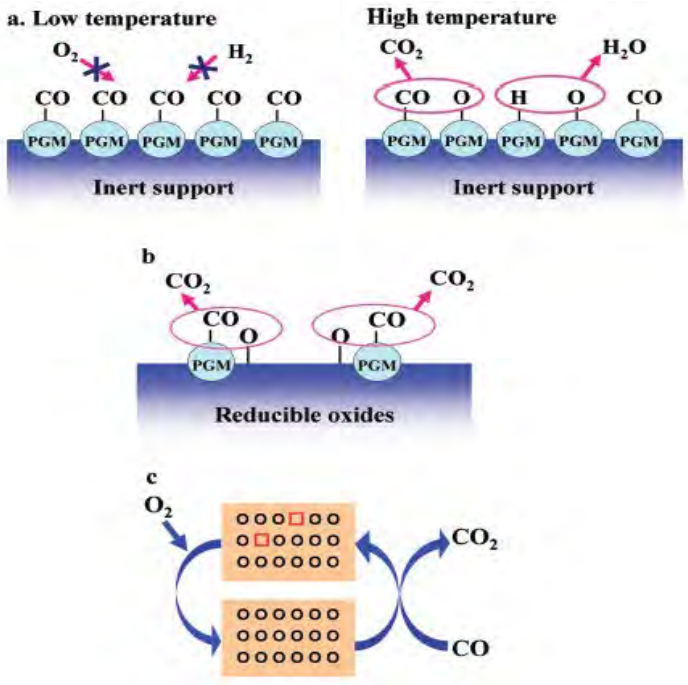


**Figure 2-7: Reaction mechanisms for PrOx a) Competitive Langmuir-Hinshelwood mechanism over nonpromoted PGM catalysts b) Non-competitive Langmuir-Hinshelwood mechanism over promoted PGM catalysts c) Mars-van Krevelen mechanism over promoted PGM catalysts adapted from (Liu et al., 2012).**

In Figure 2-7a, CO and $O_2$ both compete for the same active sites on the PGM. This mechanism is observed for non-promoted PGM catalysts. Figure 2-7b and c represent non-competitive mechanisms involving an alternate active site for the $O_2$ which is provided by either the reducible metal oxide promoter (Figure 2-7b) or the support (Figure 2-7c). In Figure 2-7b the reducible metal oxide promoter provides an O atom for the CO that is adsorbed on the PGM metal. Whereas in Figure 2-7c the O atom for CO oxidation comes from in the reducible support lattice creating a vacant space in the support. According to the Langmuir-Hinshelwood reaction pathway catalysts are more active at a higher temperature range because at lower temperatures the sites are fully covered by CO hence $O_2$ cannot adsorb onto the catalyst surface. In the Langmuir-Hinshelwood mechanism, the catalyst surface needs to be sufficiently cleared of CO in order to allow for the dissociative adsorption of $O_2$ (Yan et al., 2004).

### 2.3.2. PGM catalyst comparison

Comparison of reported catalysts for PrOx is not an easy task due to the different conditions (e.g. space velocity, feed composition) at which the studies are performed. Furthermore, there appears to be a lack of a base parameter (CO conversion, $CO_2$ selectivity or stability) to compare the catalysts (Lopez et al., 2008).

A few studies have been done were PGM catalysts activity for PrOx were compared to each other. Oh & Sinkevitch (1993) compared the activities of Rh, Ru, Pt, and Pd supported on $Al_2O_3$ for PrOx (Figure 2-8).

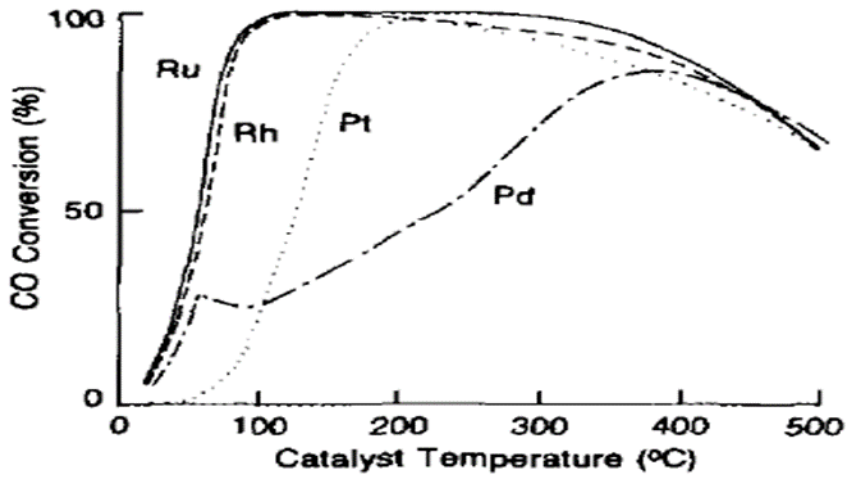


**Figure 2-8: Comparison of 0.5wt% $Ru/Al_2O_3$, 0.5wt % $Rh/Al_2O_3$, 0.5wt % $Pt/Al_2O_3$ and 0.5wt % $Pd/Al_2O_3$ for PrOx. Feed composition: 0.85 % $H_2$, 900 ppm CO, 800 ppm $O_2$, $N_2$ balance at 20 000 $h^{-1}$ taken from (Oh & Sinkevitch, 1993)**

Ru and Rh showed much higher activity for PrOx compared to Pt and Pd. However, the conditions at which this study was performed are rather unrealistic when compared to the real feed that is expected for the PrOx step in real fuel processing systems.

Another study done by Kawatsu, (1998) compared the activity of a Ru catalyst to a Pt catalyst for application in a fuel processor for an electric vehicle.

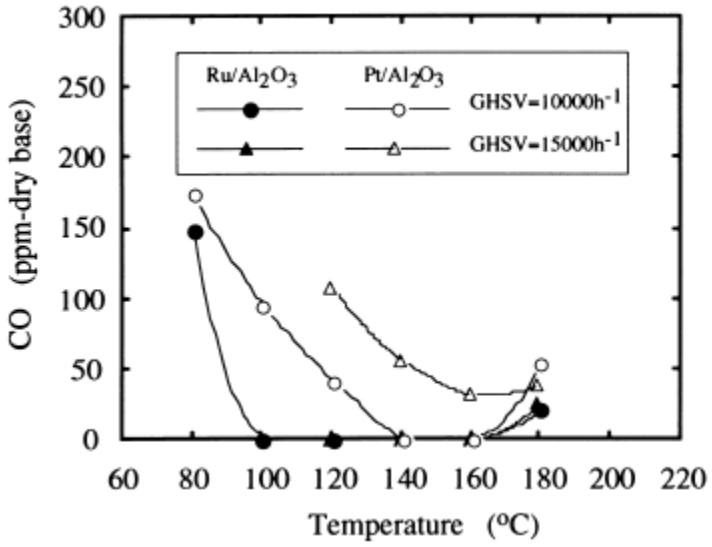


**Figure 2-9: Comparison of $Ru/Al_2O_3$ and $Pt/Al_2O_3$ for PrOx in a model gas corresponding to methanol reforming taken from (Kawatsu, 1998).**

Figure 2-9 shows that the $Ru/Al_2O_3$ catalyst has a wider operating temperature window at a high and low space velocity compared to the $Pt/Al_2O_3$. Another factor that makes Ru more favourable than Pt for PrOx is the lower rWGS activity compared to Pt catalysts (Figure 2-10).

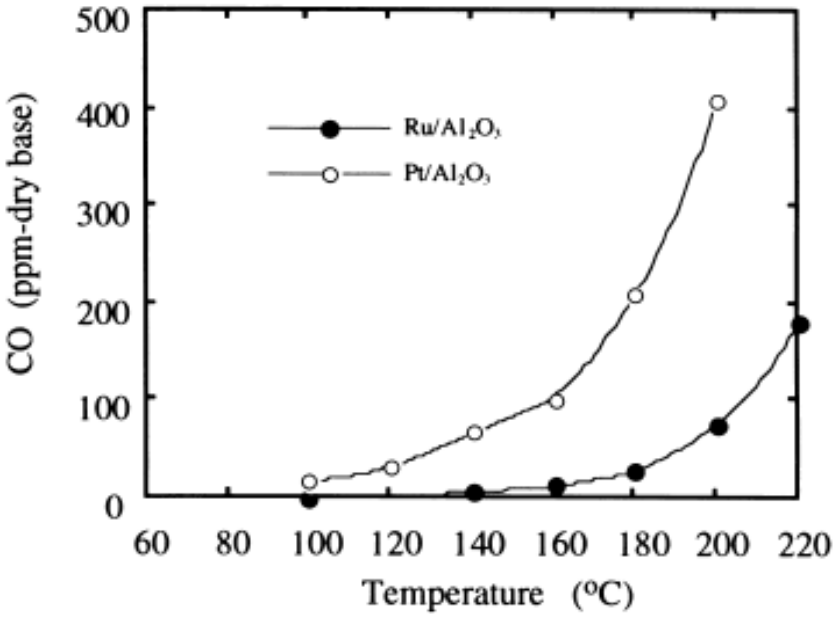


**Figure 2-10: Comparison of CO formed due to rWGS activity on $Ru/Al_2O_3$ and $Pt/Al_2O_3$ taken from (Kawatsu, 1998)**

A similar study was done by Kim et al., (2009a) to compare different noble metal catalyst for PrOx (Figure 2-11).

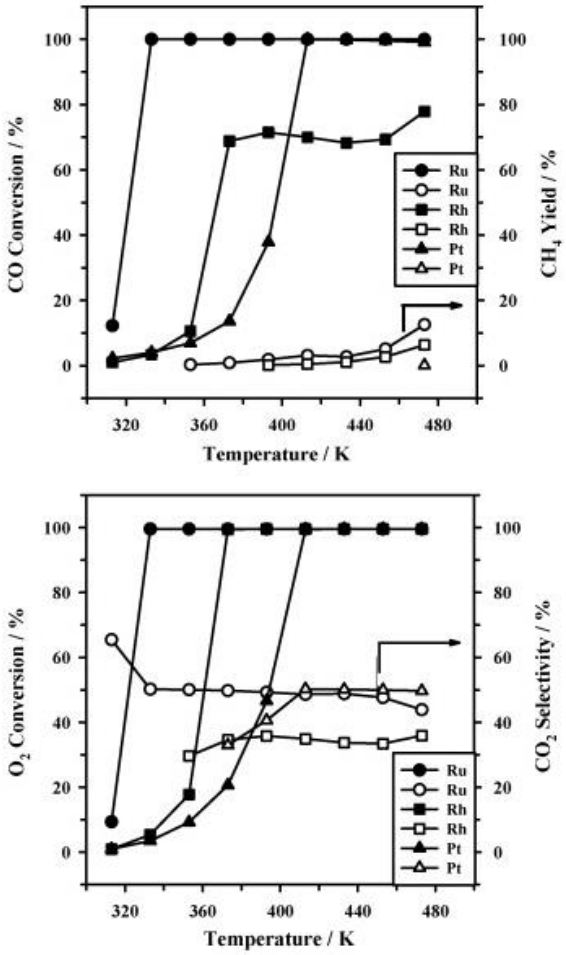


**Figure 2-11: Comparison of 5wt % $Ru/Al_2O_3$, 5wt % $Rh/Al_2O_3$ and 5wt % $Pt/Al_2O_3$ catalysts for PrOx, reaction conditions: 1 % CO, 1 % $O_2$, 50 % $H_2$, He balance, 1 000 ml/(min $g_{cat}$) adapted from (Kim et al., 2009a)**

The 5wt % $Ru/Al_2O_3$ has a higher activity for PrOx at lower temperatures (<130 °C). The Pt catalyst showed higher activity than the Rh catalyst at temperatures >130 °C. In contrast, the study by Oh & Sinkevitch (1993) (Figure 2-8) had shown that $Rh/Al_2O_3$ had a higher activity than the $Pt/Al_2O_3$. This difference could be due to the different parameters at which the studies were performed (metal loading, feed composition, space velocity).

Zhou et al., (2006) also compared PGM metal catalysts for PrOx. The results they reported are shown in Figure 2-12.

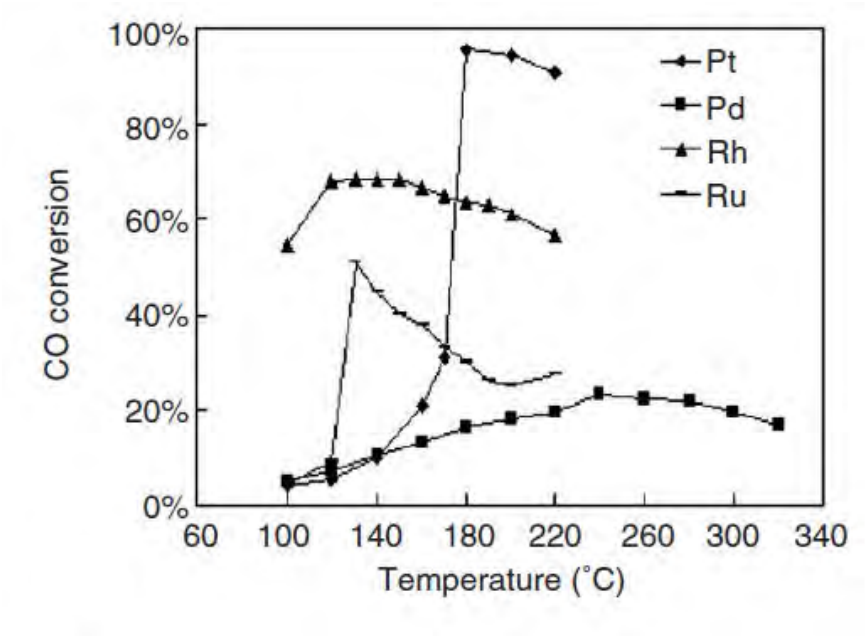


**Figure 2-12: Comparison of 0.5wt % $Ru/Al_2O_3$, 0.5w t% $Rh/Al_2O_3$, 0.5wt % $Pt/Al_2O_3$ and 0.5wt % $Pd/Al_2O_3$ catalysts for PrOx, reaction conditions: 1 % CO, 1 %$O_2$, 50 % $H_2$, 20 % $CO_2$, 20 % $H_2O$, $N_2$ balance, 30 000 h-1 adapted from Zhou et al., (2006)**

Figure 2-12 shows that at temperatures <170 °C the Rh catalyst shows the highest activity. What is interesting about this result is that Rh and Ru seem to be not as active (never achieve 100 % CO conversion) as the reports by Oh & Sinkevitch (1993) and Kim et al., (2009a). The differences could be due to the differences in the experimental conditions at which the studies were performed (metal loading, feed composition, space velocity). In contrast when Echigo et al.,(2003) compared the activity of $Pt/Al_2O_3$ to that of $Ru/Al_2O_3$ the $Ru/Al_2O_3$ showed better activity than the $Pt/Al_2O_3$ catalyst. Another study by Recupero et al., (2005) showed that higher CO conversions are obtained on $Ru/Al_2O_3$ compared to $Pt/Al_2O_3$. Furthermore, there are quite a few authors who have claimed to achieve high CO conversions using $Ru/Al_2O_3$, hence the result published by Zhou et al.,(2006) is not enough to disregard $Ru/Al_2O_3$ for PrOx. In fact, Ru catalysts have been reported to be very promising for PrOx. It has been proposed that $Ru/Al_2O_3$ is the most active noble metal catalyst (Shen et al., 2012). Rh and Ir catalysts have also been studied for PrOx however they have been found to be less selective compared to Ru and Pt catalysts (Park, Lee & Lee, 2009b). Furthermore, Pd supported catalysts have been confirmed to have a low activity and selectivity (Bion et al., 2008). The authors explained the low activity at low temperatures to be due to the formation of β-hydride which suppresses the oxidation of CO. While at high temperatures it was observed that metallic Pd had a higher affinity for $H_2$ adsorption compared to CO.

Ru catalysts have 3 main advantages (Chin et al., 2005) over Pt catalysts namely:

- Lower operating temperatures
- Can completely eliminate CO in a single step using reasonable space velocities at an $O_2$/CO ratio of 1 without compromising $CO_2$ selectivity
- Wide operating temperature window

After analysis of the above literature, Ru appears to be a good catalyst to study for PrOx.

## 2.4. Catalyst synthesis techniques

The active metal on catalysts is usually supported on a material in order to increase dispersion, increase surface area and prevent sintering. Sintering of small particles as illustrated in Figure 2-13 needs to be avoided in order to maintain the active surface area and hence the catalyst activity.

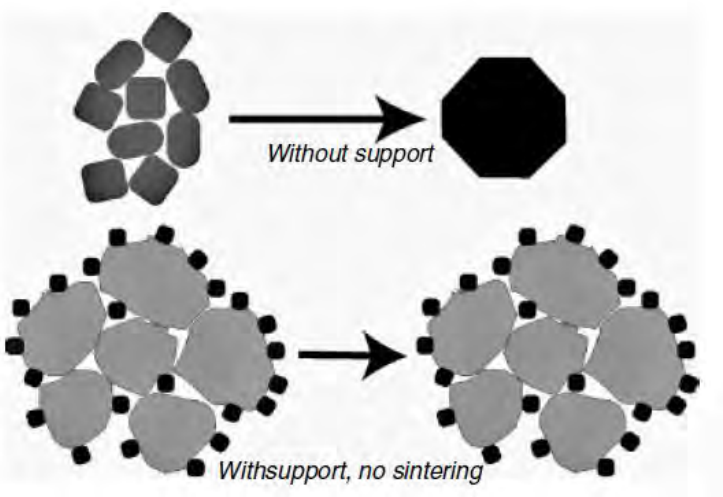


**Figure 2-13: Comparison of a supported and unsupported catalyst adapted from (Geus & Jos van Dillen, 2008)**

There are several different methods of catalyst synthesis. The method chosen depends on the desired chemical and physical characteristics of the end product. Some synthesis techniques include deposition, precipitation, co-precipitation and gel formation. Supported metal catalysts are generally prepared by impregnation, followed by drying then calcination and finally activation (Haber et al., 1995). There are three main stages of catalyst synthesis namely:

1. Preparation of the primary solid
2. Processing of that primary solid to obtain the catalyst precursor

3. Activation of the precursor to the active catalyst

During impregnation a solid is contacted with a liquid which contains the components to be deposited on the surface (Haber et al., 1995). For incipient wetness impregnation the support is contacted with a liquid with a volume that is equivalent to or slightly less than that of the total pore volume of the catalyst (Perego & Villa, 1997) (Figure 2-14). If there is excess liquid compared to the volume of the pores then the method is known as wetness impregnation.

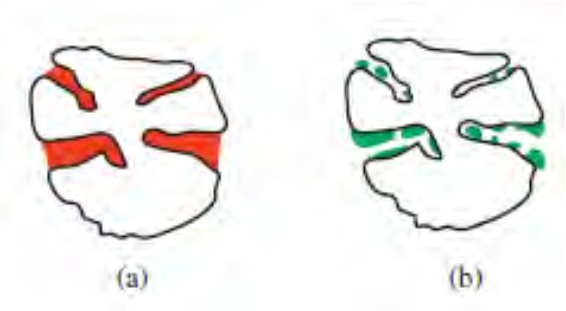


**Figure 2-14: Illustration of pore filling (a) and drying (b) method during wet impregnation, taken from (Ross, 2012)**

For incipient wetness impregnation, the main goal is to retain the species inside the pores during drying whereas for wetness impregnation specific interactions are much more significant (Ross, 2012). Redistribution of the impregnated species can occur during the drying process of an impregnated catalyst if the interactions with the support are weak leading to an inhomogeneous catalyst (Schwarz et al., 1995). Wetness impregnation can be performed whilst also doing a pH adjustment. The pH adjustment changes the overall charge of the support surface depending on whether the pH is below or above the point of zero charge (PZC) (Figure 2-15).

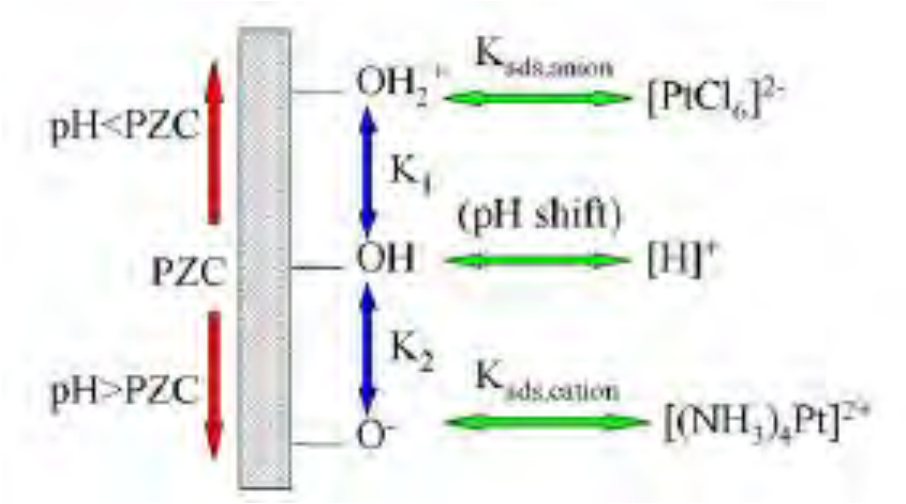

**Figure 2-15: Illustration of pH adjustment in order to enhance strong electrostatic adsorption of the metal precursor onto the catalyst support image taken from (Jiao & Regalbuto, 2008).**

The pH is adjusted in order to influence strong electrostatic adsorption of the metal precursor onto the support. Miller et al., (2004) reported that the Pt on silica catalyst that was prepared using a pH adjustment method had a higher dispersion than that prepared by dry impregnation.

Another catalyst preparation method that is mostly used for zeolites is ion exchange. During this process precursor metal cations (e.g $PtNH_3)_4^{2+}$) exchange with $K^+$, $Na^+$ or $NH_4^+$ ions on the zeolite according to the following reaction (Schwarz et al, 1995):

$$Pt(NH_3)_4^{2+}{}_{(aq)} + 2Cl^-_{(aq)} + 2K^+_{zeol} \leftrightarrow 2K^+_{(aq)} + 2Cl^-_{(aq)} + Pt(NH_3)_4^{2+}{}_{zeol} \quad \text{reaction 16}$$

The $NH_3$ ligands on the zeolite can then be removed from the surface by calcination while the $K^+$ and $Cl^-$ ions are removed during filtration and washing (Schwarz et al., 1995).

## 2.5. Factors that affect Ru catalysts activity for PrOx

The activity of Ru catalysts can be affected by various factors. In order to optimize catalyst performance it is important to understand the various factors that influence the catalyst activity. The following discussion concerns the factors that influence Ru catalyst activity for PrOx.

### 2.5.1. Catalyst preparation method

Catalyst preparation influences catalyst activity. In order to make the best catalyst it is important to understand the various factors that affect the catalyst activity.

It has been shown by Chin et al., (2005) that ruthenium nitrosyl nitrate is the best precursor for Ru catalysts compared to ruthenium chloride and ruthenium carbonyl (Figure 2-16).

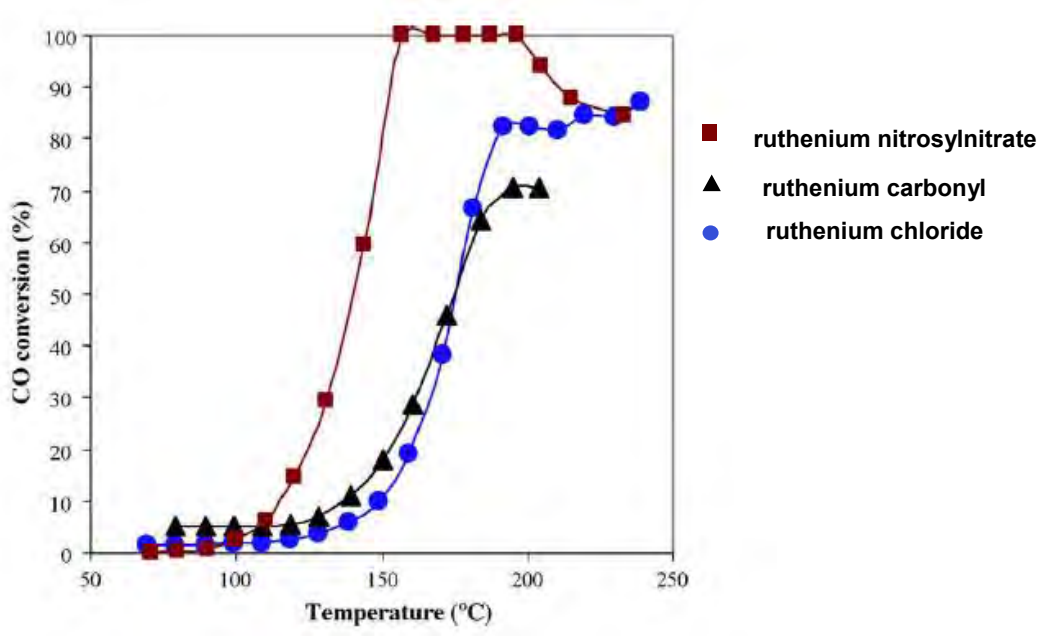


**Figure 2-16: Effect of Ru precursor on the catalyst activity at 0.5 % CO, 0.5 % $O_2$, 45 % $H_2$, 54 % $N_2$ at 120 000 ml/g h, taken from (Chin et al, 2005)**

The higher CO conversion obtained using the ruthenium nitrosyl nitrate as the precursor was attributed to the higher dispersion achieved when using the ruthenium nitrosyl nitrate precursor. Furthermore the authors suggested that using a ruthenium chloride precursor could result in a significant amount of residual chloride on the catalyst. Chlorine can alter the catalyst structure and block the active sites for CO oxidation (Narita et al., 1987). A similar explanation was also proposed with the ruthenium carbonyl precursor where some residual carbonyl groups were observed on the catalyst surface. Wörner et al., (2003) also confirmed that ruthenium nitrosyl nitrate is the best precursor for Ru catalysts in PrOx when compared to ruthenium (III) chloride and ruthenium carbonyl.

Furthermore, Chin et al., (2005) investigated the effect of reduction methods on the $Ru/Al_2O_3$ catalyst activity. One catalyst was reduced directly in $H_2$ at 300 °C and the other catalyst was first oxidized in $O_2$ at 300 °C followed by reduction in $H_2$ at 300 °C (Figure 2-17).

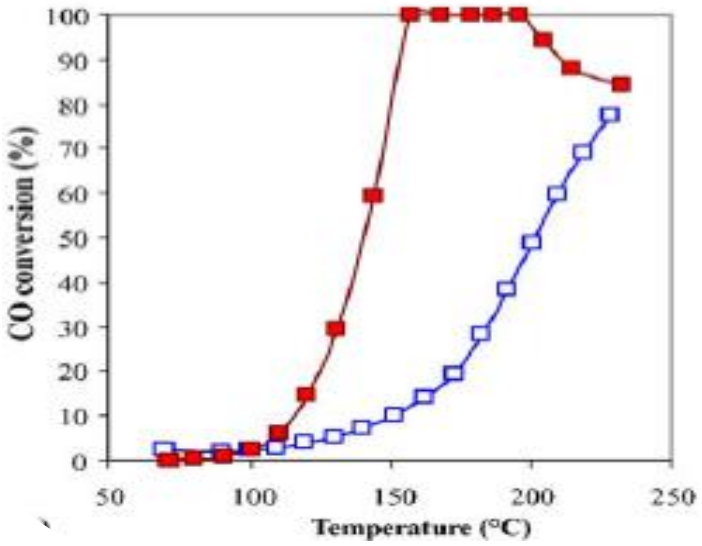


**Figure 2-17: Effect of reduction method on the activity of $Ru/Al_2O_3$, Reaction conditions: 0.5 % CO, 0.5 % $O_2$, 45 % $H_2$-balance $N_2$, 120,000 mL/g h; filled symbols: $H_2$ treatment at 300 °C; open symbols: $O_2$ at 300 °C followed by $H_2$ treatment at 300 °C, taken from (Chin et al., 2005)**

The catalyst reduced in $H_2$ showed higher conversions than the catalyst that was first oxidised and then reduced in $H_2$. This was explained to be due to the fact the catalyst directly reduced in $H_2$ had more exposed active sites since it had a higher dispersion. In addition, Echigo & Tabata, (2004) reported that CO oxidation activity at low temperatures can be improved by increasing the ratio of Ru(0) on the catalyst surface which can be achieved by reduction in $H_2/N_2$.

### 2.5.2. Reaction Temperature

The requirement for PrOx catalyst is that they achieve maximum conversion at a temperature range that is between the PEMFC and the WGS step (80 – 200 °C) in order to optimize the heat integration system.

Low CO conversions are usually observed on Ru catalysts at low temperatures. This has been attributed to low $O_2$ dissociation activity due to CO blocking the active sites (Kim et al.,2009a) and (Han et al., 2004a). The optimum temperature range at which Ru catalysts achieve maximum CO conversion varies in literature. One of the earlier studies on PrOx by Brown and Green (1960) reported that the optimum temperature for PrOx on a 0.5 wt% $Ru/Al_2O_3$ was 122 – 162 °C. Chin et al., (2005) reported an optimum temperature range of 180 – 200 °C for an impregnated 1 wt% $Ru/Al_2O_3$ catalyst with an inlet CO concentration of 0.5 vol.%. Oh and Sinkevitch (1993) reported an optimum temperature range of 102 – 302 °C for an inlet CO concentration of 900 ppm CO on a 0.5 wt% $Ru/Al_2O_3$ catalyst. A

temperature range of 240 – 300 °C for a 2 wt % $Ru/Al_2O_3$ catalyst was reported by Utaka et al., (2003) whilst Han et al.,(2004a) reported optimum temperatures below 150 °C for a 5 wt % $Ru/Al_2O_3$ catalyst. This shows that there is no uniformity in the optimum temperatures reported for PrOx using Ru catalysts.

### 2.5.3. Feed composition

Currently there is no standard feed used for PrOx in literature. Various studies done on PrOx are done in the absence of $CO_2$ and $H_2O$. It is important to understand the effects of these components since they make up part of the feed to the PrOx step in a fuel processing system. Kim & Park, (2010) found that CO conversion as well as selectivity decreased in the presence of $H_2O$ or $CO_2$ when using $Ru/\alpha\text{-}Al_2O_3$ as a catalyst. This was said to be due to the competitive adsorption of $H_2O$ and CO on the active sites as well as the strong adsorption of $CO_2$ onto the catalyst surface. Experiments done by Chin et al, (2005) showed that the addition of 10 % water to the feed stream had no effect on the activity of $Ru/SiO_2$, while a small effect (negative for T< 180 $^oC$ and positive for T> 200 $^oC$ was observed on $Ru/Al_2O_3$. In contrast, Kim et al., (2009a) reported no change in the CO oxidation rate when 10% $H_2O$ was added to the feed. However the addition of 20% $CO_2$ resulted in a decrease in $CO_2$ selectivity and CO oxidation.

According to Zhou et al., (2006), the presence of $CO_2$ in the feed stream decreases the CO conversion. Three explanations were proposed for this phenomenon. The first being that, $CO_2$ adsorbs onto the catalysts surface and dissociates to form CO. The second theory was that $CO_2$ influences the reverse WGS and the third theory was that $CO_2$ blocks the active sites. This was attributed to the competitive adsorption of CO and $CO_2$ onto the catalyst surface. Similarly, Echigo & Tabata, (2003) reported that the outlet CO concentration increases and the temperature window becomes narrower with the addition of $CO_2$ due to the rWGS reaction.

The concentration of CO in the feed stream also affects the observed exit CO concentrations. Low inlet CO concentrations (as a result of a more efficient WGS step) would result in higher CO conversions (i.e. lower exit CO concentrations). Some authors in literature use feed streams of 0.5 % CO (Echigo & Tabata, 2003), (Recupero et al., 2005) and (Rosso et al., 2004). Studies done using 1 % CO do not always achieve 100 % CO conversion (e.g Han et al., (2004a)).

### 2.5.3.1. $O_2$/CO ratio

Since most catalysts are not 100 % selective, the $O_2$/CO ratio is usually larger than the stoichiometric ratio (0.5). A term called λ is used to define the atomic oxygen to CO ratio according to the following equation:

$$\lambda = 2 * \frac{O_2}{CO} \qquad \text{equation 3}$$

It is important to apply an $O_2$/CO ratio that is high enough to achieve low CO concentrations (<10 ppm) whilst minimizing $H_2$ oxidation. Another issue that could arise from high $O_2$/CO ratios is thermal management since both CO and $H_2$ oxidation are exothermic reactions. This is mostly important when considering upscaling the laboratory experiments (Dagle et al., 2011).

Brown & Green (1960) reported that as the inlet CO concentration increases, the required $O_2$/CO ratio to decrease the CO concentration to less than 10 ppm increases. They reported that for a commercial 0.5 wt % $Ru/Al_2O_3$ catalyst, λ>3.5 was required to decrease 0.5 % CO to less than 10 ppm at 122 - 180 °C. Echigo et al.,(2003) used λ=3 to decrease the CO concentration from 0.5 % to less than 1 ppm at 10 700 ml/(h $g_{cat}$) for a 1 wt % $Ru/Al_2O_3$ catalyst. Whilst λ=2 was used by Chin et al.,(2005) to decrease the CO concentration from 0.5 % to less than 30 ppm at 120 000 ml/(h $g_{cat}$). Hence there is no general consensus in literature for a λ value. This could be due to the different operating conditions at which the studies are done.

The amount of $O_2$ can be reduced without the compromising the CO conversion by a multistage CO removal process. Brown & Green, (1960) suggested the use of a 2 stage reactor in order to remove CO from a $H_2$ rich stream. The main advantage of this is that the $CO_2$ selectivity increases and also the temperature control becomes simpler since the less heat is emitted in each stage (Echigo et al., 2003). However, this results in a more complex heat integration and air injection system (Echigo et al., 2003). As a result single stage PrOx systems are more desirable.

### 2.5.4. Effect of catalyst support

Various studies have been done to assess the effect of the Ru catalyst support on the PrOx activity. Shen et al., (2012) decreased the CO concentration from 1 % to less than 100 ppm using a 4 wt % $Ru/Al_2O_3$ at 60 000 ml/(h $g_{cat}$). They attributed the high CO conversion at high space velocity to be due to the meso-macroporous γ-$Al_2O_3$ support they made. However this could also have been due to the higher metal loading of the catalyst. Rosso et al.,(2004)

prepared Ru catalysts supported on γ-$Al_2O_3$, 3A- type zeolite, 4A-type zeolite and 5A-type zeolite (Figure 2-18).

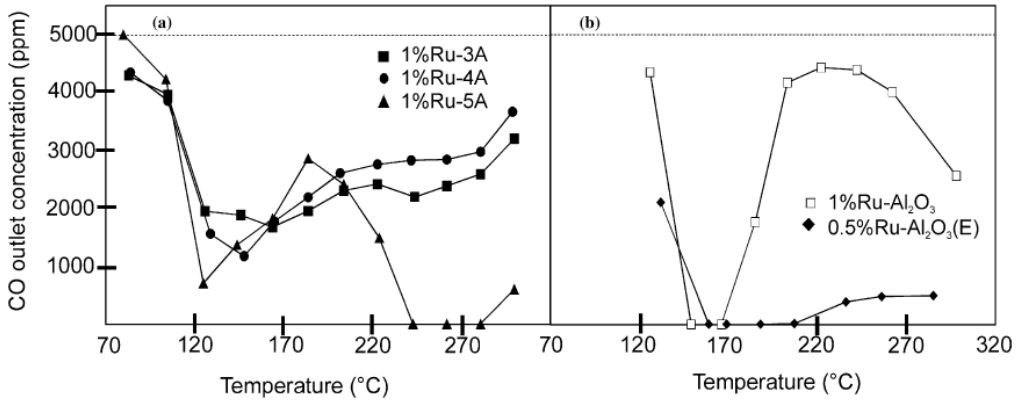


**Figure 2-18: Comparison of CO outlet concentration on the a) zeolite supported catalysts b) alumina supported catalysts. Feed conditions, 37 % $H_2$, 18 % $CO_2$, 0.5 % CO, 5 % $H_2O$, 1 % $O_2$, He balance at 40 000 ml/(h $g_{cat}$) adapted from (Rosso et al., 2004)**

The 1 wt % Ru-3A and the 1 wt % Ru-4A did not achieve high CO conversions (low CO outlet concentration) unlike the 1 wt % Ru-5A which achieved high CO (10 ppm) conversions at 250 °C. Kim & Park (2010) tested the effect of crystalline phase of aluminium oxide supports on Ru catalyst activity. They reported that Ru/α-$Al_2O_3$ had the highest CO conversion compared to Ru/κ-$Al_2O_3$, Ru/γ-$Al_2O_3$, Ru/η-$Al_2O_3$, Ru/δ-$Al_2O_3$ and Ru/θ-$Al_2O_3$ especially at low temperature. The activity of Ru supported on alumina was also compared to that supported on silica in a study by Chin et al., (2005). It was observed the highest CO conversion (~100 %) for Ru/$SiO_2$ was between 120 – 150 °C and 160 - 180 °C for Ru/$Al_2O_3$. This was explained to be due to the higher thermal stability of CO adsorbed onto $Al_2O_3$ supported Ru compared to $SiO_2$ supported Ru (i.e. $CO_2$ species can desorb from $SiO_2$ supported Ru at lower temperatures than from $Al_2O_3$ supported Ru). Another paper by Kim et al., (2009a) compared Ru catalysts supported on YSZ, $ZrO_2$, $TiO_2$, $SiO_2$ and γ-$Al_2O_3$. In this study the catalyst supported on YSZ showed superior activity for PrOx. Unlike the results published by Chin et al.,(2005) the Ru/$Al_2O_3$ and Ru/SiO2 studied by Kim et al., (2009a) did not reach 100 % CO conversion. The difference in the results could be due to the different experimental conditions (Table 2-3).

**Table 2-3: Comparison of experimental conditions used by Kim et al.,(2009a) and Chin et al.,(2005)**

| | **(Kim et al., 2009a)** | **Chin et al., (2005)** |
|---|---|---|
| Ru preparation | Impregnation with $Ru(NO)(NO_3)_3{\cdot}XH_2O$ | Impregnation with $Ru(NO)(NO_3)_3{\cdot}XH_2O$ |
| Reduction | 300 °C in $H_2$ | 300 °C in $H_2$ |
| Ru content (wt %) | 0.58 | 1.0 |
| Feed composition | 1 % CO, 1 % $O_2$, 50 % $H_2$ in He | 0.5 % CO, 0.5 % $O_2$, 45 % $H_2$ in He |
| Space velocity | 60 000 ml/(h $g_{cat}$) | 120 000 ml/(h $g_{cat}$) |

Another study was also done by the same authors (Kim & Park, (2010)) where they investigate the effect of the support on the Ru catalysts Kim et al.,(2009a). What is interesting to note is the differences in the performance of Ru/γ-$Al_2O_3$ reported in the 2009 paper and that in the 2010 paper (Table 2-4).

**Table 2-4: Comparison of observed data by Kim & Park, 2010 and Kim et al., 2009a**

| | **(Kim et al., 2009a)** | **Kim & Park (2010)** |
|---|---|---|
| Ru preparation | Impregnation with $Ru(NO)(NO_3)_3{\cdot}XH_2O$ | Impregnation with $Ru(NO)(NO_3)_3{\cdot}XH_2O$ |
| Reduction | 300 °C in $H_2$ | 300 °C in $H_2$ |
| Ru content | 0.58 | 0.688 |
| Feed composition | 1 % CO, 1 % $O_2$, 50 % $H_2$ in He | 1 % CO, 1 % $O_2$, 50 % $H_2$ in He |
| Space velocity | 1 000 ml/min/$g_{cat}$ | 1 000 ml/min/$g_{cat}$ |
| $X_{co}$ at 200 °C | 5 % | 55 % |
| $X_{O2}$ at 200 °C | 10 % | 40 % |
| $S_{co}$ at 200 °C | 20 % | 75 % |

From Table 2-4 we can see the Ru/γ-$Al_2O_3$ catalysts were prepared and reduced at the same conditions. Furthermore they have comparable Ru loadings but the observed CO conversions in the 2 papers are very different. This brings into question the reliability of the reported results.

Furthermore, one of the co-authors in the Kim & Park (2010) also co-authored another paper Park &Park (2014) in which they investigated Ru/κ-$Al_2O_3$ for PrOx. The claim was that the high surface area of the κ-$Al_2O_3$ is favorable to the external mass transfer of $O_2$ during PrOx. This is after they had published that Ru/α-$Al_2O_3$ is the best for PrOx compared to other phases of $Al_2O_3$ due to the stability of the Ru metal under the PrOx conditions (Kim & Park 2010). This was based on the view that the metallic phase of Ru is more superior for PrOx activity compared to oxidized Ru phase. Park & Park (2014) claim that the Ru/α-$Al_2O_3$ investigated by Kim & Park (2010) could not achieve full CO conversion. However, Kim & Park (2010) had claimed that "Ru/α-$Al_2O_3$ can reduce the high inlet CO concentration to less than 10 ppm".

### 2.5.5. Particle size

Metal or metal oxide particle size is an important factor in catalysis because it affects the surface to volume ratio which influences the activity and selectivity of molecules adsorbed onto the catalyst surface (Kim et al., 2012).

Chin et al., (2005) reported that the 1 wt % Ru/γ-$Al_2O_3$ with smaller particles (1.6 nm) showed superior activity for PrOx compared to the 1 wt % Ru/γ-$Al_2O_3$ with larger particles (7.8 nm). However, Kim et al., (2012) suggested that as the Ru particle size increases, PrOx activity increases and they stated that this was closely related to the $O_2$ adsorption behavior on Ru. In their paper they suggested an activation method that can control the Ru particle size to an optimum size (6 nm) for 5 wt % Ru/$Al_2O_3$. This result is the complete opposite of what the same authors published a few years earlier when they tested the activity of Ru supported on different types of alumina for PrOx. Kim & Park, (2010) reported that Ru supported on α-$Al_2O_3$ showed the best activity for PrOx. The 0.7 wt % Ru/α-$Al_2O_3$ had the smallest average particle size (2.6 nm). Furthermore, they showed that as the amount of chemisorbed CO increased, the Ru particle size decreased. But the opposite was reported in their 2012 paper as shown in Table 2-5.

**Table 2-5: Comparison of observed data by Kim & Park, 2010 and Kim et al., 2012**

| ***Kim & Park (2010)*** | | ***Kim et al., (2012)*** | |
|---|---|---|---|
| Particle size (TEM) | Chemisorbed CO (μmol CO/$g_{cat}$) | Particle size (TEM) | Chemisorbed CO (μmol CO/$g_{cat}$) |
| 2.9 | 32.6 | 5.7 | 8.2 |
| 4.0 | 26.0 | 6.3 | 13.6 |

| | | | |
|---|---|---|---|
| 6.2 | 16.6 | 7.1 | 22.6 |

An increase in the amount of the CO chemisorbed is usually an indicator of increase in surface area (hence decrease in particle size).

Later on in 2014 one of the co-authors in the Kim et al.,(2012) paper co-authored another paper where they report that increasing Ru particle size increases PrOx but only up to 3 nm. They claimed that once the particles are larger than 3 nm $H_2$ oxidation is further enhanced thus reducing $CO_2$ selectivity (Park & Park, 2014).

Kim et al., (2012) reported that for 1 wt % $Ru/SiO_2$, higher PrOx activity was observed on the larger Ru particles (6.4 nm) than the smaller particles (1.5 nm). In contrast, Chin et al., (2005) reported that the 1 wt % $Ru/SiO_2$ with smaller particles (2.4 nm) showed much superior activity for PrOx compared to the 1 wt % $Ru/SiO_2$ with larger particles (19.0 nm).

### 2.5.6. Methanation

Methane formation is usually obtained on Ru catalysts especially at high temperatures. The methane formed could be as a result of CO or/and $CO_2$ methanation. CO methanation is quite beneficial because it aids in lowering the CO concentration. $CO_2$ methanation however results in further $H_2$ consumption which is undesirable. Kim et al., (2012) reported that at high temperatures (>200 °C) more methane formation was observed on smaller Ru particles (5.7 nm) than on larger Ru particles (6.3 nm). Kim & Park (2010) observed that on $Ru/Al_2O_3$ catalyst, methane formation is only observed after $O_2$ was completely consumed. Echigo et al., (2003) calculated that generating 500 ppm of $CH_4$ reduced the fuel processor efficiency by approximately 0.1 %. Therefore several ppm of $CH_4$ have no major impact on the fuel processor efficiency.

### 2.5.7. Percentage metal loading

The metal loading on the catalyst contributes to catalyst activity. A study done by Kim et al., (2009a) showed that a 5wt % $Ru/Al_2O_3$ could achieve 100 % CO conversion (<10 ppm CO) at temperatures between 60 – 150 °C. However, the 0.5wt % $Ru/Al_2O_3$ only achieved a maximum conversion of 80% at 100 °C at the same conditions (1 % CO, 1 % $O_2$, 50 % $H_2$, He balance, 1000 ml/(min $g_{cat}$). When the 0.5wt% $Ru/Al_2O_3$ was tested at a lower space velocity (100 ml/(min $g_{cat}$), 100% CO conversion was achieved at 100 °C, however there was no wide temperature window at maximum conversion. The turnover frequency (TOF) for the 5 wt % $Al_2O_3$ was three times higher than that of the 0.5 wt % $Ru/Al_2O_3$. Furthermore, the

0.5 wt % $Ru/Al_2O_3$ showed lower $CO_2$ selectivity than the 5 wt % $Ru/Al_2O_3$. As a result, the authors decided that 5wt% $Ru/Al_2O_3$ was the optimum PrOx catalyst. In contrast, Huang et al., (2007) reported that the CO conversion was affected by the Ru metal loading at temperatures lower than 100 °C. Increasing the metal loading from 0.1 wt % to 5 wt % increased the CO conversion for temperatures below 100 °C. It was suggested that the optimal Ru loading is the 1 wt % $Ru/Al_2O_3$ which achieved the highest CO conversion at the lowest temperature (100 °C).

### 2.5.8. Space velocity

High space velocities (SV) (i.e. low contact time) result in a reduction of not only the size but also the cost of the system (Watanabe et al., 2003). According to Echigo & Tabata (2003) a space velocity of 10 700 ml/(h $g_{cat}$) is sufficient for the CO removal reactor.

0.7 % Ru/α-$Al_2O_3$ catalyst by Kim & Park, (2010) showed a CO conversion close to 100 % at a $CO_2$ selectivity of 50 % and $O_2$/CO ratio of 1. However the space velocity was quite low (6 000 ml/ g h). Echigo & Tabata (2003) reduced the CO concentration from 0.5 % to less than 10 ppm using a 1 wt % Ru/γ-$Al_2O_3$ at 10 700 ml/(h $g_{cat}$) and λ = 2. Recupero et al., (2005) reported an exit CO concentration of less than 10 ppm from 0.5 vol. % at 6 500 $h^{-1}$ but with λ = 4. Whilst Chin et al., (2005) achieved complete CO removal at a space velocity of 120 000 ml/(h $g_{cat}$) with 0.5 % CO in the feed. Once again we can see that there is a wide range of space velocities used in literature and no uniformity.

### 2.5.9. Ru catalyst promotion effects

A promoter can be added to the Ru catalyst to influence catalyst activity. Niu et al., (2014) doped $Ru/SiO_2$ with potassium (K) and reported an improved CO oxidation activity and selectivity. Addition of K improved the dissociation of $O_2$ on the Ru surface due to the weakened adsorption of CO on the catalyst active site thus increasing PrOx activity (Niu et al., 2013). $CO_2$ selectivity was improved due to weak adsorption of $H_2$ onto the catalyst active sites at high temperatures as a result of the K (Niu et al., 2013). There is very little work published on the promotion of Ru with alkali metals for PrOx.

## 2.6. Pt catalysts

Igarashi et al., (1997) published a paper where they looked into using the molecular sieve effect of zeolites in order to improve the $CO_2$ selectivity of Pt catalysts in PrOx. Mordenite is a zeolite and the benefit of zeolite structures is the sieving effect of the zeolite cages. According to Igarashi et al., (1997) CO and $O_2$ molecules are more concentrated in the

mordenite cages because of the higher polarity and/or molecular weight compared to $H_2$. This results in increased $CO_2$ selectivity. They had also proposed the use of a multistage reactor (2 stages) to decrease the CO concentration and improve $CO_2$ selectivity using a 6 wt% Pt/Mordenite catalyst. In 2003 the same authors published another paper where they proposed the use of Pt-Fe/Mordenite as a PrOx catalyst. Pt-Fe/Mordenite was superior to their previous Pt/Mordenite catalyst and achieved 100 % CO conversion with 100 % selectivity at λ=1 in a single stage reactor (Watanabe et al., 2003). The catalyst activity was improved by the addition of Fe which lowered the bond strength of CO to Pt. The proposed mechanism on the Pt-Fe/Mordenite is a bi-functional mechanism were the CO adsorbs onto Pt and the $O_2$ adsorption and dissociation occurs on Fe (Figure 2-19).

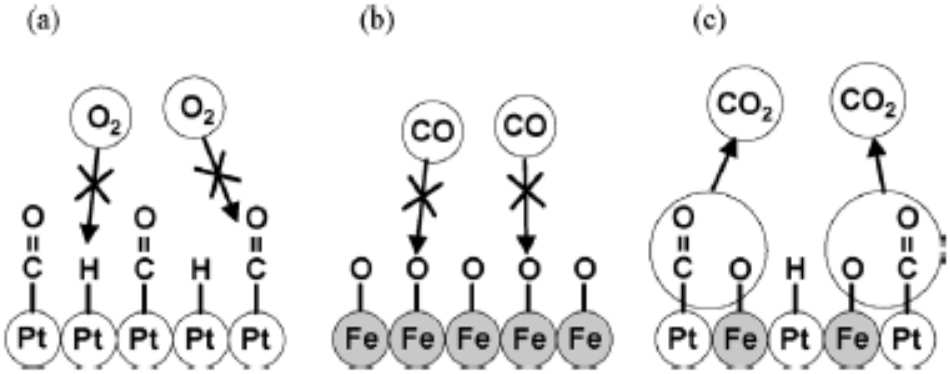


**Figure 2-19: The mechanism of PrOx on a) Pt/Mordenite b) Fe/Mordenite c) Pt-Fe/Mordenite taken from (Kotobuki et al., 2005)**

The addition of Fe results in a non-competitive Langmuir-Hinshelwood mechanism in which CO and $O_2$ do not compete for the same active sites. Pt-Fe/Mordenite is a good catalyst to investigate further for PrOx due to the high CO conversion (100 %) and selectivity (100 %) as reported by Watanabe et al., (2003). The Pt-Fe/Mordenite catalyst was prepared by a conventional ion exchange method followed by oxidation at 500 °C for 0.5 h then reduction at 500 °C in $H_2$ for 1 h.

In this MSc study a solid state ion exchange for the Fe followed by a competitive ion exchange for the Pt is proposed as an improvement to the catalyst preparation method. Kogel et al., (1998) reported that solid state ion exchange of Fe onto MFI zeolite showed an improved catalyst activity for the reduction of NO to $N_2O$ compared to the catalyst prepared by aqueous ion exchange. They also reported that the addition of Pt increased the yield of $CO_2$ formed by the oxidation of CO during the NO reduction process. Preparation by aqueous ion exchange results in the precipitation of iron hydroxide (Kogel et al., 1998).

Therefore, this study used solid state ion exchange to deposit Fe onto Mordenite. This study used a competitive ion exchange method to deposit Pt onto Mordenite because competitive ion exchange increases the dispersion of Pt (Philippaerts et al., 2010). Furthermore the Pt-Fe/Mordenite in this study was oxidized at 350 °C for 1 h at a heating rate of 0.3 °C/min and reduced in $H_2$ at 250 °C for 8 hours at a heating rate of 0.4 °C/min. According to Philippaerts et al., (2010) this oxidation and reduction method results in better Pt dispersion.

## 2.7. Heat and mass transfer limitations

CO oxidation is a very rapid reaction which is controlled by mass transfer (Shen et al., 2012). It has been proposed that a macroporous structure promotes mass and heat transfer (Roberts et al., 2003) and (Lu et al., 2009). The macroporous structure enhances the diffusion of the reactants into the pores to the active site. The study done by Rosso et al., (2004) in which the zeolite with larger pore size (5A) exhibited the highest CO conversion, shows that macro pores favour mass transfer.

Since CO oxidation is an exothermic reaction, there is potential for hot spot formation on the catalyst surface (Rozovskii et al., 2008). The formation of hot spots enhances the rWGS reaction thus forming more CO causing a decrease in CO conversion. Thus, efficient heat transfer is desired.

## 2.8. Research motivation

### 2.8.1. Ru catalyst

From the given literature review, one can observe that there is a lot of information on Ru catalysts for PrOx. Most of work published is either just for laboratory tests or for specific PrOx reactors or fuel processors. Ranking these catalysts is however a challenging task due to the different conditions (space velocity, metal loading, feed composition etc.) at which the studies where done. This presents a lack of systematic characterization of the catalysts.

Furthermore, a more critical review of the published literature highlights some contradictions.

As a result it is very important to do an in-house test for the HySA fuel processing project in order to obtain more reliable results that are at the specific conditions at which the fuel processor is expected to run.

### 2.8.2. Pt – Fe/Mordenite

The results obtained by Watanabe et al.,(2003) present a very promising Pt-Fe/Mordenite catalyst that not only achieves 100 % CO conversion but also 100 % $CO_2$ selectivity at λ=1. This result has never been reported for Ru catalyst which generally have a selectivity of ~50 % as the best result. Investigating Pt-Fe/Mordenite further using a different catalyst preparation and reduction method to determine its applicability in the HySA fuel processor appears to be a worthwhile venture.

# 3. Objectives of Study

## 3.1. Aim

The aim of this study is to evaluate the performance of in house synthesized $Ru/Al_2O_3$ catalyst and compare it to a commercial catalyst for PrOx activity in a fuel processor system.

## 3.2. Objectives

The objectives of this study were to:

- Synthesise $Ru/Al_2O_3$ using incipient wetness impregnation and pH adjusted wetness impregnation.
- Synthesise a $Ru/Al_2O_3$ catalyst by incipient wetness impregnation.
- Evaluate the activity of the synthesised catalysts at different temperatures, space velocity as well as $O_2$/CO ratio in order to determine the operation window.
- Compare the synthesised catalyst activity to a commercial PrOx catalyst.

## 3.3. Hypothesis

The following hypothesis was then proposed:

- The Ru catalyst prepared using pH adjustment is more active than the incipient wetness impregnation prepared catalyst because the pH adjustment method increases dispersion and hence PrOx activity

## 3.4. Key questions

The key questions to be assessed based on this hypothesis are therefore;

- How does temperature, space velocity and $O_2$/CO ratio affect catalytic activity?
- Does pH adjustment during wetness impregnation improve catalyst dispersion and hence PrOx activity?
- How do the synthesised catalysts compare to the commercial catalyst?

Towards the end of the study, a Pt-Fe/Mordenite catalyst found in literature and exhibited remarkable results for PrOx (high CO conversion and selectivity)

An attempt was then made to synthesize the same catalyst using a modified method. An additional hypothesis was then proposed as follows:

- The Pt-Fe/Mordenite prepared using solid state ion exchange and competitive ion exchange will exhibit higher $CO_2$ selectivity compared to the Ru catalysts. Since the

active sites are located in the zeolite cages, a sieving mechanism can be utilized favouring CO diffusion compared to $H_2$ diffusion thus increasing $CO_2$ selectivity.

The key question was:

- Can the catalyst preparation method for Pt-Fe/Mordenite by Watanabe et al. 2003 be improved by using solid state ion exchange and competitive ion exchange?

# 4. Experimental

## 4.1. Catalyst preparation

In this study two Ru catalysts supported on alumina as well as a Pt-Fe supported on mordenite were prepared.

### 4.1.1. Ru catalyst

#### 4.1.1.1. Wetness impregnation with high pH

A 1 wt % $Ru/Al_2O_3$ catalyst was prepared using wetness impregnation at a high pH in order to influence strong electrostatic adsorption of the Ru precursor onto the γ-$Al_2O_3$. γ-$Al_2O_3$ (Puralox SCCa 5-150) was calcined at 1 100 °C for 5 hours using a heating rate of 3.5 °C/min to change the phase to α-$Al_2O_3$. This was done in order to change the phase of the γ-$Al_2O_3$ to α-$Al_2O_3$ because Kim et al., (2010) reported that the catalyst supported on α-$Al_2O_3$ exhibited better PrOx activity. The calcined support (3.96 g) was added to a 1 L solution of 2.667 ml $Ru(NO)(NO_3)_3$ (Sigma Aldrich) mixed with water and 0.056 g NaOH (Kimix) to raise the pH to>9. Since the point of zero charge (PZC) of α-$Al_2O_3$ is 9.1 ±0.1 (Yopps and Fuerstenau 1964, 61-71), at pH>9.1 the support would have an overall positive charge. This results in strong electrostatic adsorption of the Ru precursor anion ($Ru(NO)(H_2O)_{x-1}OH^-_{aq}$) with the support. The mixture was stirred overnight then filtered and dried at room temperature overnight. Before analysis the catalyst was reduced in 5% $H_2/N_2$ at 300 °C at a heating rate of 3 °C/min. This catalyst will be referred to as Ru_high pH.

#### 4.1.1.2. Incipient Wetness Impregnation

Another Ru catalyst was also prepared by incipient wetness impregnation according to the method described by Chin et al., (2005). The γ-$Al_2O_3$ (Puralox SCCa 5-150) support was first calcined at 500 °C at a heating rate of 3.5 °C/min. Four grams of catalyst was made by impregnating 3.96 g of γ-$Al_2O_3$ with 2.67 ml of $Ru(NO)(NO_3)_3$. The catalyst was dried overnight at 60 °C then reduced in 5% $H_2/N_2$ at 300 °C at a heating rate of 3 °C/min before analysis. This catalyst will be referred to as Ru_IWI.

### 4.1.2. Pt-Fe/Mordenite catalyst

To prepare the 4 wt% Pt-0.5 wt % Fe/mordenite catalyst, 1 g of Mordenite ($NH_4$-MOR-20 supplied by SC zeolites) was ground with a mortar and pistol. Iron(II) chloride tetrahydrate (Sigma Aldrich) was added to the mordenite and the powder was ground further before micronizng (McCrone Micronising Mill) for 20 minutes following the procedure of Kogel et

al., (1998) The Fe exchanged mordenite was heated to 550 °C in 3 hours then kept at that temperature for 6 h in air. This was then followed by a competitive ion exchange of Na and Pt for 24 h with an atomic Na/Pt ratio of 25 in order to enhance the Pt dispersion on Mordenite. Competitive ion exchange was used because Philippaerts et al., (2010) found that competitive ion exchange led to higher dispersion of Pt on ZSM-5. The catalyst was washed and filtered until there was no Cl detected in the filtrate. To test for Cl, $AgNO_3$(aq) was added to the filtrate. The formation of a milky precipitate (AgCl) indicates the presence of Cl. The catalyst was then dried at room temperature overnight.

Before analysis the catalyst was first oxidised at 350 °C in $O_2$ at 100 ml/min using a heating of 0.3 °C/min. The temperature was kept at 350 °C for an hour then the reactor was cooled in $N_2$ to room temperature. The catalyst was then reduced in $H_2$ at 250 °C for 8 hours using a heating rate of 0.4 °C/min. This catalyst is referred to as Pt-Fe/M.

## 4.2. Catalyst Characterization

Various characterization techniques were used in order to determine the physical characteristics of the catalysts and supports.

### 4.2.1. Brunauer–Emmett–Teller surface area

The surface area as well as the pore diameter of the different types of alumina used where determined by the Brunauer–Emmett–Teller (BET) method using $N_2$ adsorption and desorption in a Micromeritics ASAP 2000 analyser. The samples were degassed at 120 °C for (1 hour under vacuum) $N_2$ adsorption and desorption were measured at the temperature of liquid $N_2$.

### 4.2.2. Inductively coupled plasma optical emission spectrometry analysis

The percentage metal loading on the prepared catalysts was determined by inductively coupled plasma optical emission spectrometry (ICP–OES) using a Varian ICP 730-ES spectrophotometer. In this technique a liquid sample is introduced to a radiofrequency (RF)-induced argon plasma causing the sample to dissociate into its atoms or ions. These atoms or ions are then excited to a state where they emit light of a characteristic wavelength (Hou and Jones 2000).

A 50 mg sample was dissolved in a mixture of 6ml concentrated hydrochloric acid (HCl), 2 ml concentrated hydrofluoric acid (HF) and 2 ml concentrated nitric acid ($HNO_3$). This was

then followed by digestion in a MARS-5 Microwave digester before ICP-OES analysis. The metal loading was determined by means of a calibrated curve with known metal concentrations.

### 4.2.3. Chemisorption

For the Ru catalysts, $O_2$ chemisorption was performed in order to determine the particle size as well as metal dispersion on the support. $H_2$ chemisorption and CO chemisorption where not performed due to the issue of the $H_2$ spillover effect or the formation of carbonyl groups which may affect the results obtained using these methods (Chin et al., 2005). $O_2$ chemisorption was performed using an ASAP 2020 C unit. The catalyst was first evacuated in He then reduced according to the reduction procedure in Section 4.1.1. The sample was then evacuated and $O_2$ chemisorption was performed at 40 °C.

The diameter of the particle can be calculated from $O_2$ chemisorption according to the following equation:

$$d=\frac{6\cdot V_m}{D\cdot a_m}$$

d – Particle diameter [nm]
$V_m$ – volume occupied by metal atom [$nm^3$]
$a_m$ – surface area occupied by an exposed surface metal ion [$nm^2$]

$V_m$ and $a_m$ are 13.65 x $10^{-3}$ $nm^3$ and 6.35 x $10^{-2}$ $nm^2$ respectively (Shen et al., 2008).

### 4.2.4. Temperature programme reduction

Temperature programmed reduction (TPR) was performed on the catalysts to determine the catalyst reduction behaviour using a Micromeritics Autochem HP II 2950 Chemisorption Analyzer with a TCD detector. A 50mg sample was placed in a quartz tube reactor and the sample was first dried in Ar at 120 °C then cooled. TPR analysis was done in 5% $H_2$/Ar at a flowrate of 20 ml/min and a heating rate of 10 °C/min up to a temperature of 400 °C. A thermal conductivity detector (TCD) measured the $H_2$ uptake.

### 4.2.5. Transmission electron microscopy

Transmission electron microscopy (TEM) analysis was performed using a Tecnai $G^2$ electron microscope operating at 200 kV. Before analysis the sample was first reduced according to the method described in Section 4.1. The sample was then ground using a mortar to fine

particles. A few drops of acetone were added to the sample which was then ultrasonicated for 15 minutes before being deposited onto a carbon coated copper grid for TEM analysis.

## 4.3. Test unit

A process flow diagram of the experimental setup of this project is shown in Figure 4 -1.

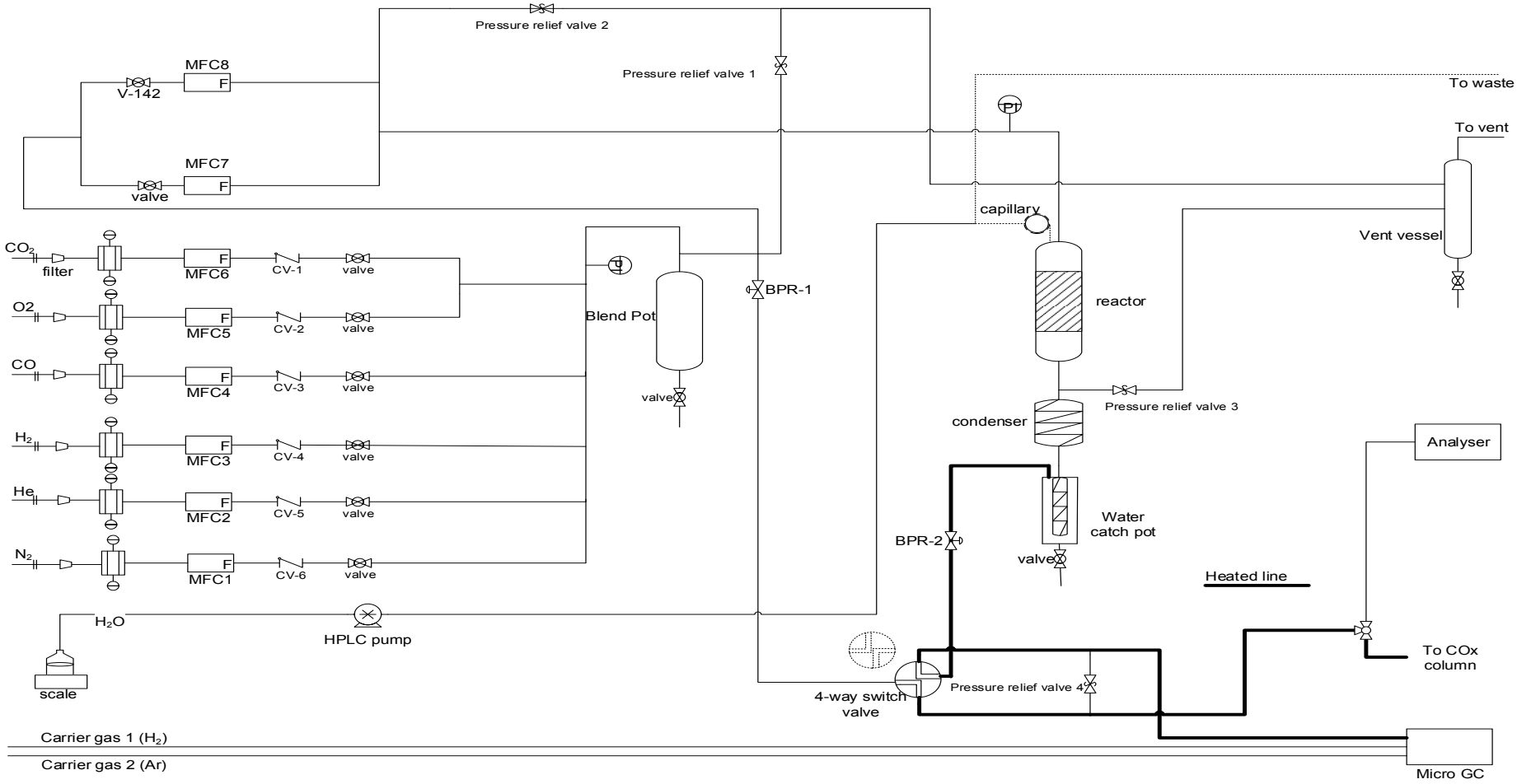


**Figure 4-1: Process flow diagram of the equipment setup used in this study**

### 4.3.1. Mass flow controllers

Brooks mass flow controllers with a proportional-integral-derivative (PID) control loop where used to control the gas flow rates.

### 4.3.2. Temperature controllers

Temperature controllers (Gefran 800P) were used to set the reactor as well as the heating line to the required temperature. A J-type thermocouple (Uni Temp) was used to measure the temperature of the catalyst bed as well as the heating line.

### 4.3.3. Pressure reducing regulators

The analysis gases were passed through filters before flowing through pressure reducing regulators (Tescom). Pressure reducing regulators are used to maintain the required outlet pressure and provide the required flow that meets a variable demand downstream. The purpose of the pressure reducing regulator was to not only decrease the outlet pressure but to also regulate the inlet pressure to the mass flow controllers.

### 4.3.4. Back pressure regulator

Spring loaded back pressure regulators (Tescom 150) were used to maintain the pressure in the blend pot and in the reactor. A back pressure regulator maintains the upstream pressure by means of a sensing element which cracks open when the set pressure is exceeded to return the upstream pressure to the set point.

### 4.3.5. Pressure relief valves

In the event of a drastic increase in pressure, pressure relief valves were put in place to vent out the excess gas thus reducing the pressure.

### 4.3.6. 2-way (4-port) by-pass switch valve

A 4-way switch valve with two inlet and two outlet ports as shown in Figure 4-1 was used to sample either the reactor product stream or the reactor by-pass (i.e. feed). When the valve was set to sample the reactor product on the micro GC, the reactor by-pass stream was sent to vent vessel and vice versa when the by-pass stream was sampled.

### 4.3.7. Fixed bed reactor

All experiments were done in a fixed bed reactor setup shown in Figure 4-2.

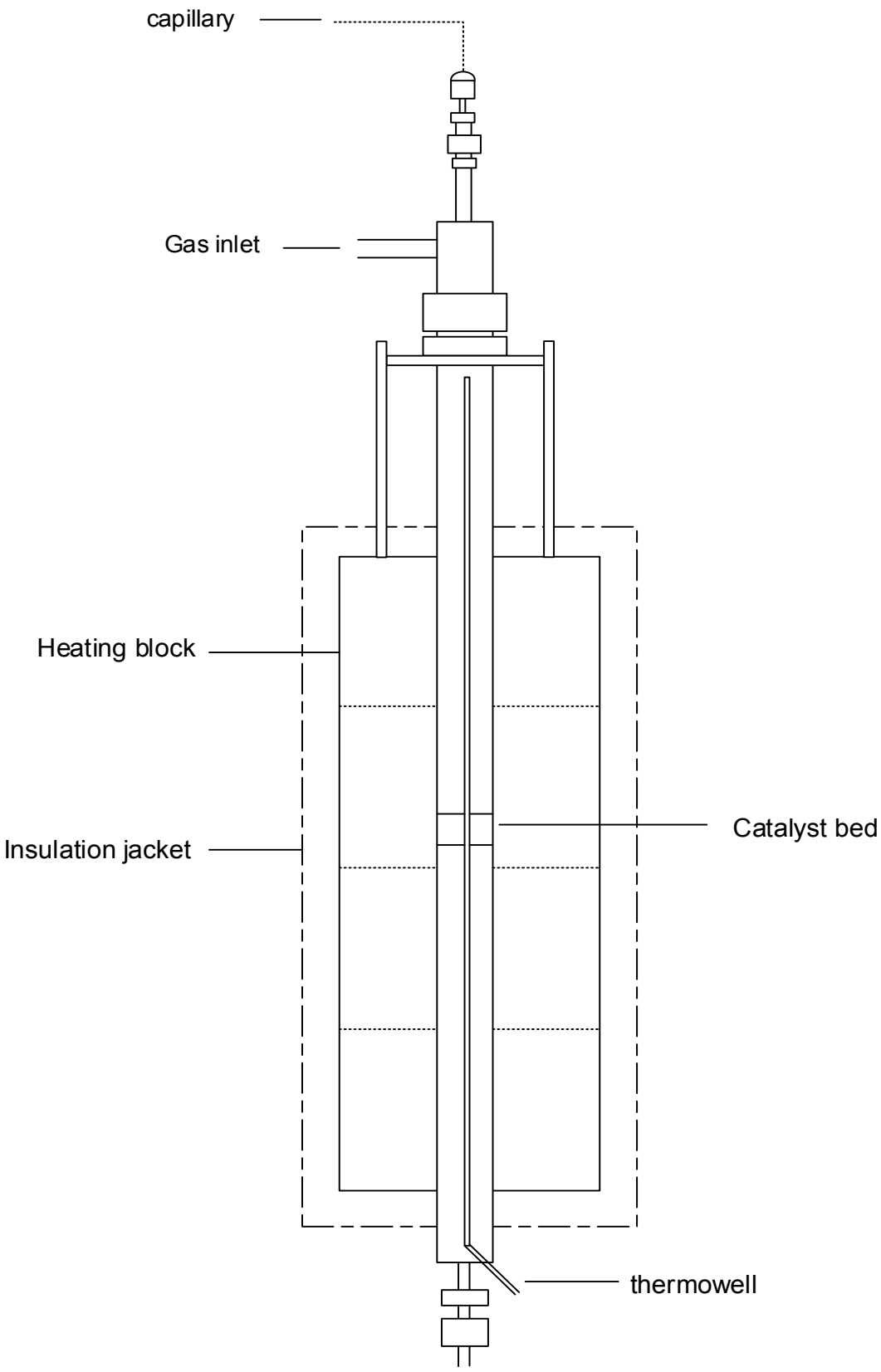


**Figure 4-2: Fixed bed reactor setup**

### 4.3.8. Condenser

A condenser with a counter current coolant (ethylene glycol-water mixture) at 4 °C was used to condense water from the reactor outlet. The coolant was cycled through a cooling bath (Lauda Alpha) kept at 4 °C. The condensed water was collected in a knock-out pot which was drained regularly.

### 4.3.9. Heating line

The reactor product line to the micro GC was heated after the condenser in order to prevent water condensation which could damage the molsieve columns in the micro GC. The heating line was kept at 60 °C.

### 4.3.10. Water pump

Water was fed from an HPLC pump (Lab alliance series 1500). A capillary (internal diameter 50 µm) with a splitter was used to flow water from the pump discharge to the reactor. A capillary was used in order to stabilize the flow of water since low flowrates were used. The capillary stabilized the flow of water by creating a pressure gradient between the reactor and the pump head.

## 4.4. Test unit commissioning

The test unit was commissioned before any experiments began.

### 4.4.1. Mass flow controller calibration

A bubble flow meter was used to calibrate the mass flow controllers (MFC). A plot of the measured flow rate vs the set flow rate was used to check for linearity and offset of the mass flow controllers (Figure 4-3). The calibration plots for all the MFC's can be found in Appendix II.

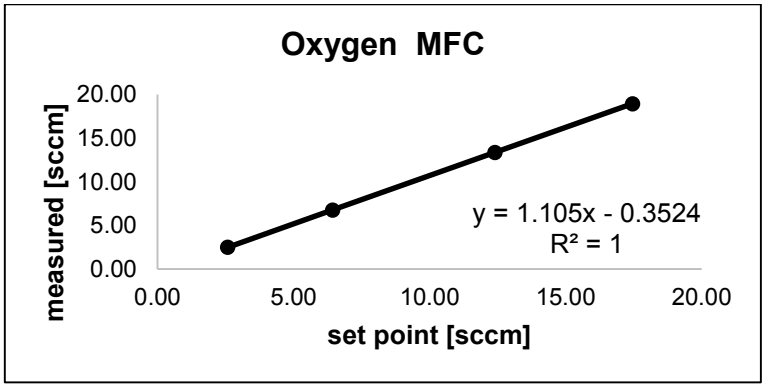


**Figure 4-3: Oxygen mass flow controller calibration**

The equation of the line obtained in the calibration plot (Figure 4-3) was then used to calculate the required set point in order to flow the required gas flowrate. The following equation was used:

$$\text{MFC set point} = \frac{\text{Required gas flow rate} - c_A}{m_A} \qquad \text{equation 4}$$

$m_A$ = gradient of calibration plot for gas A, $C_A$= y- intercept of calibration plot for gas A

### 4.4.2. Reactor Isothermal zone

A temperature profile for the reactor was performed at various temperatures in a reactor packed with silicone carbide particles under $N_2$ flow. The reactor was mounted into a heating block with four heating bands. The temperature of each heating band was adjusted in order to establish an isothermal zone in the reactor. A J-type thermocouple was used to measure the temperature at every 1cm along the reactor length (Figure 4-4).

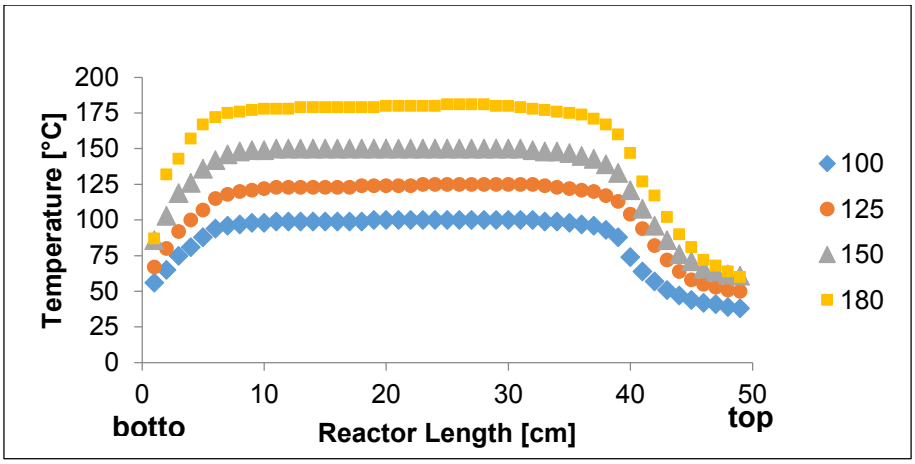


**Figure 4-4: Temperature profiles along a packed reactor filled with SiC**

The isothermal zone was determined to be between 20 cm and 30 cm from the bottom of the reactor. As a result the catalyst bed was placed in this region during catalyst activity testing.

### 4.4.3. Pump calibration

A schematic of the pump set up described in Section 4.3.9 is shown in Figure 4-5.

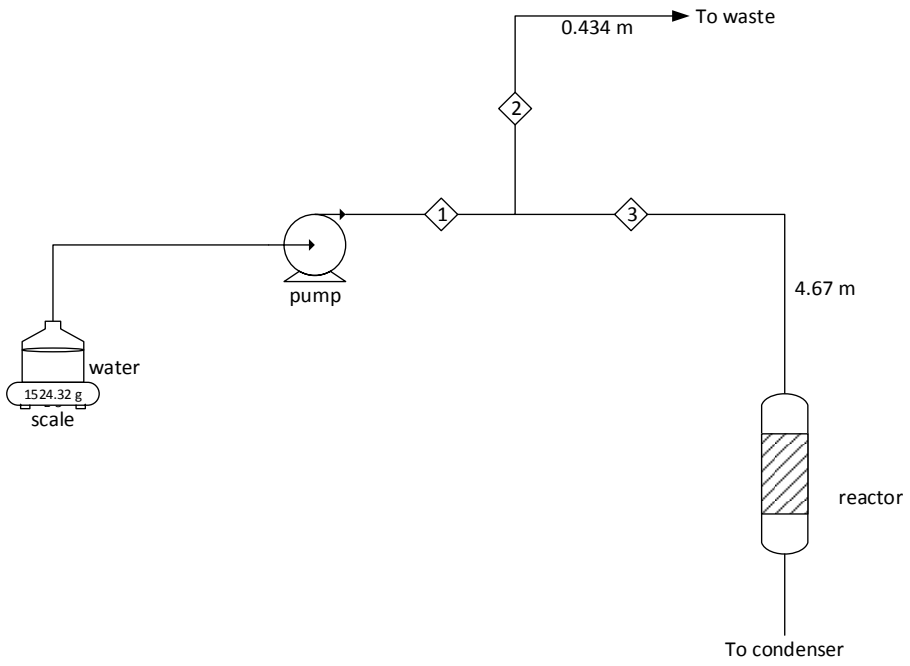


**Figure 4-5: Pump setup for the water feed to the reactor.**

The split ratio of water going to the reactor versus the pump flowrate was defined as:

$$\text{Split ratio} = \frac{f_{w,2}}{f_{w,1}} \qquad \text{equation 5}$$

with fw,i being the flowrate of water in stream i.

The experimental split fraction was determined by measuring the water collected in streams 2 and 3 over time at a constant pump rate. In addition, a theoretical split fraction was also calculated by using the Hagen-Poiseuille equation.

$$\Delta P = \frac{8 \cdot Q \cdot \eta \cdot L}{\pi \cdot r^4} \qquad \text{equation 6}$$

Equation 6 can be rewritten as;

$$Q = \frac{\pi \cdot r^4 \cdot \Delta P}{8 \cdot \eta \cdot L} \qquad \text{equation 7}$$

Where Q= flow rate [$m_3$/s], η= dynamic viscosity [kg/m.s], L=length of capillary [m], r= capillary radius [m], ΔP = pressure drop [Pa]

Since the pressure at which the water leaves the pump as well as the final pressure (1 $bar_g$ for the stream going to waste and 1.5 $bar_g$ for the stream to the reactor) is known, the

pressure drop can be calculated. The flowrate in capillary 2 and 3 can then be calculated and hence the split ratio. The difference obtained between the experimental split ratio and the theoretical split ratio was found to be approximately 4 %. The split ratio between the capillaries was determined to be 9 % of the pump discharge going to the reactor. All data and calculations are show in Appendix III.

### 4.4.4. Leak test

The reactor was pressurized to 5 $bar_g$ using BPR-2 and left for 2 hours to determine if there was a pressure drop which would indicate leaks. Pressure relief valve 1 was detected to have a leak when the valve was closed. The leak was measured at different pressures to obtain the data below.

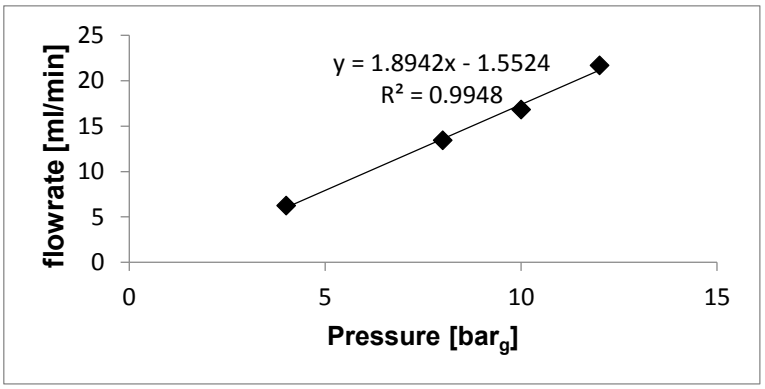


**Figure 4-6: Data for the rate of gas leak through pressure relief valve 1 at different pressures.**

The pressure relief valve was not replaced because the loss was accounted for in the feed gas which was always fed with an excess of at least 25 % of the required flow to the reactor. Excess gas was also flowed in order to keep the pressure in the blend pot higher than in the reactor to create a pressure difference allowing for gas flow.

## 4.5. Activity tests

The variables that were investigated for their effect on PrOx are space velocity, temperature and $O_2$/CO ratio using the setup in Figure 4-1.

In the literature for PrOx there are various feed compositions that different researchers use. In this study, 2 feed compositions were tested (Table 4-1).

**Table 4-1: Feed concentration used for the catalyst activity testing**

| Gas | Feed 1[a] | Feed 2[b] |
|---|---|---|
| CO | 1.0 % | 0.5 % |
| $CO_2$ | 20.0 % | 15.0 % |
| $O_2$ | 1.0 % | 0.5 % |
| $H_2$ | 50.0 % | 45.0 % |
| $H_2O$ | 10.0 % | 10.0 % |
| $N_2$ | 16.0 % | 27.0 % |
| He | 2 % | 2 % |

[a] Feed from Kim and Park 2010

[b] Feed from Chin et al., (2005)

The gases used in this study were supplied by Afrox at a purity of 99.99 % except for $O_2$ which was 99.5 %.

## 4.6. Data analysis using gas chromatography

To sample the reactor gas feed as well as the product gas an online micro gas chromatograph (Varian CP-4900 micro GC) was used. The system comprised of four modules with each module consisting of an injector, column and a thermal conductivity detector (TCD). The conditions of each of these are summarized in the Table 4-2. He gas was chosen as a reference gas instead of Ar because Ar and $O_2$ have the same retention time in a molsieve column.

**Table 4-2: Micro GC specifications and settings**

| **Channel** | 1 | 2 | 3 | 4 |
|---|---|---|---|---|
| **Column** | Molsieve 5A | Molsieve 5A | 5CB | PPQ |
| **Column length [m]** | 10 | 20 | 8 | 10 |
| **Injector temperature [°C]** | 110 | 110 | 50 | 50 |
| **Oven temperature [°C]** | 110 | 100 | 40 | 40 |
| **Pressure [kPa]** | 200 | 200 | 50 | 50 |
| **Carrier gas** | Ar | $H_2$ | $H_2$ | $H_2$ |
| **Gas analysed** | $H_2$, He | He, $O_2$, CO, $N_2$, $CH_4$ | $CO_2$ | He, $CO_2$, $CH_4$ |

Although $O_2$, $N_2$ and CO show peaks in the Molsieve 5A column with Ar as a carrier gas (Channel 1), they were only analysed in the Molsieve 5A column with $H_2$ as a carrier gas (Channel 2). This is because at low CO and $O_2$ concentrations, no CO and $O_2$ peaks would appear in channel 1 due to the very large $H_2$ peak. As a result Channel 2 was used to analyse $O_2$ and CO because no $H_2$ peak appears since $H_2$ is the carrier gas.

Channel 4 instead of 3 was used to analyse $CO_2$ since the internal standard (He) shows a separate peak in Channel 4. This was done to avoid the use of an internal standard in one column to calculate the area of a gas in another column thus reducing errors. Methane was analysed in Channel 4 because the peak area was larger compared to Channel 2.

### 4.6.1. GC calibration

Before calibrating the micro GC, the molsieve columns (Channel 1 and 2) were baked out for 2 days at 180 °C. It is important to bake the molsieve columns regularly because the zeolite stationary phase in molsieves adsorbs water until the micro pores are filled. $CO_2$ can then react with the water forming carbonic acid which overtime increases in concentration and may cause damage to the zeolite framework. It was not necessary to bake the 5CB and PPQ columns (Channels 3 and 4) because unlike molsieve columns, water does not permanently adsorb.

It can be seen in Figure 4-7 that the peaks shift to a longer retention time after baking the columns.

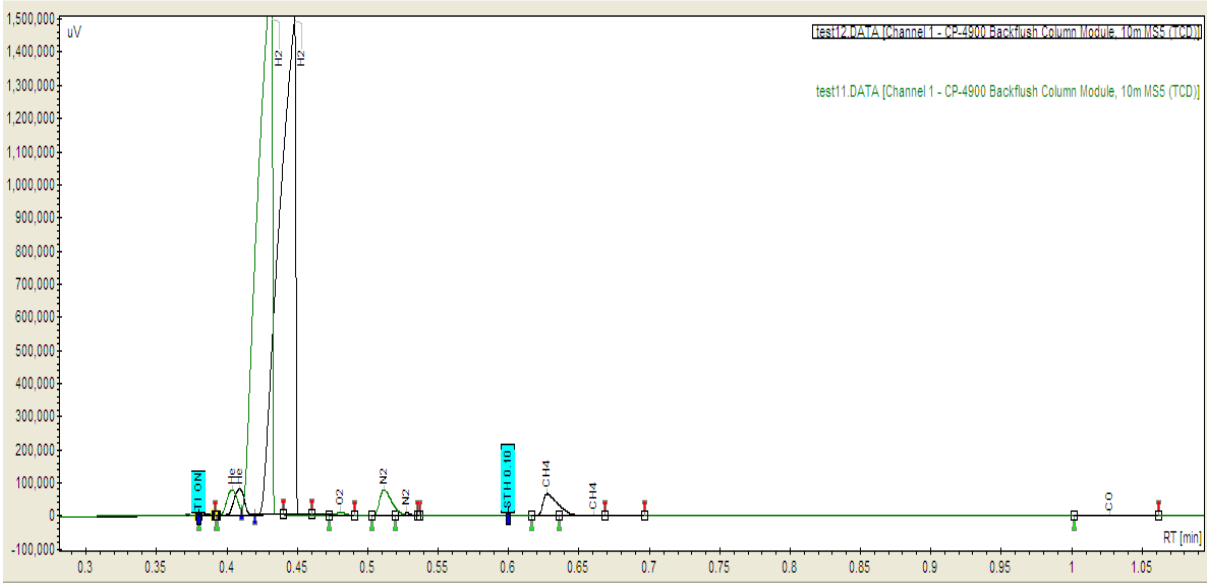


**Figure 4-7: Chromatograms showing the shift in peaks after baking the molsieve column**

In Figure 4-7, test 11 (green) was performed before the molsieve column was baked and test 12 (black) was performed after the column was baked for 2 days.

The sample gas passed through a pre-column before the molsieve column. In this pre-column $CO_2$ has the longest retention time because it strongly adsorbs onto the column. Therefore a back-flush time can be set in order to prevent injecting $CO_2$ into the molsieve column. The back-flush mechanism works in such a way that at the set time a valve after the pre-column switches and reverses the flow in the pre-column. The pre-column, which is a short PPQ column separates $CO_2$ from the other gases, hence all the other gases are injected onto the molsieve column when the valve switches and $CO_2$ is vented out the front of the pre-column. This mechanism is shown in Figure 4-8.

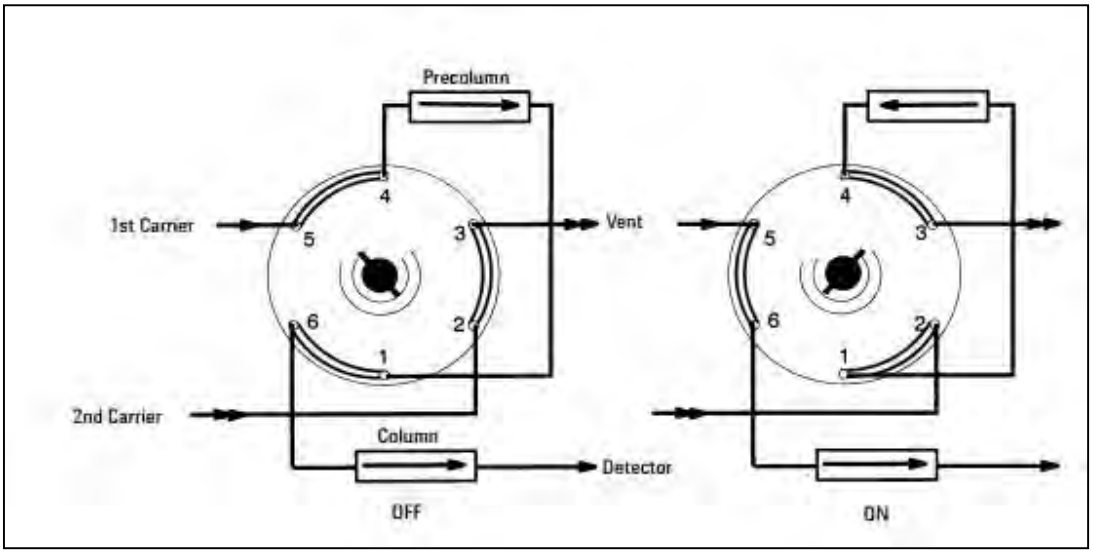


**Figure 4-8: Back-flush mechanism for a pre-column to vent (Agilent 2001)**

The retention time of each gas was determined by flowing the individual gas and sampling the reactor by-pass on the micro-GC. The retention times as well as the columns in which the gases elude are shown in Table 4-3.

**Table 4-3: Retention times of the analysis gases in the micro GC channels**

| Gas | Retention time [min] | | | |
|---|---|---|---|---|
| | **MS5 (10 m)** | **MS5 (20 m)** | **5CB** | **PPQ** |
| $H_2$ | 0.41 | - | - | - |
| $CO_2$ | - | - | 0.41 | 0.71 |
| $O_2$ | - | 0.56 | - | - |
| CO | - | 1.3 | - | - |
| He | 0.37 | 0.39 | - | 0.49 |
| $N_2$ | - | 0.7 | - | - |
| $CH_4$ | - | 0.9 | - | 0.58 |
| H2O* | - | - | 0.53 | 2.68 |

* traces of water in the reactor product are observed in the 5CB and PPQ column

After determining the back-flush time of each gas, the optimal back-flash time could be determined. This was done by sampling a standard gas mixture ($CO_2$, CO, $N_2$, $H_2$, $O_2$ and He) on the micro GC then the back-flush time was reduced according to Table 4-4.

**Table 4-4: Procedure for decreasing the back-flush time in order to determine the optimum**

| Sample name | Channel 1 back-flush time (s) | Channel 2 back-flush time (s) |
|---|---|---|
| Test 14 | 11.5 | 11.5 |
| Test 15 | 6 | 6 |
| Test 16 | 5 | 5 |
| Test 17 | 4 | 4 |
| Test 18 | 5 | 3 |
| Test 19 | 5 | 2 |
| Test 20 | 5 | 2 |
| Test 21 | 5 | 3 |

The times indicated in red show the time at which some of the gases were not injected onto the molsieve (i.e. the valve switches too soon). This is observed on the chromatogram in Figure 4-9.

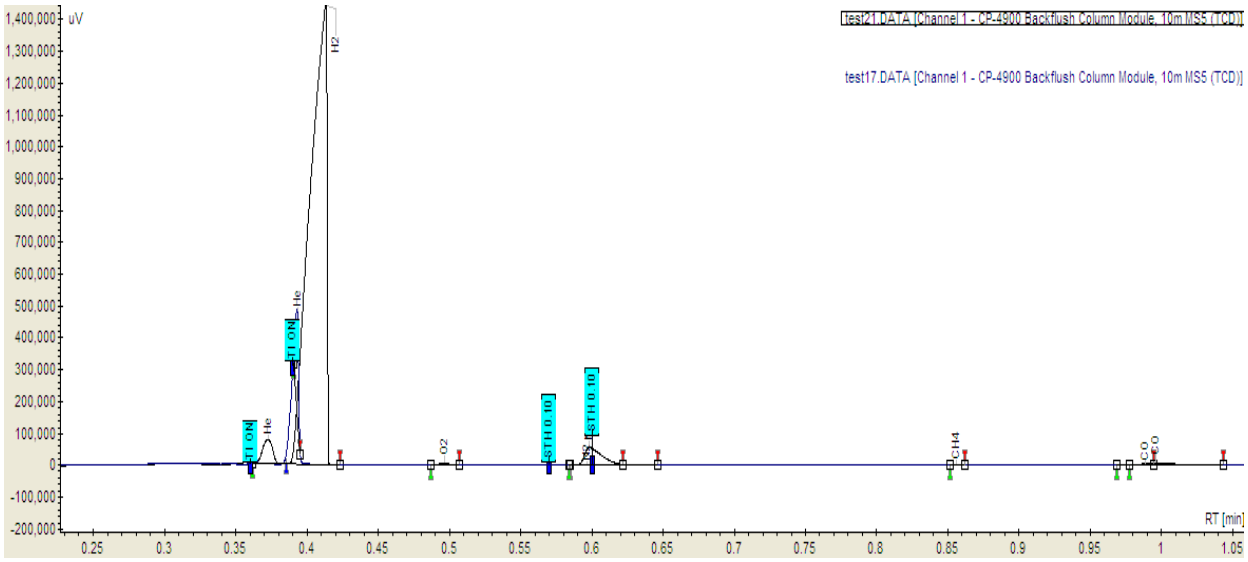


**Figure 4-9: Comparison of chromatograms at back-flush times 4 s and 5 s**

For a back-flush time of 4 s (blue in Figure 4-9) there are no $H_2$ and $O_2$ peaks which indicate that the valve switches too soon. The $H_2$ and $O_2$ peaks reappear when the back-flush time is

increased to 5 s (black in Figure 4-9). It was determined the optimum back-flush times for Channel 1 and Channel 2 are 5 s and 3 s respectively.

A bump in the chromatogram baseline indicates the valve switching as shown in Figure 4-10.

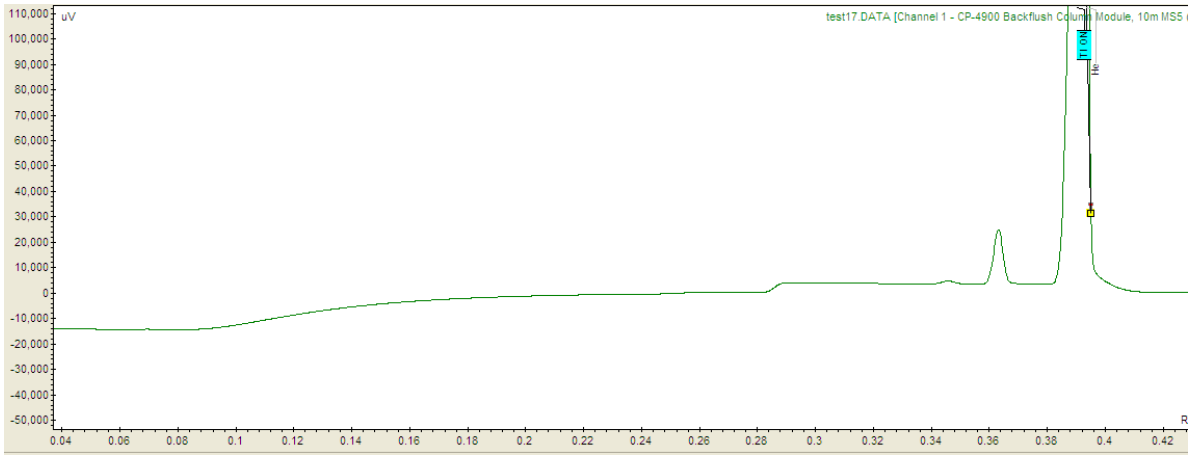


**Figure 4-10: Chromatogram showing a bump in the baseline as a result of the valve switching**

Changing the back-flush time also results in a small shift of the retention times. However the peak area remains unchanged. This is demonstrated in the chromatograms in Figure 4-11.

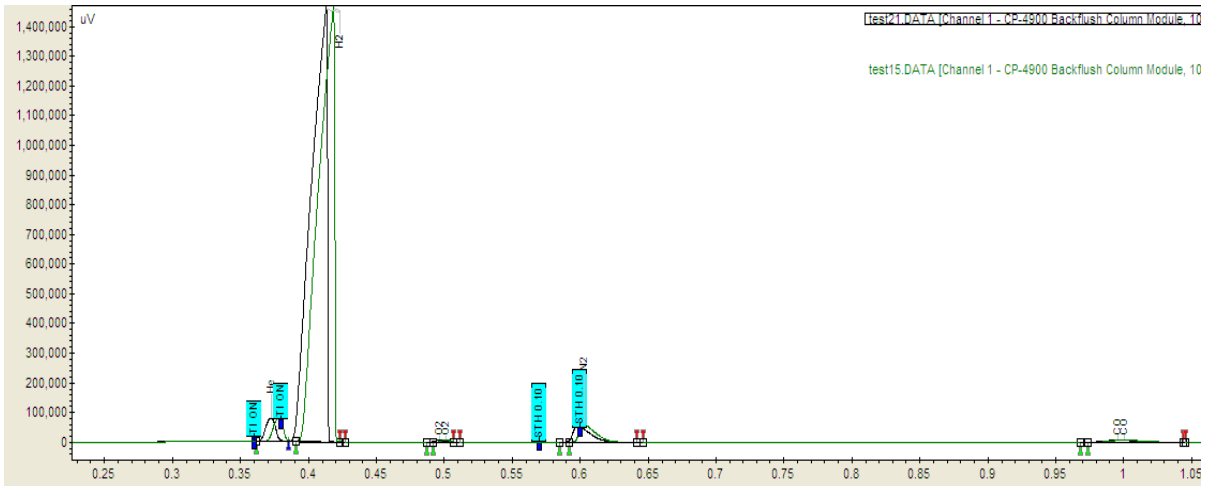


**Figure 4-11: Chromatograms showing the effect of changing the back-flush time on retention time and peak area**

Test 21 (black) in Figure 4-11 was performed at a back-flush time of 5 s and Test 15 (green) was at a back-flush time of 6 s. After changing the back-flush time peaks have same area even though the peaks have shifted.

#### 4.6.1.1. Data calculations

To calibrate the micro GC, a mixture of gases of known concentrations was set on the mass flow controllers. The gases were allowed to mix in the blend pot for an hour before being sampled on the micro GC. For each mixture 8-10 data points after the mixture was well mixed were used to determine an average area for each gas. He gas was used as the internal standard and its concentration was kept constant in all the mixtures.

Based on the GC working principle that the ratio of peak area to concentration is constant the following equations can be applied using He as the internal standard:

$$\frac{\left(\frac{\text{Area, A}}{\text{Area, He}}\right)}{\left(\frac{\text{mole fraction, A}}{\text{mole fraction , He}}\right)} = RF_A \qquad \text{equation 8}$$

With the following definitions: Area, A = peak area of gas A,
$RF_A$ = response factor of gas A

Equation 8 can also be re- written as:

$$\frac{\left(\frac{\text{Area, A}}{\text{Area, He}}\right)}{\left(\frac{\text{moles, A}}{\text{moles He}}\right)} = RF_A \qquad \text{equation 9}$$

Since the total number of moles used to determine the mole fraction of gas A and He is the same.

This equation can be simplified further since moles are proportional to volume based on the ideal gas law. Thus Equation 9 becomes:

$$\frac{\left(\frac{\text{Area, A}}{\text{Area, He}}\right)}{\left(\frac{F_A}{F_{He}}\right)} = RF_A \qquad \text{equation 10}$$

Were $F_A$ is the volumetric flowrate of gas A.

A graph of $\frac{\text{Area ,A}}{\text{Area, He}}$ vs $\frac{F_A}{F_{He}}$ gives a straight line and the slope represents $RF_A$. An example of a calibration graph is shown in Figure 4-12.

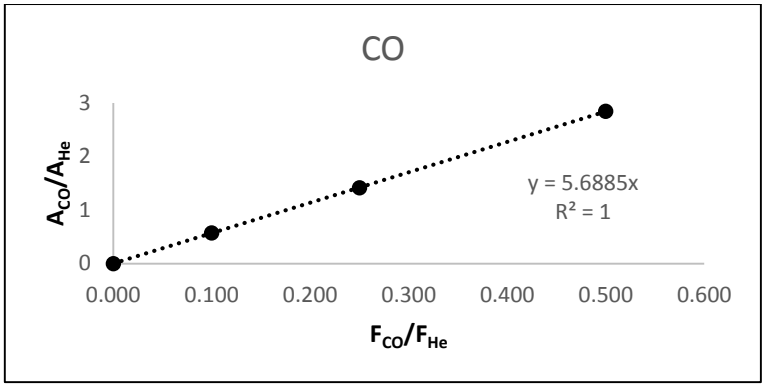


**Figure 4-12: CO peak GC calibration graph**

If the trend line in the GC calibration graph has a y-intercept that was not at zero, then equation 10 can be re written as:

$$\frac{\text{Area,A}}{\text{Area,He}} = RF_A \cdot \left(\frac{F_A}{F_{He}}\right) + C_A \qquad \text{equation 11}$$

$C_A$ = y-intercept value of gas A

From equation 11 the molar fraction of a compound can be calculated as

$$F_A = F_{He,feed} \cdot \left(\frac{\frac{Area_A}{Area_{He}} - C_A}{RF_A}\right) \qquad \text{equation 12}$$

Using Equation 12 the CO ($X_{CO}$) and $O_2$ ($X_{O_2}$)conversions as well as $CO_2$ selectivity ($S_{CO_2}$) can be calculated as follows.

$$X_{CO} = \frac{F_{CO,in} - F_{CO,out}}{F_{CO,in}} \qquad \text{equation 13}$$

$$X_{O_2} = \frac{F_{O_2,in} - F_{O_2,out}}{F_{O_2,in}} \qquad \text{equation 14}$$

$$S_{CO_2} = 0.5 * \frac{F_{CO,in} - F_{CO,out}}{F_{O_{2,in}} - F_{O_{2,out}}} \qquad \text{equation 15}$$

A carbon balance was done after each run according to the following equation.

$$\text{Carbon Balance} = \frac{F_{CO,in} + F_{co_2,in}}{F_{CO,out} + F_{co_2,out} + F_{CH_4,out}} \qquad \text{equation 16}$$

### 4.6.2. $CO_2$ solubility in water

The solubility of each gas in water is shown in Table 4-5.

**Table 4-5: List of gas solubility in water for the analysis gases**

| Gas | Solubility in water at 30 °C (g gas/kg water) |
|---|---|
| CO | 0.025 |
| $CO_2$ | 1.25 |
| $CH_4$ | 0.02 |
| $H_2$ | 0.00145 |
| $N_2$ | 0.017 |
| He | 0.0014 |
| $O_2$ | 0.036 |

There is a possibility that some gases could be absorbed in the water condensing in the water catch pot before the reactor product is sampled on the online micro GC. From Table 4-5, $CO_2$ has the highest solubility in water, thus there is a high probability of some $CO_2$ dissolving in water. As a result, the measured product $CO_2$ concentration measured could be lower than the actual $CO_2$ concentration that was in the reactor product stream. This however will have no effect on the calculated CO conversion and $CO_2$ selectivity since the CO solubility in water is low and the assumption that the amount of CO and O2 that dissolves in water is negligible. However the carbon balance can be affected since the $CO_2$ solubility in water is quite significant (see calculations in Appendix V).

## 4.7. Data analysis using analyser

Low CO concentration which could not be detected using the micro GC were determined using an analyser (ABB AO2040) which had a CO detection range of 0 – 400 ppm. The analyser was calibrated regularly in order to maintain accurate CO measurements. This was done by using the built in calibration cells in the analyser.

## 4.8. Start-up procedure

Before each test the empty reactor was first cleaned with acetone then dried by blowing compressed air. The catalyst was mixed with silicon carbide (Si/C) particles then loaded in to the reactor isothermal zone with Si/C packed at the bottom and at the top of the catalyst bed.

The following start-up procedure was followed once the catalyst was loaded into the reactor and a leak test performed.

- The catalyst was reduced according to the procedures described in Section 4.1.1.
- The catalyst bed temperature was monitored using a thermocouple placed in the thermowell of the reactor.
- The reactor was then cooled after catalyst reduction to reaction temperature in $N_2$.
- The cooling bath was switched on and set to 4 °C.
- Once the reaction temperature was reached the pump was switched on and water was pumped through capillary into the reactor.
- The mass flow controllers (MFC 1 – MFC 6) were set to the required reaction flowrates.
- The pressure in the blend pot was set to 6 $bar_g$ using the back pressure regulator (BPR-1).
- The reactor was pressurised to 1.5 bar using the back pressure regulator (BPR-2).
- The 4-way switch valve was set to sample the reactor by-pass (i.e. feed).
- The by-pass was sampled until the desired feed gas composition was achieved then the 4 way switch valve was changed to sample the reactor product.

## 4.9. Changing operation conditions

The operating conditions were changed after the system had reached steady state and after taking an average of 8 – 10 data points. To change the reactor temperature, the required temperature settings for each block were set and the sampling was resumed until steady state was achieved.

To change the space velocity, MFC 7 or 8 were set to the required flowrate and the required water flowrate was set on the pump. In this study the space velocity is the total reactor feed

flowrate relative to the catalyst mass. In this study the space velocity was calculated as follows:

$$SV = \frac{\text{Total flowrate}_{in}}{m_{cat}} \qquad \text{equation 17}$$

Where $m_{cat}$ = catalyst mass [g]

To change the $O_2$/CO ratio, the $O_2$ and $N_2$ flowrate were adjusted accordingly. The feed stream was then sampled until the required $O_2$/CO ratio was achieved. Thereafter the 4-way switch valve was set to sample the reactor product.

## 4.10. Shut-down procedure

The following shut-down procedure was followed:

- The water pump and the micro GC were switched off.
- The reactor was depressurised by opening BPR-2.
- To prevent any water condensation in the reactor the heating bands were switched off to cool the reactor after approximately 1 h.
- The gases were all switched off except for $N_2$ gas which was left to flow through the reactor while it cooled down.
- The cooling bath was then switched off.
- When the reactor had cooled, the $N_2$ gas was then switched off.

# 5. Results and discussion

In this chapter the results of the experiments performed in order to evaluate the objectives of this project (Chapter 3) are presented and discussed. The prepared three catalysts (Ru_high pH, Ru_IWI and Pt-Fe/M) as described in Chapter 4 as well as a commercial catalyst (referred to as commercial) were tested for PrOx activity using the reactor setup shown in Figure 4-1.

## 5.1. Characterisation results

Characterisation tests were performed in order to determine the physical characteristics of the catalysts which have the potential to affect PrOx activity.

### 5.1.1. ICP-OES results

The prepared catalyst samples were sent for ICP-OES analysis to determine the metal loading. The results obtained are shown in Table 5-1.

**Table 5-1: ICP-OES results showing the metal loading results for the prepared catalysts**

| Sample | | Intended loading | ICP-OES loading |
|---|---|---|---|
| Ru_high pH | | 1 wt % | 0.8 wt % * |
| Ru_IWI | | 1 wt % | 0.8 wt % |
| Pt – Fe/M | Pt | 4 wt % | 2.7 wt % |
| | Fe | 0.5 wt % | 0.2 wt % |

* 0.06 wt % Na was detected

For all the catalysts, the metal loading measured by ICP-OES (Table 5-1) was slightly lower than the intended metal loading. For the Ru_high pH catalyst this was due to the loss of Ru during filtration as some Ru was detected in the filtrate. The same explanation can also be used for the Pt-Fe/M catalyst even though the filtrate was not sampled. The lower loading on the Ru_IWI catalyst could be due to some of the precursor solution not being deposited onto the support, but sticking the walls of the beaker.

### 5.1.2. BET surface area

The isotherms for $N_2$ adsorption and desorption on the supports are shown in Figure 5-1. The temperature in the parenthesis is the temperature at which the support was calcined.

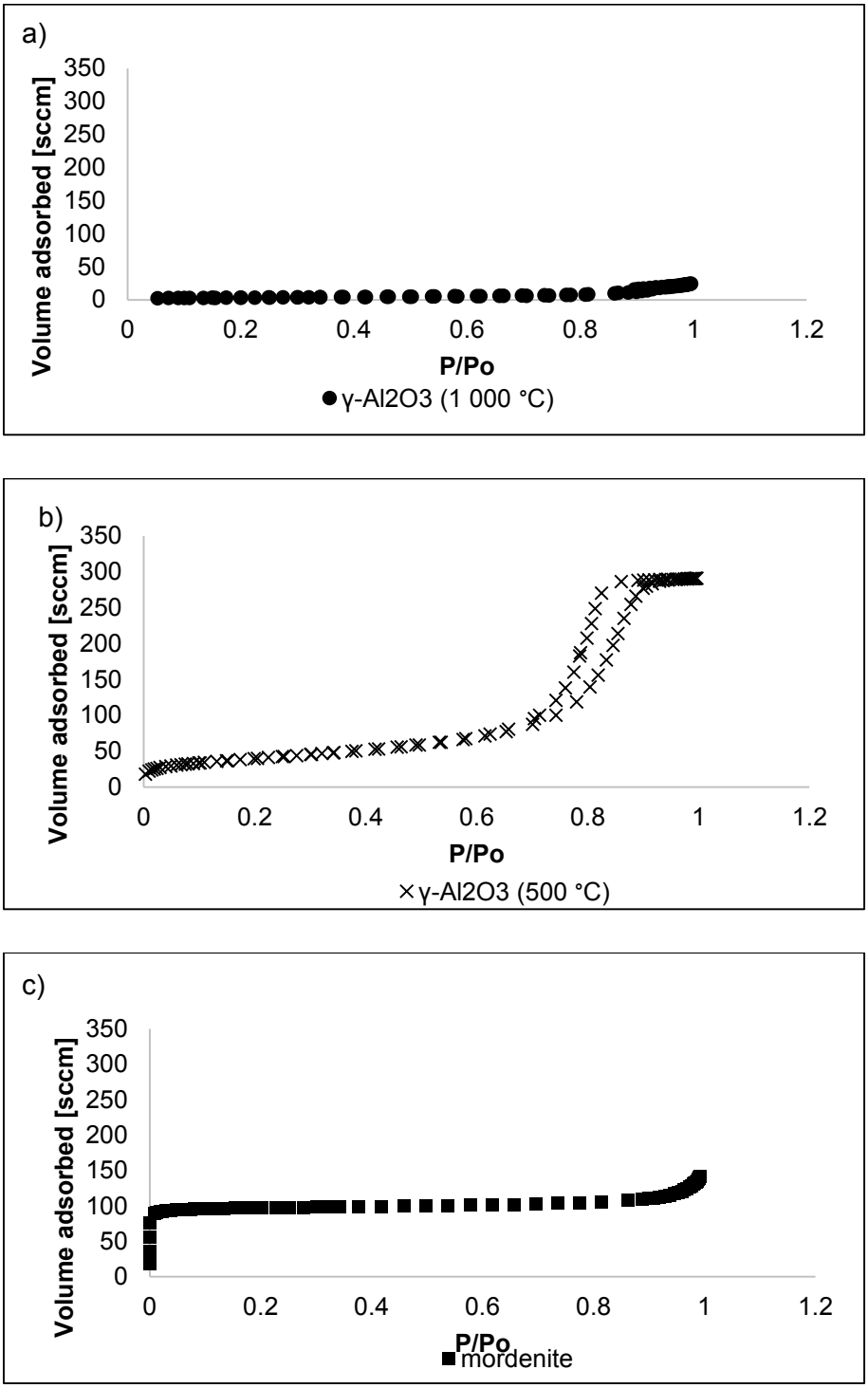


**Figure 5-1: $N_2$ adsorption and desorption curves for the $Al_2O_3$ calcined at a) 1 000 °C and b) 500 °C and c) mordenite.**

The volume of $N_2$ adsorbed increases with increasing pressure for the two types of alumina as well as for mordenite. In addition, the BET surface area decreases as the calcination temperature of alumina increases (Table 5-2). Furthermore, the pore volume decreases with increase in calcination temperature as shown in Table 5-2.

**Table 5-2: BET surface area as well as pore volume data obtained from $N_2$ physisorption experiments for the $Al_2O_3$ calcined at 1 000 °C and 500 °C and mordenite**

| Sample | BET Surface Area [$m^2/g$] | Pore volume [$cm^3/g$]* |
|---|---|---|
| γ-$Al_2O_3$ calcined (500 °C) | 143.3 | 0.48 |
| γ-$Al_2O_3$ calcined (1000 °C) | 12.4 | 0.038 |
| mordenite | 395.5 | 0.08 |

* determined form BJH desorption

The results in Table 5-2 show that increasing the calcination temperature results in loss of surface area hence the volume of $N_2$ adsorbed decreases with increasing calcination temperature. Mordenite was observed to have a much higher surface area compared to both types of alumina.

The pore size distribution of each support determined from the $N_2$ desorption isotherm is shown in Figure 5-2.

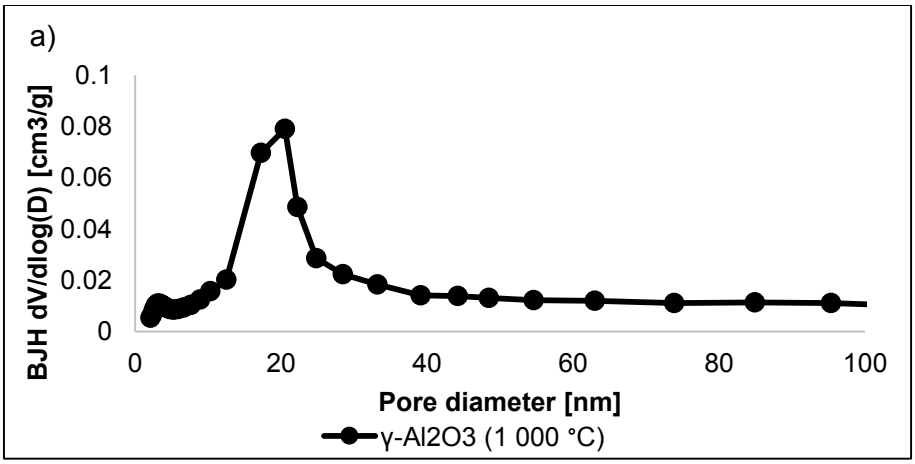

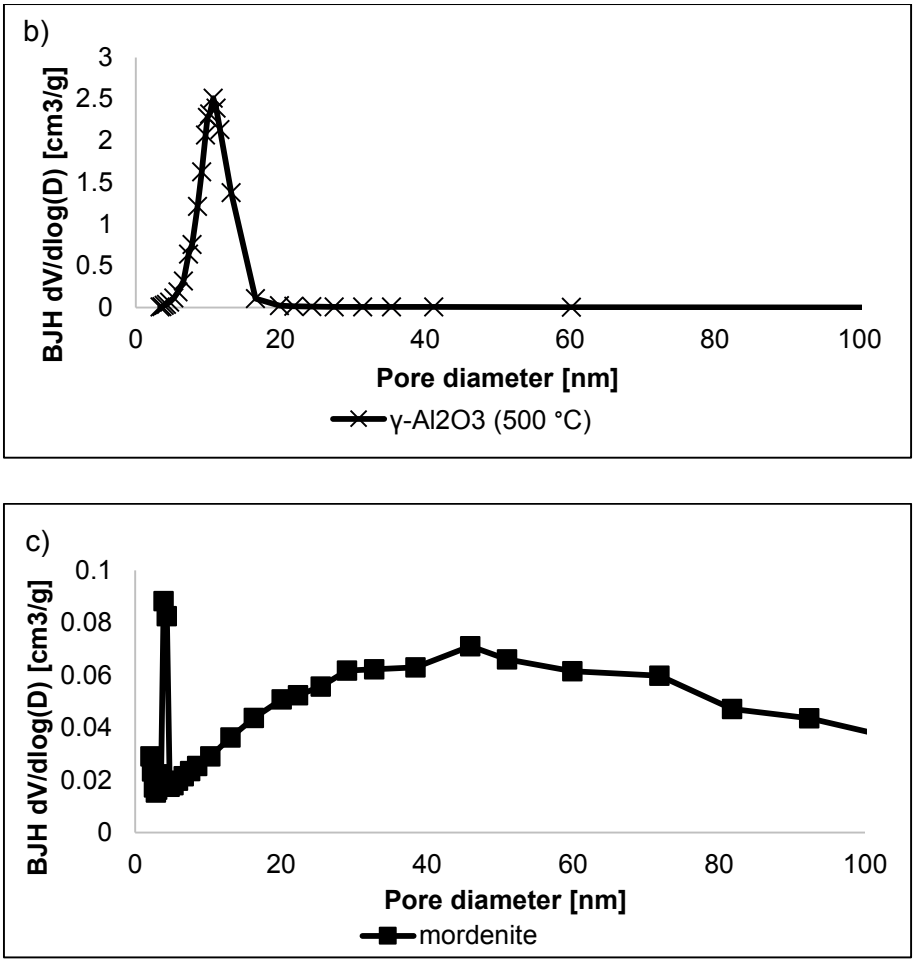


**Figure 5-2: Pore size distribution data for the $Al_2O_3$ calcined at a) 1 000 °C and b) 500 °C and c) mordenite obtained from the $N_2$ desorption isotherm using the BJH method.**

The pore size distribution shows the presence of a mesoporous pore structure for γ-$Al_2O_3$ (1 000 °C) and γ-$Al_2O_3$ (500 °C). Mordenite showed no distinct peak for a mesoporous or macro porous pore structure.

These characterisation results show that the $Al_2O_3$ support for the Ru_IWI catalyst had a larger surface area compared to the Ru_high pH catalyst support. Furthermore the $Al_2O_3$ support for the Ru_IWI catalyst had larger pore volume compared to the $Al_2O_3$ support for Ru_high pH.

### 5.1.3. TEM analysis results

The TEM images of the reduced catalysts as well as the particle size distribution were analysed and the results obtained are shown in Figure 5-3.

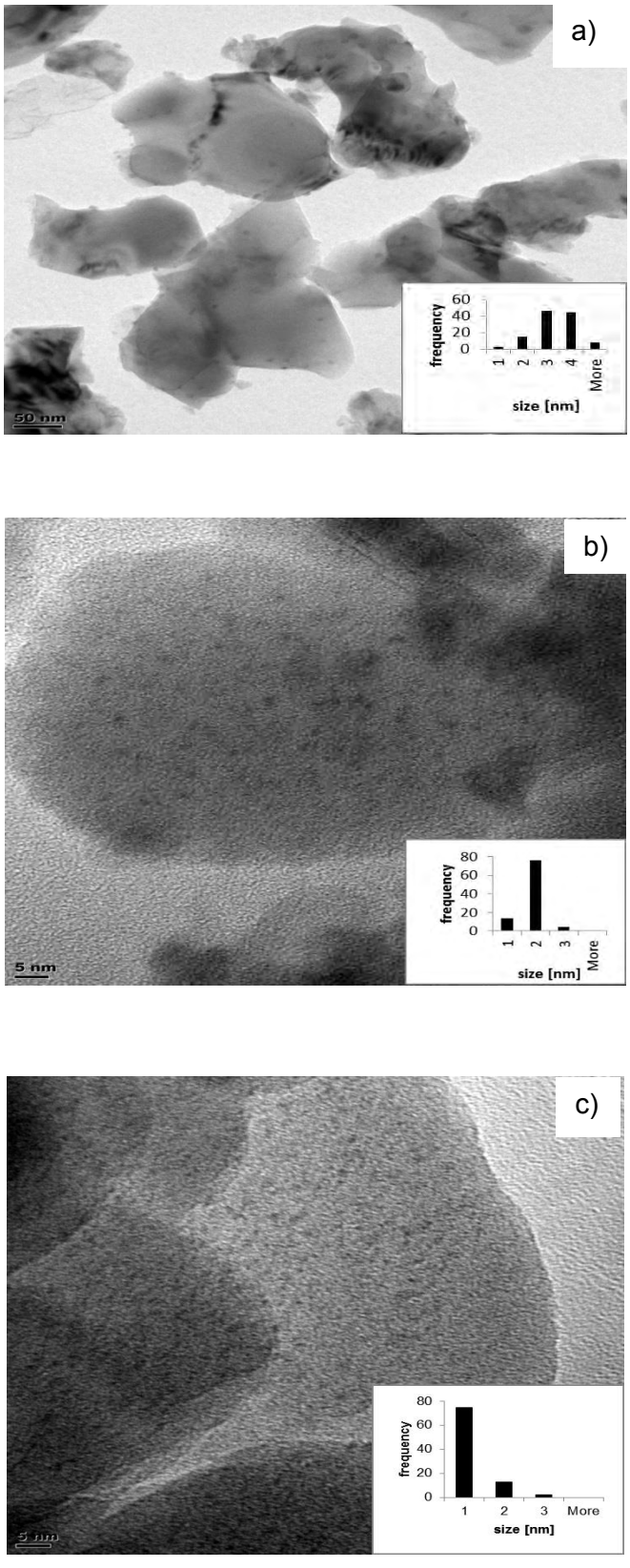


**Figure 5-3: TEM images as well as particle size distributions for a) Ru_high pH b) Ru_IWI c) Pt_Fe/M catalyst after reduction.**

The difference in the support structure of the γ-$Al_2O_3$ (1 000 °C) and γ-$Al_2O_3$ (500 °C) can be seen in the TEM images. The average particle sizes were 1.3 ± 0.3 nm and 2.9 ± 0.8 nm for Ru_IWI and Ru_high pH respectively. Most of the Pt particles in the Pt-Fe/M catalyst (Figure 5-3c) were less than 1 nm. However it is difficult to conclude from the TEM images if the particles are inside or outside the mordenite pores.

### 5.1.4. TPR results

TPR was performed on the prepared Ru catalysts in order to develop TPR profiles Figure 5-4 to show the temperature at which the catalysts are reduced.

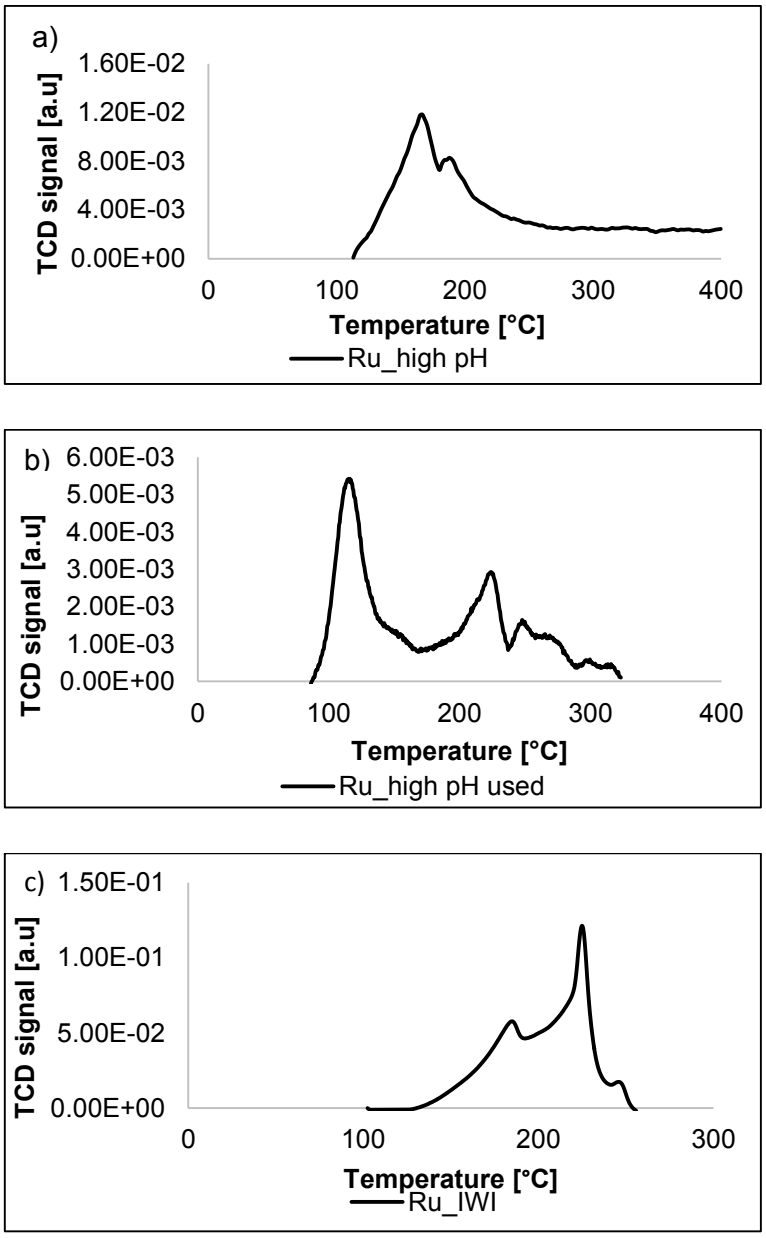


**Figure 5-4: TPR profile for a) Ru_high pH b) used Ru_high pH and c) Ru_IWI catalyst**

The proposed reduction reactions for the TPR profiles in Figure 5-4 are as follows:

$RuO_2 + H_2 \rightarrow RuO + H_2O$

$RuO + H_2 \rightarrow Ru + H_2O$

It has been proposed that the peak at lower temperature is due to well dispersed $RuO_2$ and the peak at higher temperature is due to crystallized $RuO_2$ (Bion et al., 2008).

The Ru_high pH and Ru_IWI catalysts before reaction (Figure 5-4 a and c) exhibit slightly different TPR profiles. However, both catalysts are reduced below 300 °C. Thus the reduction temperature used for the catalyst is sufficient to ensure that the Ru on the catalysts is reduced to the metallic state. The used Ru_high pH catalyst (Figure 5-4 b) exhibits a different temperature profile compared to that of the fresh catalyst (Figure 5-4 c). This shows that there is a change in the catalyst structure during the reaction. It should be noted that to recover the use Ru_high pH catalyst, it had to be sieved in order to separate the catalyst from the Si/C. However some very fine Si/C could not be separated from the catalyst. The residual Si/C would not affect the TPR profiles because it does not reduce at these temperatures.

### 5.1.5. $O_2$ chemisorption

$O_2$ chemisorption was used to determine dispersion of Ru on the support as well as the particle size of the Ru. The particle size obtained using chemisorption was compared to the TEM particle size (Table 5-3).

**Table 5-3: Catalyst dispersion calculated from $O_2$ chemisorption as well comparison of chemisorption particle size to TEM particle size**

| Catalyst | $Al_2O_3$ support surface area [m2/g] | Dispersion | $O_2$ Chemisorption size [nm] | TEM size [nm] |
|---|---|---|---|---|
| Ru_high pH | 12.4 | 64 % | 2.0 | 2.9 ± 0.8 |
| Ru_IWI | 143.3 | 78 % | 1.6 | 1.3 ± 0.3 |

The particle sizes from TEM are comparable to the $O_2$ chemisorption particle sizes (Table 5-3). The Ru_IWI catalyst had a higher dispersion (14 % higher) compared to the Ru_high pH catalyst. This result makes sense considering that the surface area of Ru_high pH was much lower than Ru_IWI (Table 5-3).The dispersion on Ru_high pH could probably have been

higher if the alumina support had a higher surface area. The first part of the hypothesis could not be either proved or disproved because the $Al_2O_3$ supports were calcined at different temperatures and hence had different surface areas.

## 5.2. Ru catalyst activity tests

The variables tested for the activity tests were temperature, space velocity and $O_2$/CO ratio. By understanding the effects of these variables on CO conversion a well as $CO_2$ selectivity an optimum operation window for the catalysts can be determined.

### 5.2.1. Initial results for Ru_high pH

Initially the observed CO conversion as well as $CO_2$ selectivity on the Ru_high pH catalyst was very low compared to data reported for $Ru/Al_2O_3$ catalysts in literature. An example of the initial results obtained is shown in Figure 5-5.

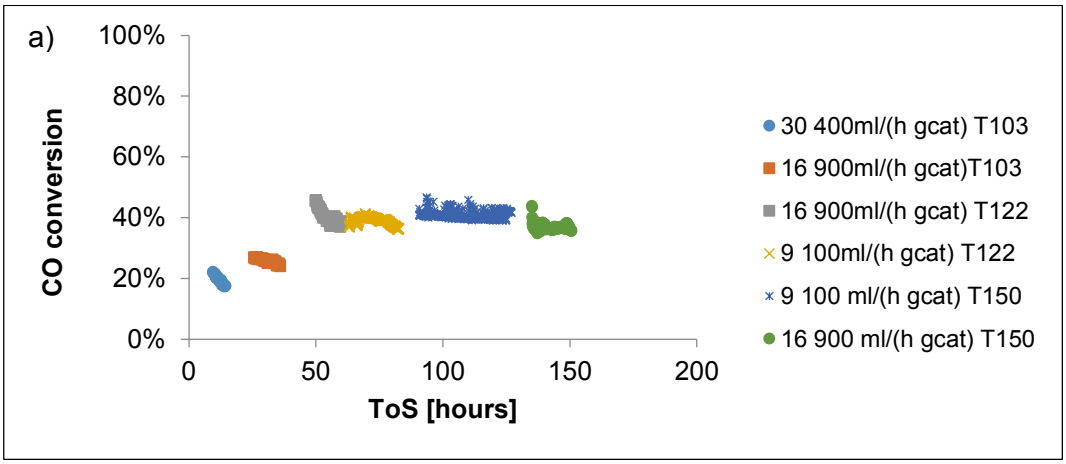


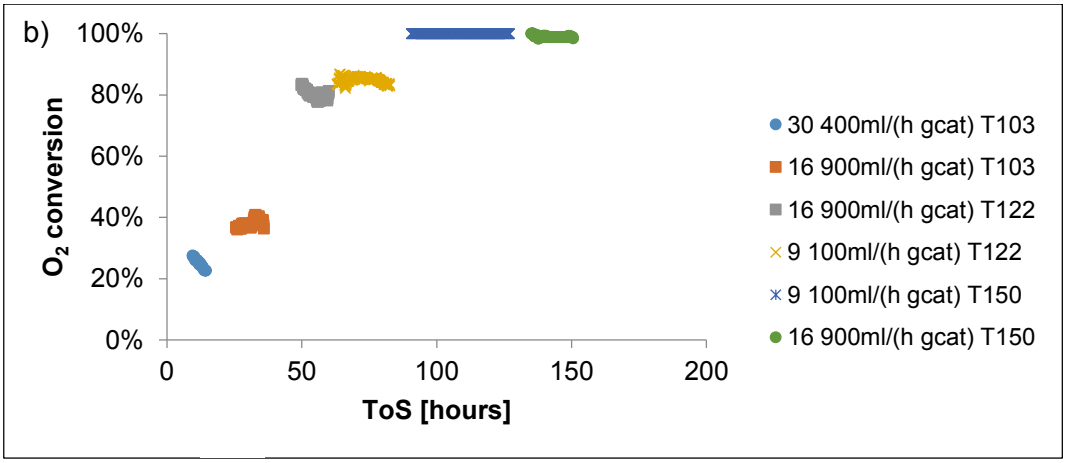

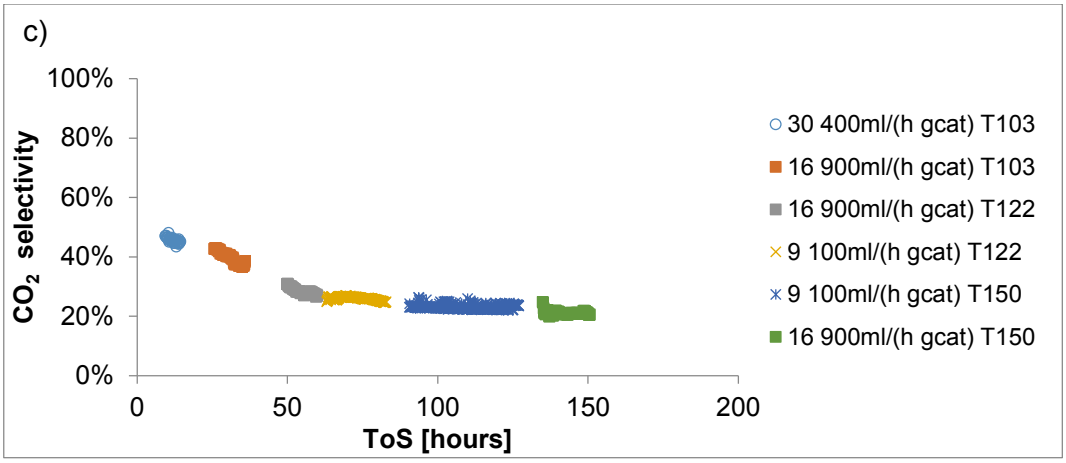


**Figure 5-5: Effect of changing space velocity and temperature on a) CO conversion b) $O_2$ conversion c) $CO_2$ selectivity Feed conditions: 1 % CO, 1 % $O_2$, 50 % $H_2$, 10 % $H_2O$, 20 % $CO_2$, 2 %He, $N_2$ balance**

The CO conversion could not be increased to even 50 % even after increasing the reaction temperature and decreasing the space velocity. The selectivity values were also quite low.

In an attempt to increase the CO conversion, the $O_2$/CO ratio was increased (Figure 5-6)

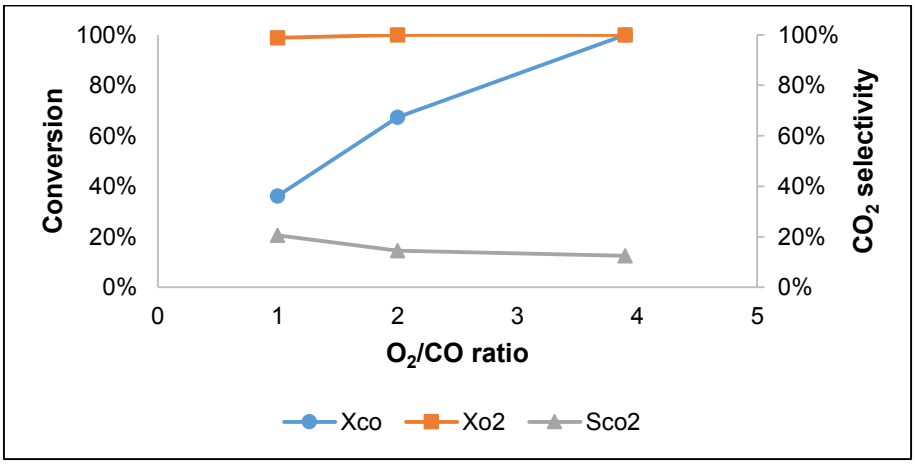


**Figure 5-6: Effect of changing space velocity and temperature on CO conversion, $O_2$ conversion and $CO_2$ selectivity. Feed conditions: 1 % CO, (1-3.9) % $O_2$, 50 % $H_2$, 10 % $H_2O$, 20 % $CO_2$, 2 %He, $N_2$ balance at SV 16 900 ml/(h $g_{cat}$)**

Increasing the $O_2$/CO ratio increased the CO conversion however this resulted in an even lower $CO_2$ selectivity. An $O_2$/CO ratio of 3.9 is simply unrealistic for a fuel processor as this only results in a larger $H_2$ consumption which is undesirable.

After these initial results, a more in depth literature study was done in order to try and explain these poor results. A paper by Chin et al., (2005) showed poor activity for the catalyst that was first oxidised then reduced compared to the catalyst that was reduced in $H_2$

only. The reduction in $O_2$ led to the sintering of the Ru particles resulting in a lower particle dispersion and hence a decreased PrOx activity.

Based on this, a new hypothesis was then formed that there is $O_2$ present in the system during reduction thus resulting in the sintering of the particles which show poor activity and selectivity. To test this hypothesis the time it takes to completely flush out $O_2$ from the system after an experiment using $N_2$ was investigated (Figure 5-7).

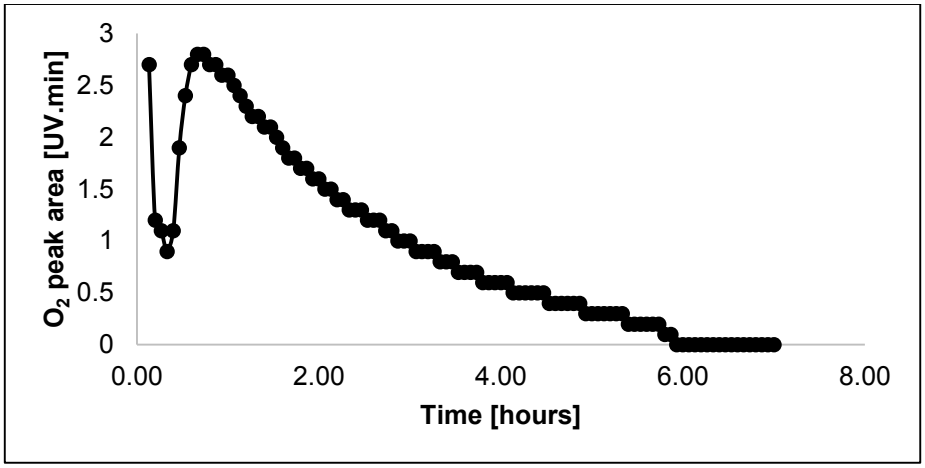


**Figure 5-7: Time it takes to flush out $O_2$ after experimental runs from the system using $N_2$ at 50 ml/min**

The results in Figure 5-7 show that it takes approximately 6 hours to completely flush out $O_2$ from the system. During the initial catalyst activity testing, the system was not purged with $N_2$ in order to flush out $O_2$ before the catalyst reduction. Therefore it is highly possible that there was still $O_2$ present in the system during the catalyst reduction since the reduction process took approximately 3.5 hours. This would have led to the sintering of Ru particles during reduction which explains the low activity of the catalyst. After obtaining these results it was decided that for the next experiments, $O_2$ should be completely flushed out of the system before starting the catalyst reduction step. A comparison of the results obtained without flushing and after flushing out $O_2$ is shown in Figure 5-8.

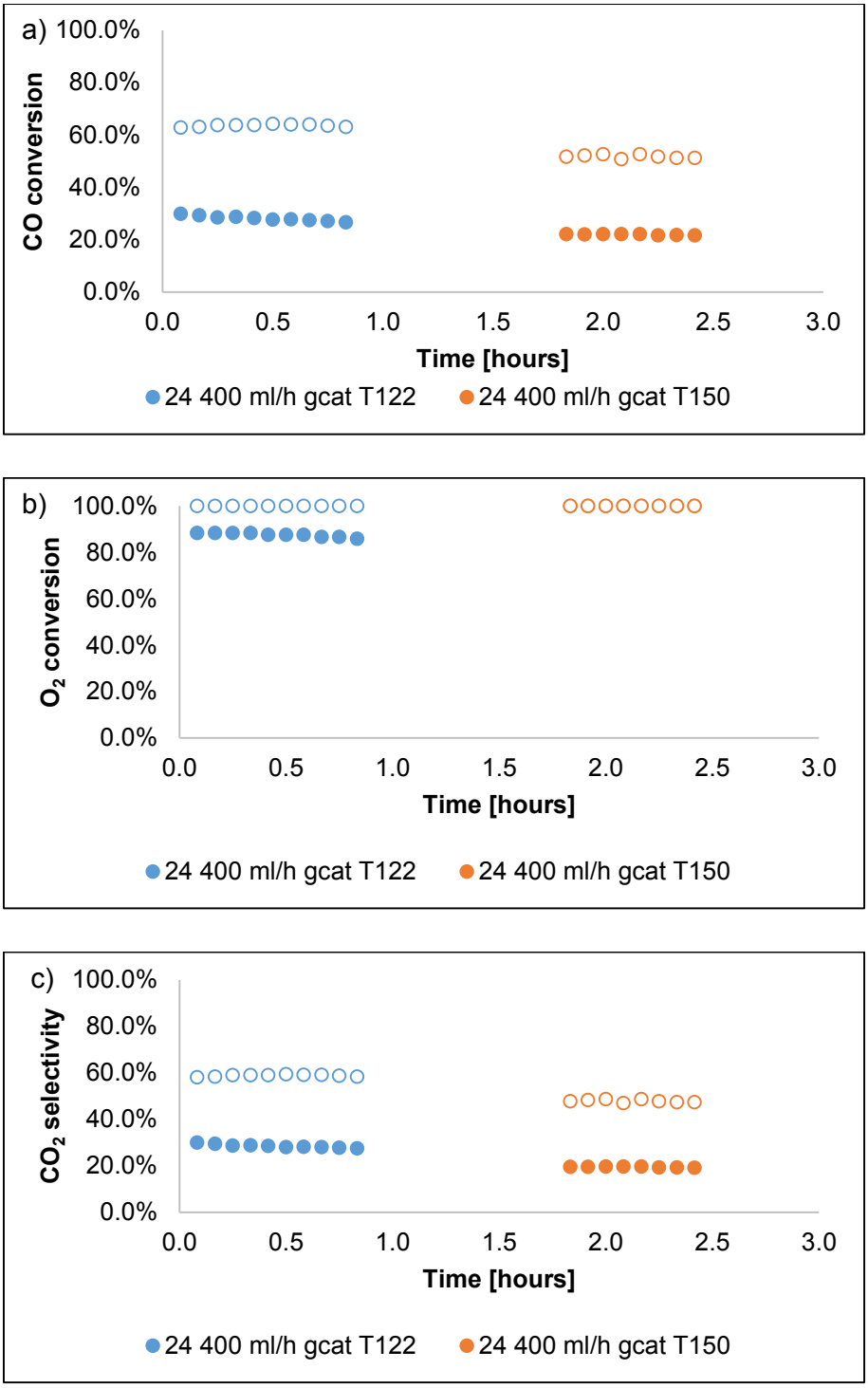


**Figure 5-8: Effect of flushing out $O_2$ before catalyst reduction on a) CO conversion b) $O_2$ conversion c) $CO_2$ selectivity Feed conditions: 1 % CO, 1 % $O_2$, 50 % $H_2$, 10 % $H_2O$, 20 % $CO_2$, 2 % He, $N_2$ balance. Filled symbols represent initial results without flushing.**

Flushing out $O_2$ results in higher CO conversions as well as higher $CO_2$ selectivity. A possible explanation is that a small amount of $O_2$ during the reduction process results in the

sintering of Ru particles. The sintering of Ru particles results in lower Ru particle dispersion which decreases PrOx activity as was observed by Chin et al., 2005.

## 5.3. Ru_high pH results

The Ru_high pH catalyst was then tested at various temperatures, space velocities as well as $O_2$/CO ratios in order to determine the optimum operation window in a fuel processor system.

### 5.3.1. Effect of Temperature

The CO conversion, $O_2$ conversion and $CO_2$ selectivity were investigated at varying temperatures.

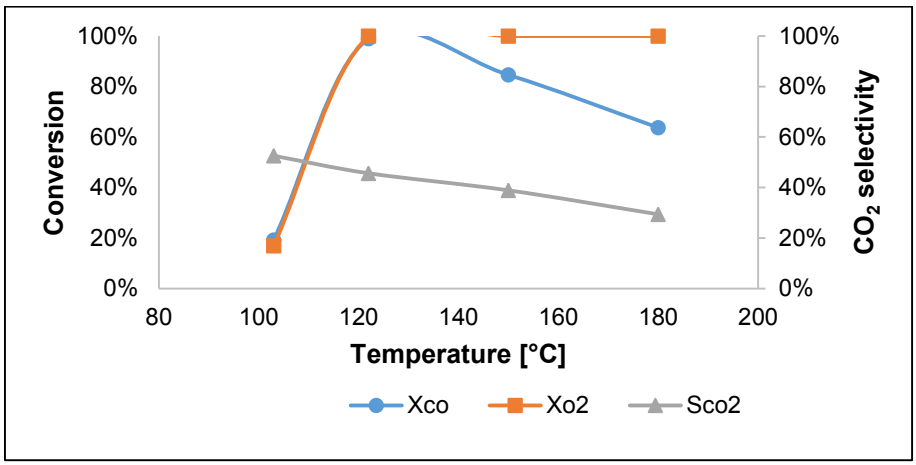


**Figure 5-9: Effect of temperature on CO conversion, $O_2$ conversion and $CO_2$ selectivity on Ru_high pH catalyst using Chin et al., (2005) feed at 120 000 ml/(h $g_{cat}$) and 160 ml/min. Feed conditions: 0.5 % CO, 0.5 % $O_2$, 45 % $H_2$, 10 % $H_2O$, 15 % $CO_2$, 2 % He, $N_2$ balance. Catalyst mass: 80 mg.**

Increasing the temperature increases the CO conversion to a maximum value after which a further increase in temperature results in a decrease in CO conversion. At low temperatures, low CO conversions are observed due to the strong CO adsorption to the Ru active sites (Han et al., 2004b). This strong adsorption limits the $O_2$ adsorption and dissociation rate because the active sites are blocked by CO. Increasing the temperature weakens the CO adsorption bond thus increasing the $O_2$ adsorption dissociation rate (Liu et al., 2012).This leads to an increase in the rate of CO oxidation. The decrease in CO conversion observed as the temperature increases further is due to the increase in the rate of the $H_2$ oxidation

reaction. This also explains the decrease in $CO_2$ selectivity with temperature. Furthermore, at higher temperatures the rWGS reaction becomes more significant thus lowering the CO conversion. Figure 5-9 shows that there exists an optimum temperature for PrOx at which CO oxidation rate is not too low and $H_2$ oxidation as well as the rWGS are not as prominent.

The catalyst was tested for rWGS activity. For this test, no CO or $O_2$ were in the feed stream. As a result, any CO observed in the reactor product stream will be due to the rWGS reaction. The results for rWGS activity on Ru_high pH are shown in Figure 5 -10.

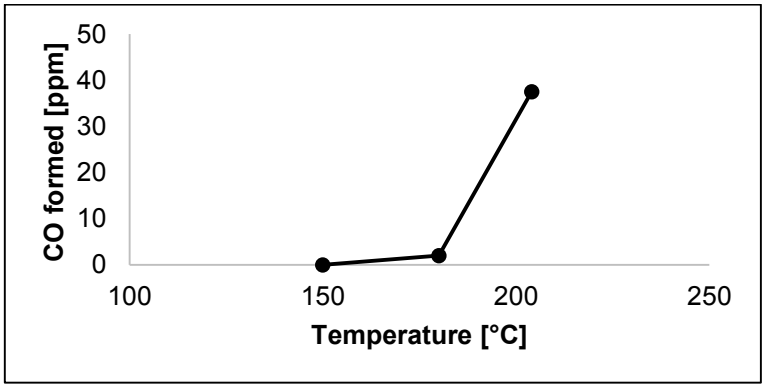


**Figure 5-10: Effect of temperature on rWGS activity on Ru_high pH catalyst. Feed conditions: 20 % $CO_2$, 50 % $H_2$, 10 % $H_2O$, 2 % He, $N_2$ balance on Ru_high pH catalyst at 25 000 ml/(h $g_{cat}$) at 32 ml/min. Catalyst mass: 80 mg.**

Figure 5-10 shows that there is rWGS activity on the Ru_high pH catalyst and the amount of CO formed during the rWGS reaction increases as the temperature increases. This is because rWGS is an endothermic reaction which is favoured by increasing temperature. However, only a few ppm of CO were formed with no CO formation at temperatures <150 °C. Han et al., (2004b) also found the rWGS reaction on $Ru/Al_2O_3$ to be negligible for temperatures <120 °C. The observed amount of CO formed could however be much higher during normal PrOx conditions since CO and $H_2$ oxidation are exothermic reactions. The temperature on the catalyst surface could be much higher than the bulk gas temperature. This was observed by Roberts et al., (2003) when the formed CO was larger than the calculated equilibrium CO content. To explain this, it was suggested that the catalyst surface temperature was higher than the bulk gas temperature. However, this explanation alone cannot account for the large decrease in CO conversion observed at higher temperatures. The decrease is due to the combined effect of rWGS and an increase in $H_2$ oxidation which uses up $O_2$ thus reducing CO oxidation.

The rate of the rWGS reaction is 4 orders of magnitude less than the CO oxidation reaction (Han et al., 2004a). Thus the rWGS reaction can be supressed by increasing the space velocity since the rWGS reaction is slower than CO oxidation.

The benefits of running the PrOx reactor at higher space velocity are two folds:

1) a more compact reactor

2) supressed rWGS activity

### 5.3.2. Effect of Space velocity

The space velocity was varied (Figure 5-11) in order to investigate its effect on CO conversion, $O_2$ conversion and $CO_2$ selectivity. Operation at high space velocity is desirable since it will make the PrOx reactor in the fuel processor more compact.

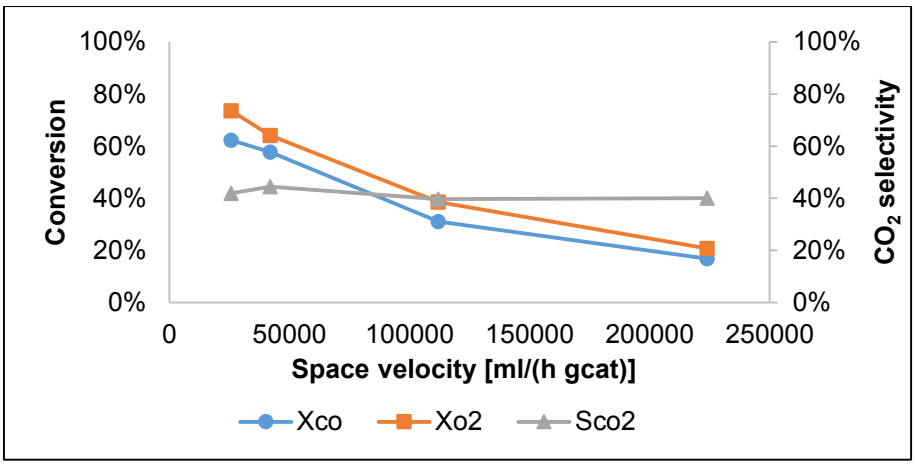


**Figure 5-11: Effect of space velocity on CO conversion, $O_2$ conversion and $CO_2$ selectivity on the Ru_high pH catalyst using feed at 122 °C. Feed conditions: 1 % CO, 1 % $O_2$, 50 % $H_2$, 10 % $H_2O$, 20 % $CO_2$, 2 % He, $N_2$ balance. Catalyst mass: 80 mg.**

At a lower temperature (122 °C), increasing space velocity decreases the CO conversion. This is because the reaction is limited at low temperature (due to limited $O_2$ dissociation). Thus, increasing the space velocity (i.e. decreasing the residence time) only results in lower conversion because the contact time of the reactants with the catalyst surface is shortened. The $CO_2$ selectivity remains almost constant with decreasing the space velocity. This could be because the $H_2$ oxidation reaction is still limited at lower temperature. Thus decreasing the space velocity (i.e. increasing residence time) does not greatly increase the $H_2$ oxidation reaction thus the selectivity remains almost unchanged.

The effect of space velocity was also tested at higher temperature and the results obtained are shown in Figure 5-12.

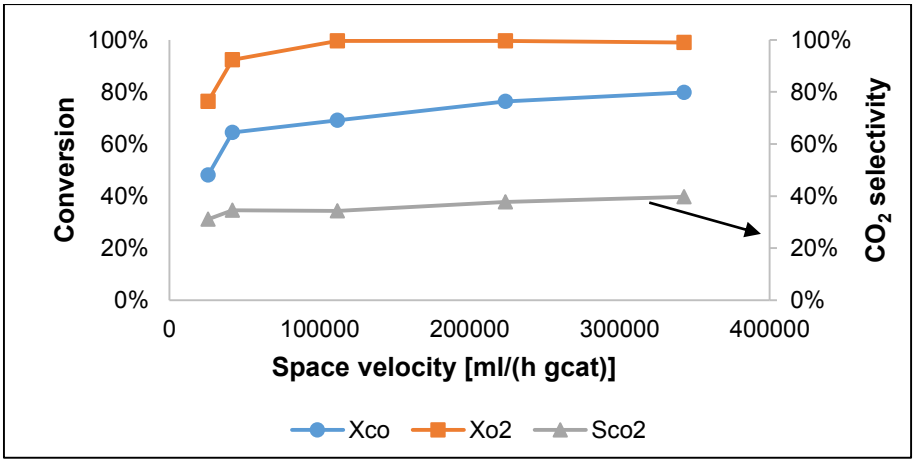


**Figure 5-12: Effect of space velocity on CO conversion, $O_2$ conversion and $CO_2$ selectivity on the Ru_high pH catalyst using feed at 150 °C. Feed conditions: 1 % CO, 1 % $O_2$, 50 % $H_2$, 10 % $H_2O$, 20 % $CO_2$, 2 % He, $N_2$ balance. Catalyst mass: 80 mg.**

At a higher temperature, increasing space velocity increases the CO conversion. This is because the rate of the $H_2$ oxidation reaction is decreased with increasing space velocity as seen from the increase in $CO_2$ selectivity.

Much lower space velocities were also investigated by loading more catalyst into the reactor to see if higher CO conversions can be achieved at a lower temperature. The CO content was also lowered to 0.5 %. The results obtained are shown in Figure 5-13.

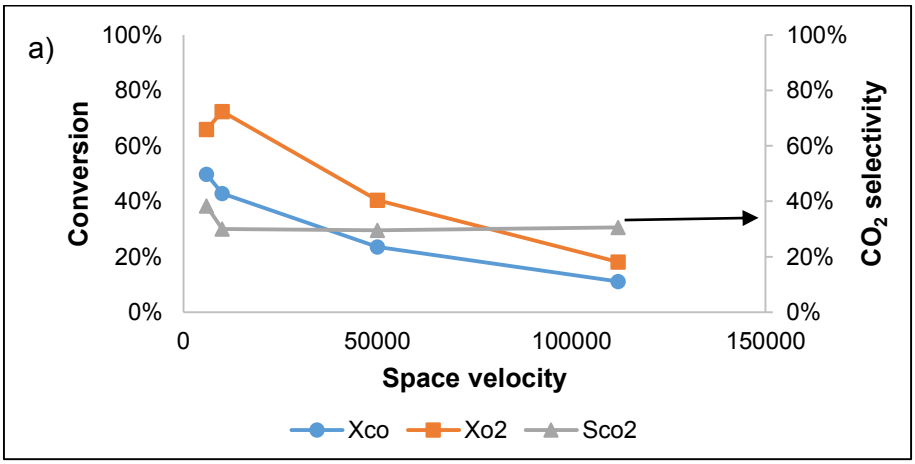

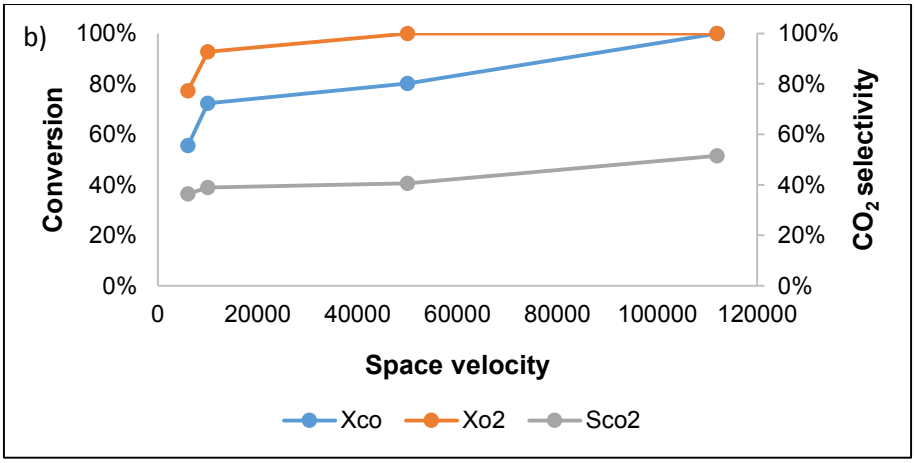


**Figure 5-13: Effect of space velocity at a) 103 °C b) 150 °C on CO conversion, $O_2$ conversion and $CO_2$ selectivity Ru_high pH catalyst using feed at. Feed conditions: 0.5 % CO, 0.5 % $O_2$, 45 % $H_2$, 10 % $H_2O$, 15 % $CO_2$, 2 % He, $N_2$ balance. Catalyst mass: 300 mg.**

High CO conversions could not be achieved at low space velocity and low temperature. This could be due to the mass transfer limitations that exist at low linear velocity and low space velocity. A higher linear velocity can be achieved at low space velocity by loading more catalyst in the reactor. Thus in order to work at lower temperatures, more catalyst needs to be loaded into the reactor leading to a larger reactor. This is less desirable since the requirement of a fuel processor is that it should be compact in size.

The effect of space velocity on the rate of methanation was also investigated (Figure 5-14).

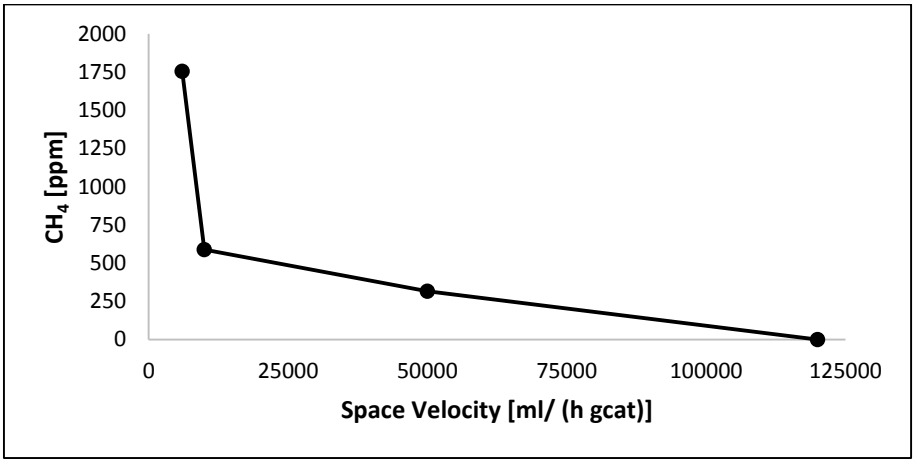


**Figure 5-14: Effect of space velocity on $CH_4$ formation. Feed conditions: 0.5 % CO, 0.5 % $O_2$, 45 % $H_2$, 10 % $H_2O$, 15 % $CO_2$, 2 % He, $N_2$ balance at 180 °C. Catalyst mass: 300 mg.**

Increasing the space velocity decreases the rate of methanation. Thus, an advantage of working at high space velocity is the reduction of methanation and hence $H_2$ consumption.

### 5.3.3. Effect of $O_2$/CO ratio

According to the CO oxidation reaction stoichiometry, only 0.25 % $O_2$ is required to completely oxidise 0.5 % CO. A test was done in order to determine how the catalyst performs at stoichiometric amounts of $O_2$ (i.e. λ=1) (Figure 5-15).

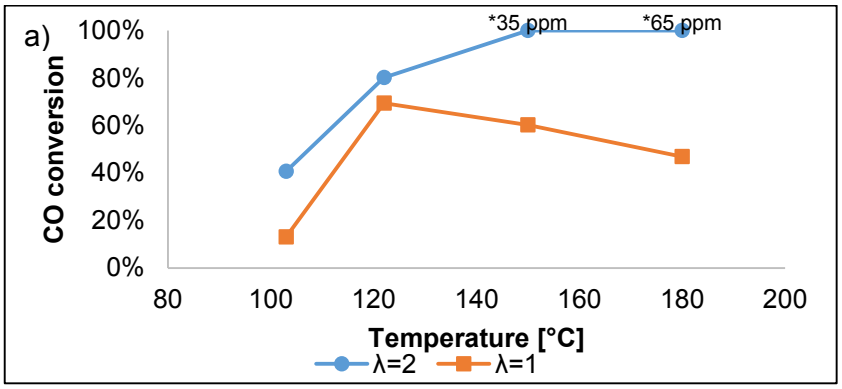


* ppm concentration measured using the analyser

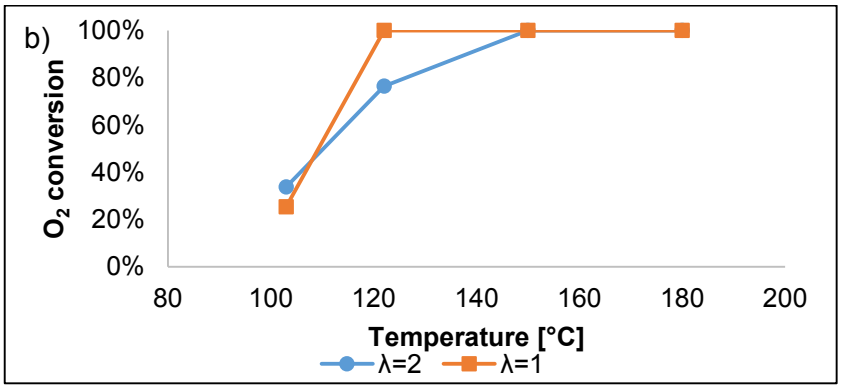


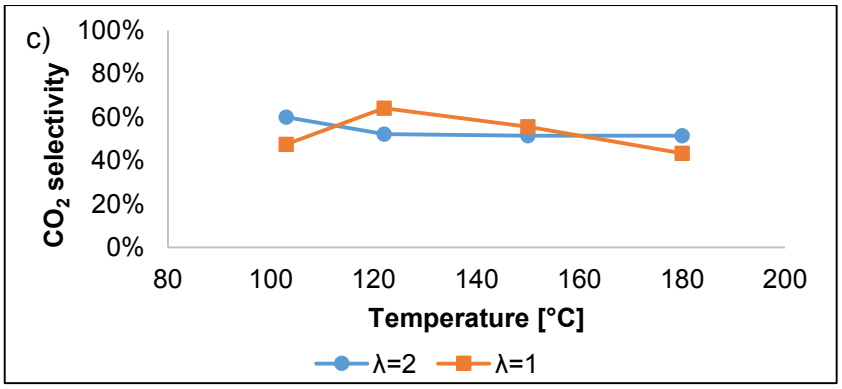


**Figure 5-15: Effect of $O_2$/CO ratio on a) CO conversion b) $O_2$ conversion c) $CO_2$ selectivity on the Ru_high pH catalyst. Feed conditions: 0.5 % CO, 0.5 % $O_2$, 45 % $H_2$, 10 % $H_2O$, 15 % $CO_2$, 2 % He, $N_2$ balance at SV 120 000 ml/(h $g_{cat}$) at 597 ml/min. Catalyst mass: 300 mg.**

Higher CO conversion was observed for the case where the $O_2$/CO ratio is 1 (i.e. λ=2). The maximum CO conversion achieved at λ = 1 was 69 %. The selectivity's did not seem to be very different. Thus the selectivity of the catalyst is not greatly affected by lowering the $O_2$ concentration. This catalyst is not selective enough for $CO_2$ to achieve 100 % CO conversion at a stoichiometric amount of $O_2$ in the feed.

### 5.3.4. Effect of feed concentration

The catalyst activity when there is 1 % CO and 0.5 % CO in the feed stream was investigated (Figure 5-16).

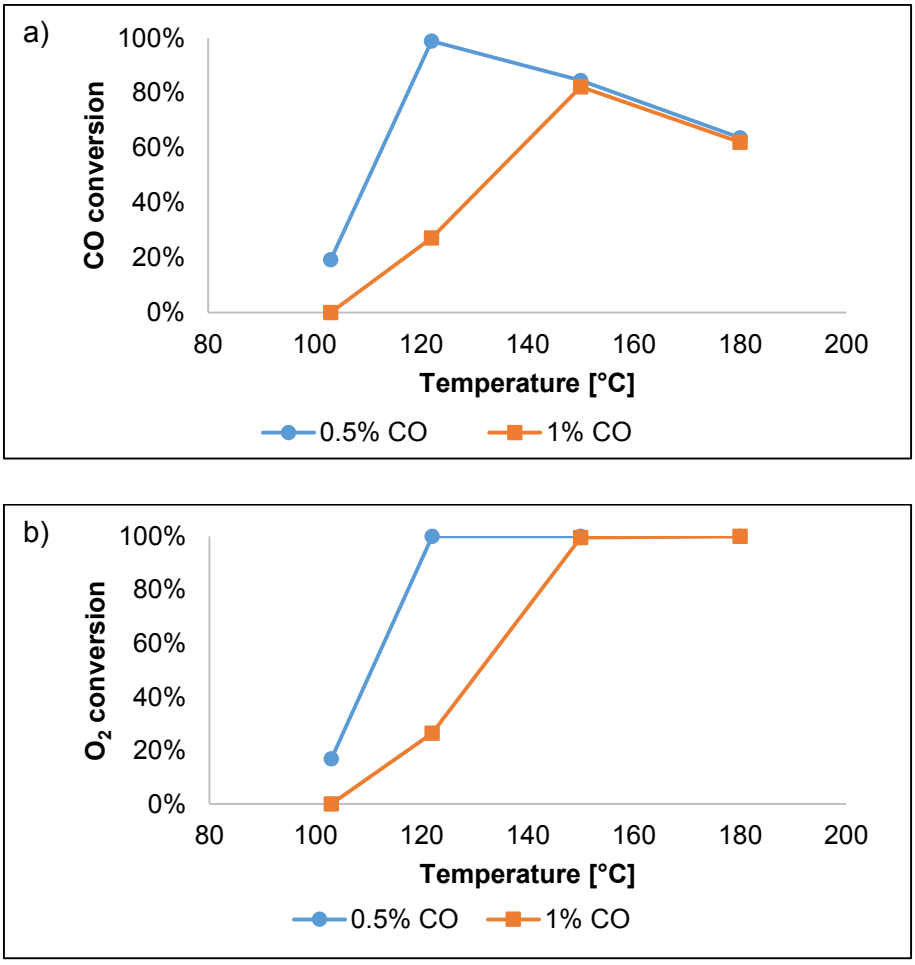

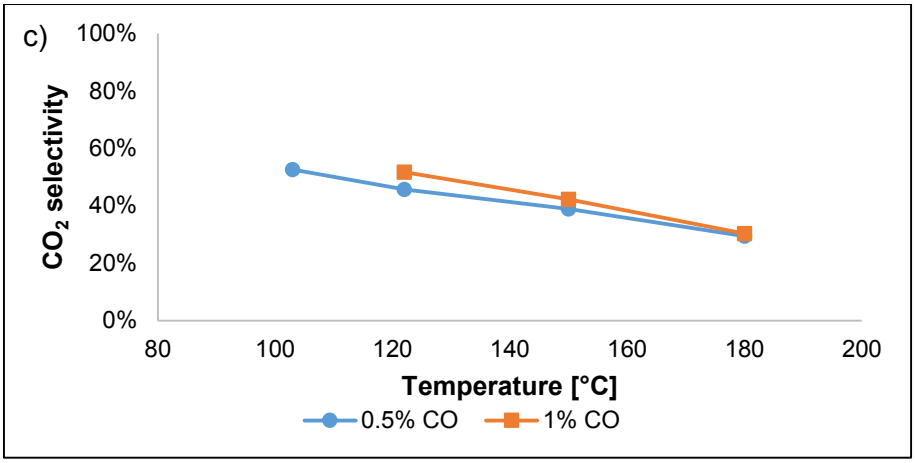


**Figure 5-16: Effect of CO feed concentration on a) CO conversion b) $O_2$ conversion c) $CO_2$ selectivity using Chin *et al.*,(2005) feed at 120 000 ml/(h $g_{cat}$) at 160 ml/min. Feed conditions: 0.5 % CO, 0.5 % $O_2$, 45 % $H_2$, 10 % $H_2O$, 15 % $CO_2$, 2 %He, $N_2$ balance and 1 % CO, 1 % $O_2$, 50 % $H_2$, 10 % $H_2O$, 20 % $CO_2$, 2 %He, $N_2$ balance. Catalyst mass: 80 mg.**

Higher CO conversions are observed when there is less CO in the feed stream i.e. the WGS step does more work to decrease the CO concentration. This could be due to the fact that with 1 % CO there is more CO that is strongly adsorbed to the active sites compared to when there is 0.5 % CO as a result there is much less active sites available for $O_2$ dissociation. The $CO_2$ selectivity's however remain similar. The selectivity at zero conversion could not be calculated since the CO conversion as well as the $O_2$ conversion was zero.

### 5.3.5. Mass transfer limitations

In order to test for mass transfer limitations the linear superficial space velocity was changed at constant space velocity by changing the catalyst mass loaded into the reactor. The catalyst mass used was approximately 80 mg for 160 ml/min and 300 mg for 597 ml/min.

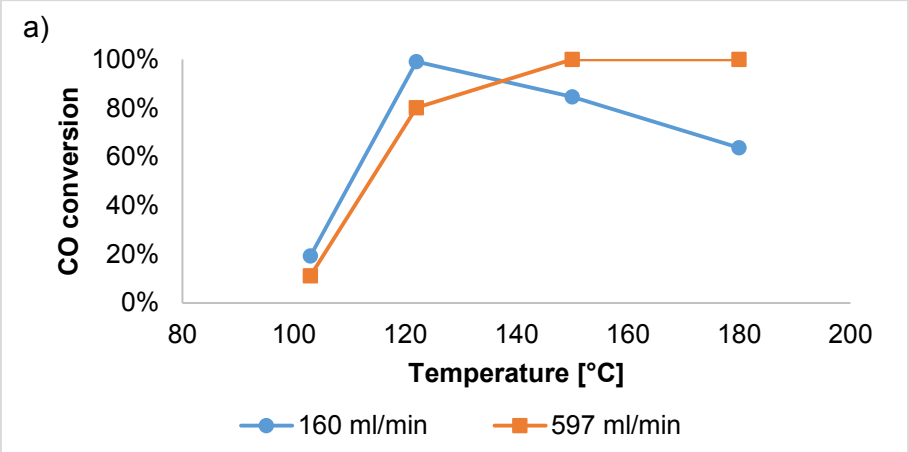

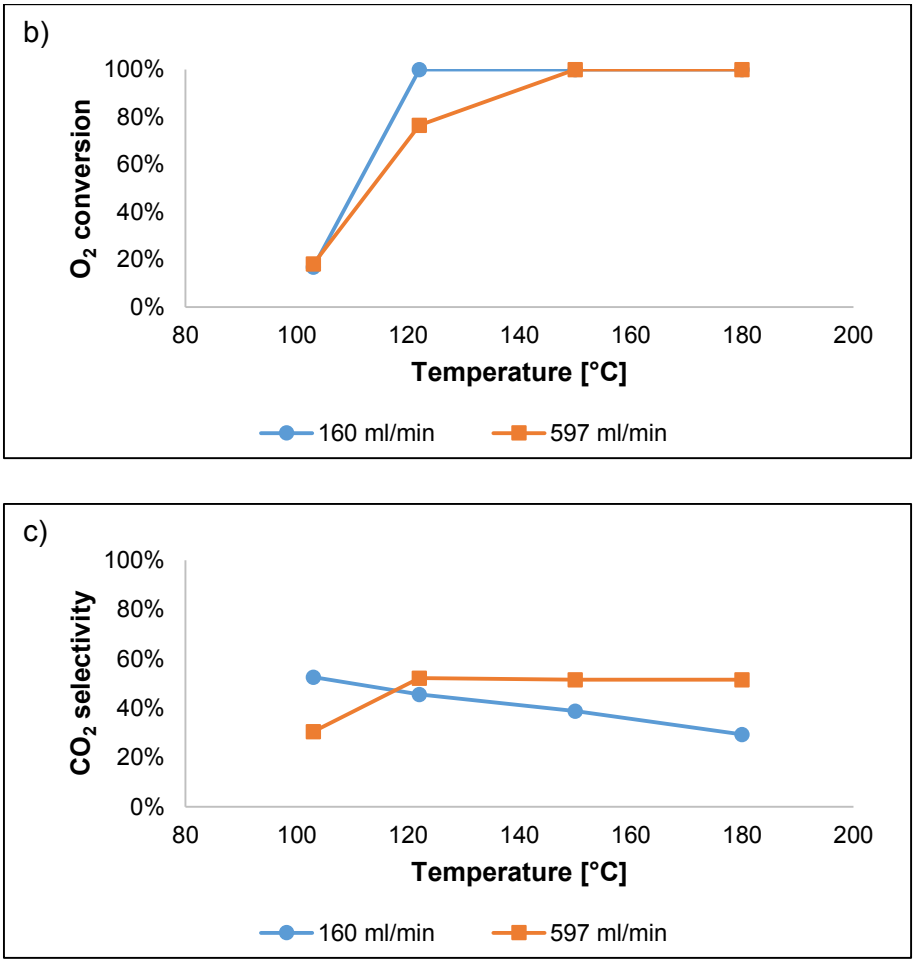


**Figure 5-17: Effect of linear velocity on a) CO conversion b) $O_2$ conversion c) $CO_2$ selectivity on the Ru_high pH catalyst at 120 000 ml/(h $g_{cat}$). Feed conditions: 0.5 % CO, 0.5 % $O_2$, 45 % $H_2$, 10 % $H_2O$, 15 % $CO_2$, 2 % He, $N_2$ balance at SV 120 000 ml/(h $g_{cat}$)**

Increasing the linear velocity at constant space velocity increases the CO conversion and $CO_2$ selectivity at higher temperatures. CO conversion increases because increasing the linear velocity decreases the boundary layer thus diffusion of the reactants to the active site is more enhanced. Since the $CO_2$ selectivity increases at higher linear velocity (except for at 103 °C) it could be said that increasing the linear velocity suppresses the $H_2$ oxidation reaction.

The increase of CO conversion with increase in linear velocity shows that CO oxidation is limited by mass transfer of $O_2$ and/or CO from the bulk gas to the catalyst surface (Roberts et al. (2003). When the reaction is no longer mass transfer limited, the reaction rate that is observed (apparent reaction rate) is given by the reaction kinetics.

At lower linear velocity, the CO conversion peaks at a lower temperature (122 °C) compared to a higher linear velocity (150 °C). One proposed explanation for this was that low linear velocity; there exists external heat transfer limitations (Roberts et al., 2003) that result in the temperature on the catalyst surface being higher than the gas temperature. Increasing the linear velocity improves heat transfer so that the temperature on the catalyst surface is not much higher than the bulk gas temperature.

### 5.3.6. Effect of water content

The effect of increasing the water content on the catalyst surface was investigated (Figure 5 -18).

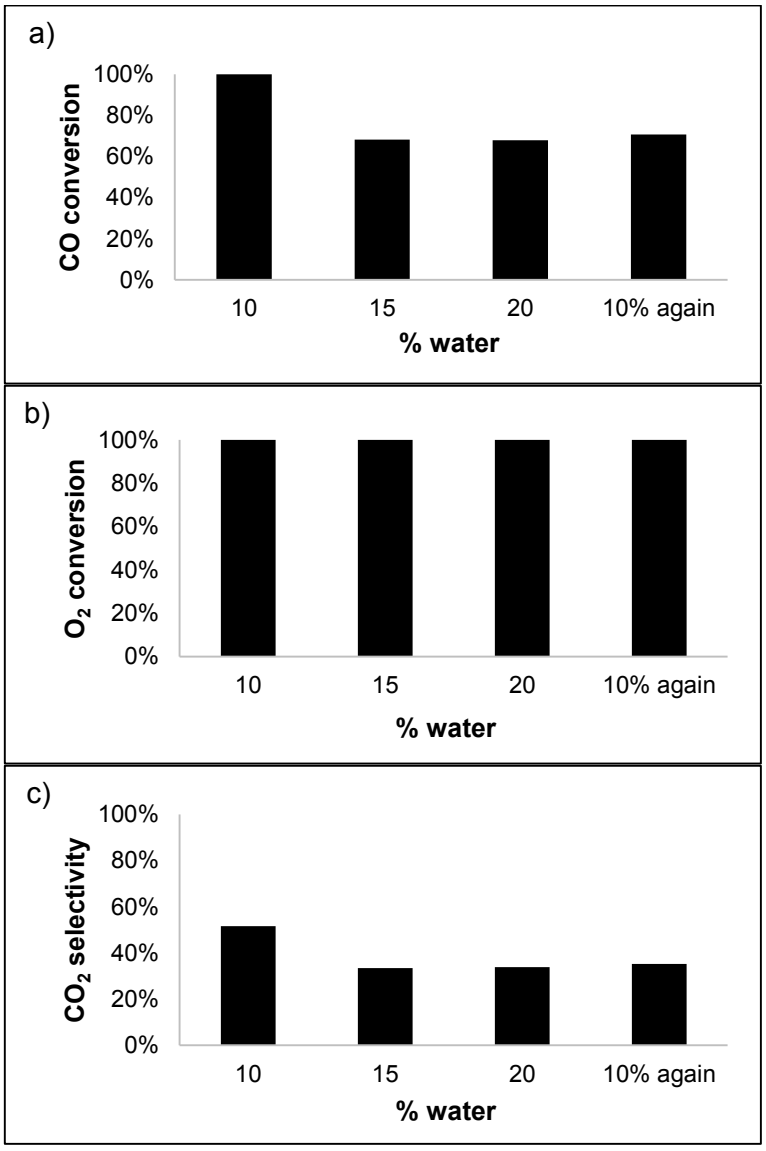

**Figure 5-18: Effect of increasing water content on a) CO conversion b) $O_2$ conversion c) $CO_2$ selectivity on the Ru_high pH catalyst. Feed conditions: 0.5 % CO, 0.5 % $O_2$, 45 % $H_2$, 10-20 % $H_2O$, 15 % $CO_2$, 2 %He, $N_2$ balance at SV 120 000 ml/(h $g_{cat}$) at 597 ml/min with temperature = 150 °C. Catalyst mas: 300 mg.**

Increasing the water resulted in the decrease in CO conversion and $CO_2$ selectivity. The $O_2$ conversion remained unchanged when the water content was increased. When the conditions were returned to 10 % water the CO conversion and $CO_2$ selectivity were much lower than before the water content increase. It appeared as if the catalyst had deactivated. An explanation for this could be that increasing the water content changes the surface structure of the catalyst making it less active for PrOx. Gottschalk et al., (2010) reported that water oxidized the surface Ru sites. According to Echigo & Tabata (2004) CO oxidation is decreased when the ratio of Ru(0) on the catalyst surface is decreased. Increasing the water content could have oxidized the Ru sites thus reducing the ratio of Ru(0) sites on the catalyst surface. This in term resulted in lower PrOx activity.

Rosso et al., (2004) reported that a $Ru/Al_2O_3$ catalyst that had been exposed to high levels of $O_2$ could be restored to its original catalytic activity by reducing the catalyst again. To test for catalyst re-activation, the catalyst was re-reduced at 300 °C.

**Table 5-4: Comparison of catalyst activity after increasing water concentration and after catalyst re-reduction at SV 120 000 ml/(h gcat) at 597 ml/min with temperature = 150 °C. Feed conditions: 0.5 % CO, 0.5 % $O_2$, 45 % $H_2$, 10-20 % $H_2O$, 15 % $CO_2$, 2 %He, $N_2$ balance. Catalyst mass: 300 mg.**

| Condition | Xco | $Sco_2$ | $Xo_2$ |
|---|---|---|---|
| Before $H_2O$ increase | 100 % | 52 % | 100 % |
| After $H_2O$ content increase | 71 % | 35 % | 100 % |
| After re-reduction | 66 % | 32 % | 100 % |

Catalyst activity could not be regained after re-reducing at 300 °C unlike the catalyst that was regenerated by Rosso et al., (2004). This could be because the catalyst by Rosso et al., (2004) was reduced at 500 °C compared to 300 °C used in this study. Furthermore, the catalyst by Rosso et al., (2004) was regenerated after being exposed to high $O_2$ concentration and not $H_2O$. The effects caused by high $H_2O$ concentration could be more permanent than the effects caused by high $O_2$ concentration. The lower CO conversion and $CO_2$ selectivity suggests that the catalyst sintered after it was re-reduced.

## 5.4. Ru_IWI results

The Ru_IWI catalyst was prepared according to the method described by Chin et al., (2005) and tested at the same conditions in order to check if he results can be reproduced and to compare its activity to the Ru_high pH catalyst.

### 5.4.1. Comparison to literature

The Ru_IWI catalyst activity was compared to the results obtained by Chin et al., (2005) at similar conditions (Figure 5-19).

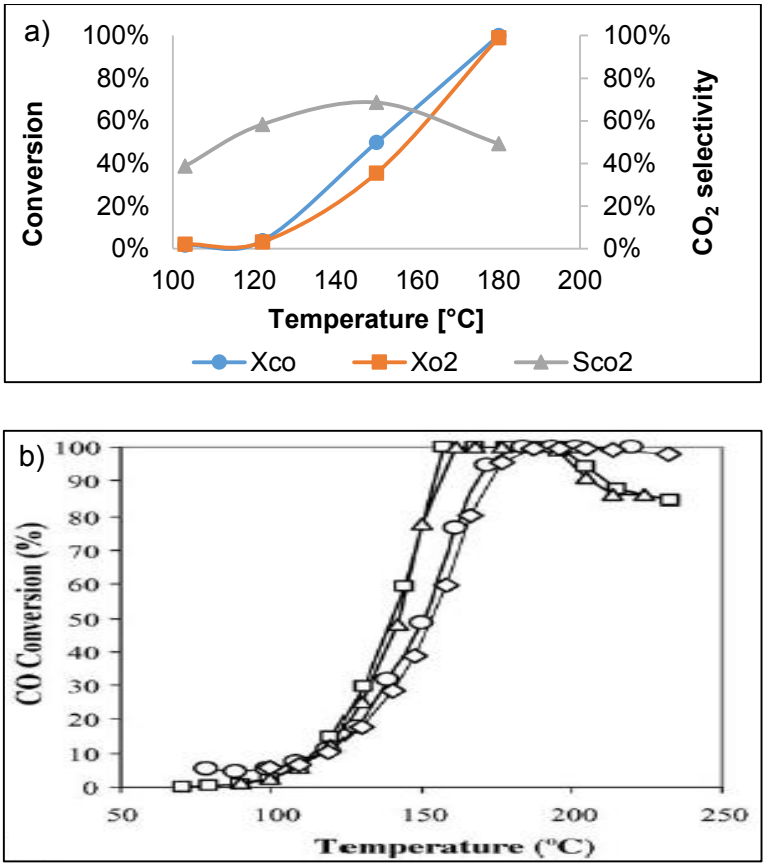


**Figure 5-19: Results obtained for a) Ru_IWI compared to b) literature results (diamond symbols). Feed conditions: 0.5 % CO, 0.5 % $O_2$, 45 % $H_2$, 10 % $H_2O$, 15 % $CO_2$, 2 % He, $N_2$ balance at 120 000 ml/ (h $g_{cat}$) at 597 ml/min. Catalyst mass: 300 mg.**

Similar results were obtained for the prepared Ru_IWI compared to the results obtained by Chin et al., (2005) at similar reaction conditions. The only difference was that in this study a higher linear velocity was used in order to decrease mass transfer limitations. It should be noted that the CO concentration obtained at 180 °C was 89 ppm. The $CO_2$ selectivity at maximum conversion was approximately 50 % which is similar to the selectivity obtained by Chin et al., (2005). Increasing temperature also results in the increase in CO conversion as

was observed on the Ru_high pH catalyst. This is due to the strong adsorption of CO onto the catalyst active site. Increasing the reaction temperature weakens the CO adsorption bond thus enhancing $O_2$ adsorption and dissociation which leads to increased CO conversion. At higher temperatures the $CO_2$ selectivity decreases due to the increase in the rate of the $H_2$ oxidation reaction.

### 5.4.2. Effect of Space velocity

The effect of space velocity was investigated on the Ru_IWI catalyst and the results obtained are shown in Figure 5-20.

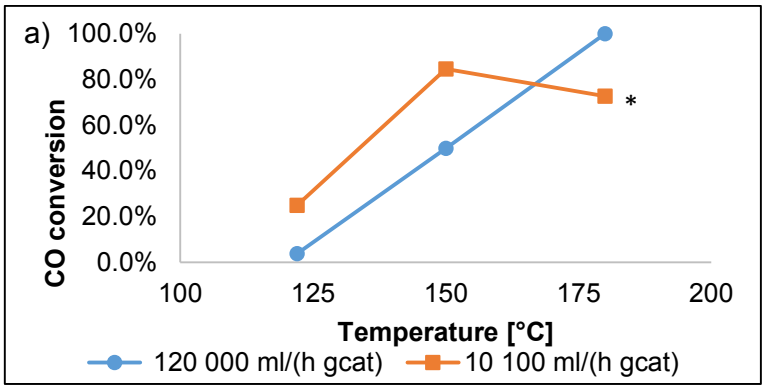


* 145 ppm $CH_4$ detected

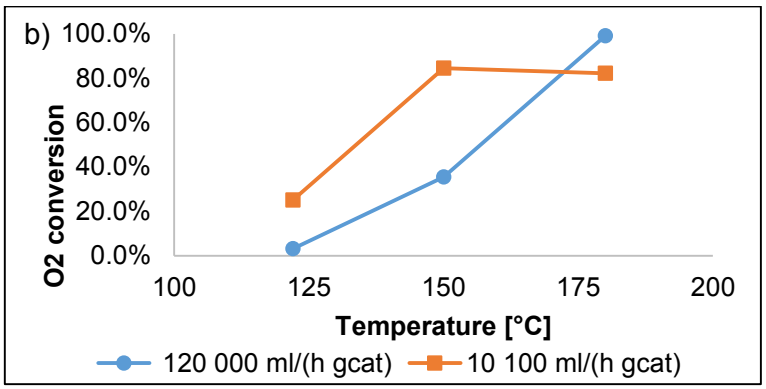


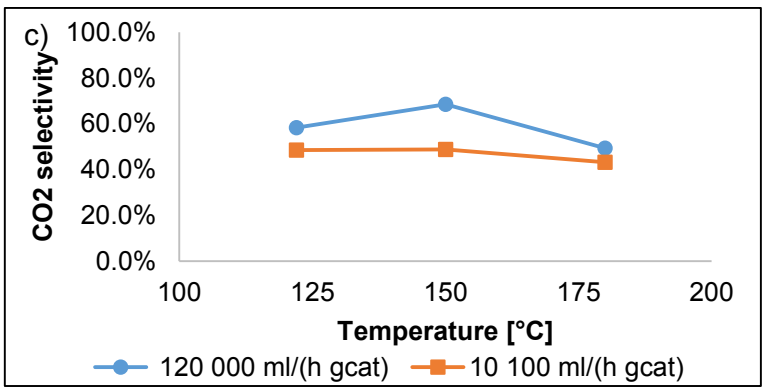

**Figure 5-20: Effect of space velocity on a) CO conversion b) $O_2$ conversion c) $CO_2$ selectivity. Feed: 0.5 % CO, 0.5 % $O_2$, 2 % He, 10 % $H_2O$, 15 % $CO_2$, 45 % $H_2$, $N_2$ balan. Catalyst mass 300 mg.**

Higher CO conversions were observed at lower space velocity up to 150 °C after which the CO conversion is higher at the higher space velocity. At higher temperatures, lower CO conversion is observed at lower space velocities. This is because at higher temperature the rWGS is more significant which lowers CO conversion. However, the rWGS reaction can be minimized by increasing the space velocity (i.e. reducing the residence time). Furthermore, one can also speculate that $H_2$ oxidation is suppressed by increasing the space velocity since the $CO_2$ selectivity is higher at higher space velocity.

### 5.4.3. Effect of $O_2$/CO ratio

The effect of decreasing the $O_2$/CO ratio to the stoichiometric amount (λ=1) was investigated on the Ru_IWI catalyst in order to assess how the catalyst performs (Figure 5-21).

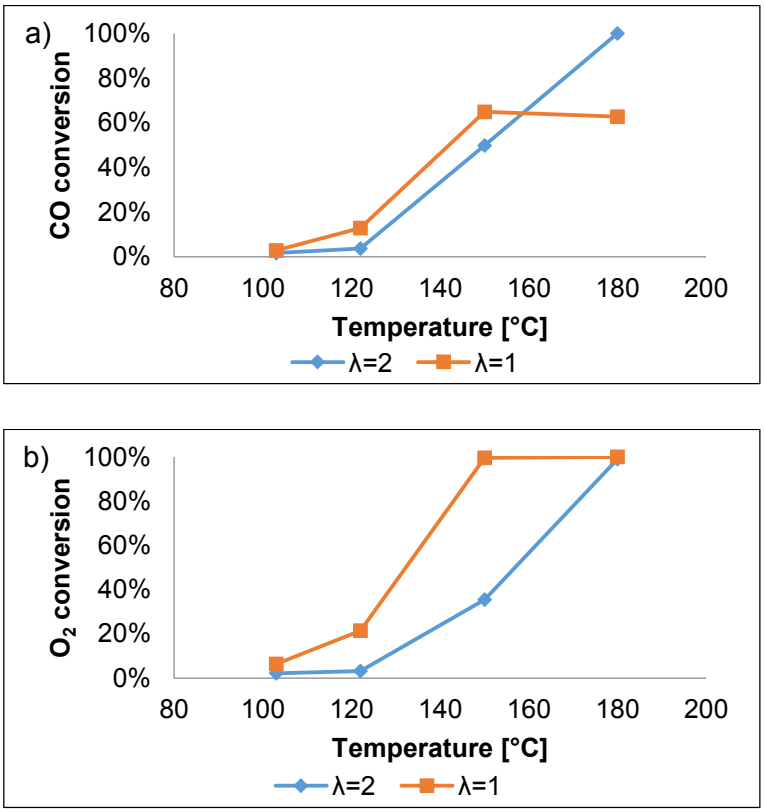

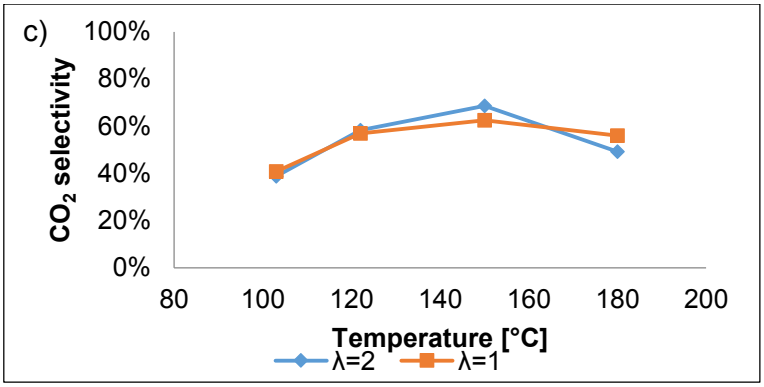


**Figure 5-21: Effect of $O_2$/CO ratio on a) CO conversion b) $O_2$ conversion c) $CO_2$ selectivity on Ru_IWI. Feed conditions: 0.5 % CO, 0.5 % $O_2$, 45 % $H_2$, 10 % $H_2O$, 15 % $CO_2$, 2 % He, $N_2$ balance at 120 000 ml/ (h $g_{cat}$), 597 ml/min. Catalyst mass: 300 mg.**

The CO conversion at λ=1 is slightly higher than the CO conversion at λ=2 up to a point where the $O_2$ becomes limiting (i.e. there is no more $O_2$ left to oxidise CO). After this point, higher CO conversion is then observed when λ=2. The selectivity at λ=1 and at λ=2 are very similar and follow a similar trend. Maximum CO conversion could not be achieved at λ=1 because the Ru_IWI catalyst is not 100 % selective towards CO oxidation.

## 5.5. Pt-Fe/Mordenite catalyst results

A Pt-Fe/M was prepared in this study with a few differences in the catalyst preparation method to that described by Watanabe et al., (2003) in attempt to improve the preparation method. A summary of the differences is shown in Table 5-5.

**Table 5-5: Comparison of the Pt-Fe/M preparation method described in literature compared to the method used in this study**

| | **Literature** | **This study** |
|---|---|---|
| Catalyst synthesis | IE of Pt followed by IE of Fe | Solid state IE of Fe followed by CIE of Pt |
| Reduction method | Oxidised in $O_2$ at 300 °C (5 °C/min) for 1h → N2 for 30 mins → $H_2$ for 1h | Oxidised in $O_2$ at 350 °C (0.3 °C/min) → cool in N2 to RT → reduced in H2 at 250 °C (0.4 °C/min) |

The prepared Pt-Fe/M was tested for PrOx activity. Results obtained by Watanabe et al., (2003) at λ=1 are shown in Figure 5-22. The results obtained using the Pt-Fe/M prepared in this study are shown in Figure 5-23.

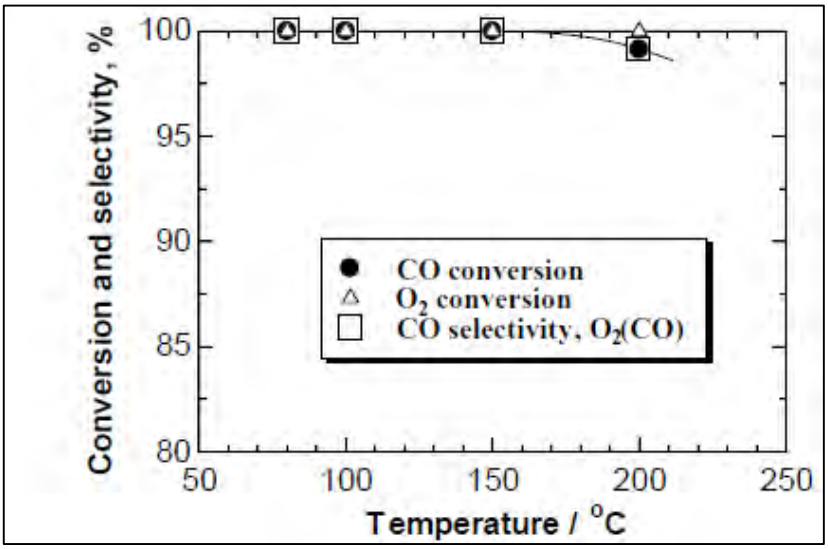


**Figure 5-22: Effect of temperature on Pt-Fe/M Feed conditions: 1 % CO, 0.5 % $O_2$, 45 % $H_2$, 20 % $H_2O$, 15 % $CO_2$, 2 % He, $N_2$ balance at 120 000 ml/(h $g_{cat}$ taken from Watanabe et al., (2003).**

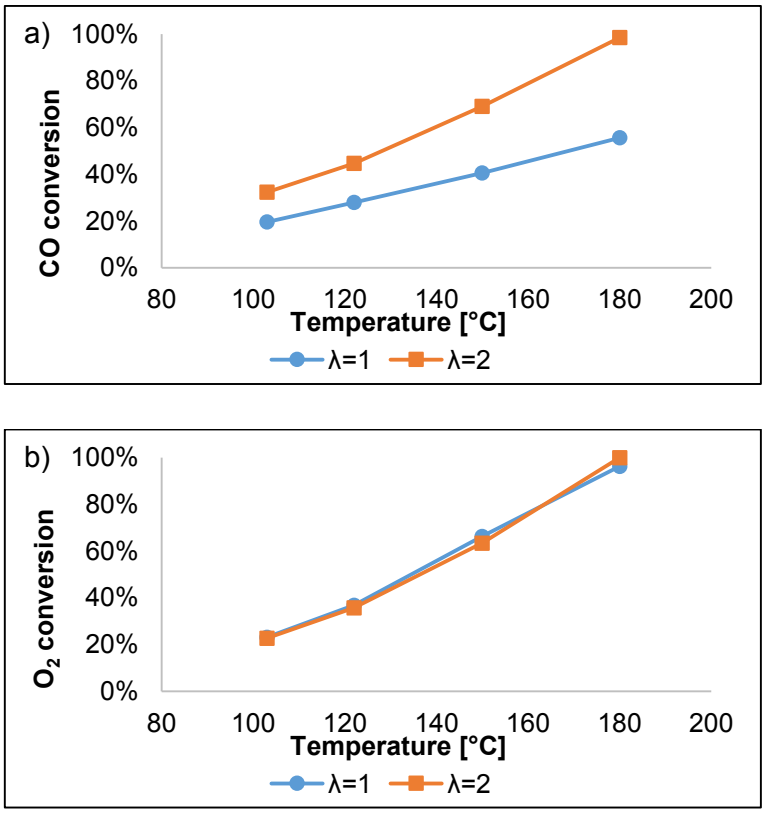

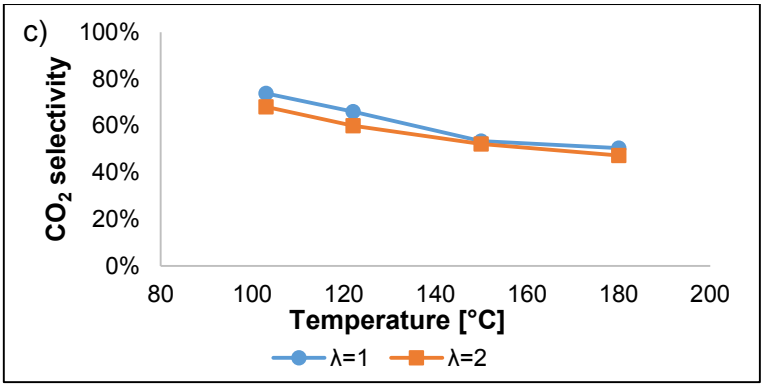


**Figure 5-23: Effect of $O_2$/CO ratio a) CO conversion b) $O_2$ conversion c) $CO_2$ selectivity on Pt-Fe/Mordenite Feed conditions: 0.5 % CO, 0.25 and 0.5 % $O_2$, 45 % $H_2$, 10 % $H_2O$, 15 % $CO_2$, 2 % He, $N_2$ balance at 120 000 ml/(h $g_{cat}$), 597 ml/min. Catalyst mass 300 mg.**

Watanabe et al., (2003) reported a CO conversion of 100 % with 100% $CO_2$ selectivity using λ=1 (Figure 5-24). The results obtained by Watanabe et al., 2003 could not be replicated using the in-house synthesised Pt-Fe/M. The maximum CO conversion obtained was 99 % at 180 °C with λ=2 and this was at a $CO_2$ selectivity of 47 %. The low selectivity at a high CO conversion suggests that the sieve effect of the zeolite is not being utilized during the reaction. Thus a large fraction of Pt particles could be located outside the zeolite pores. Watanabe et al., 2003 reported that 80 % of the metal particles were inside the mordenite cages. This explains why they achieved very high selectivity because the sieving effect of the mordenite was largely utilised. The following explanation to the result obtained can be proposed:

1. The proposed solid state ion exchange method was for MFI zeolite and in this project, mordenite was used. The difference in the pore sizes (0.7 nm for mordenite and 0.55 nm for MFI zeolite) could have had an effect on the Fe deposition on the zeolite.

## 5.6. Commercial PrOx catalyst

A commercial catalyst was also tested for PrOx activity. It should be noted that no information on the type of catalyst as well as the required pre-treatment conditions was provided. Thus the catalyst was reduced using the same method as the prepared Ru catalysts.

### 5.6.1. Effect of temperature

The reaction temperature was varied in order to investigate how temperature affects CO conversion, $O_2$ conversion and $CO_2$ selectivity (Figure 5-24).

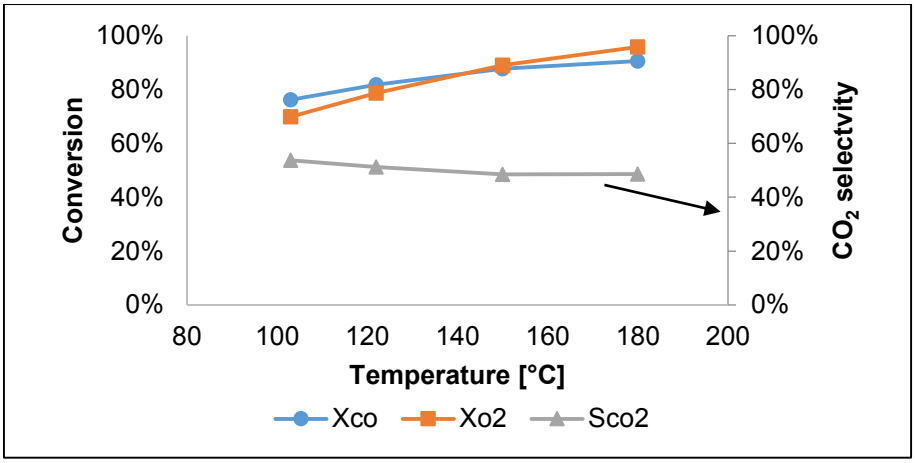


**Figure 5-24: Effect of temperature on CO conversion, $O_2$ conversion and $CO_2$ selectivity commercial catalyst. Feed conditions: 0.5 % CO, 0.5 % $O_2$, 45 % $H_2$, 10 % $H_2O$, 15 % $CO_2$, 2 % He, $N_2$ balance at 120 000 ml/ (h $g_{cat}$), 597 ml/min. Catalyst mass: 300 mg.**

Increasing the temperature increased the catalyst activity. The $O_2$ conversion did not reach 100 % even at temperatures as high as 180 °C. It should be noted that no methane formation was observed on this catalyst.

### 5.6.2. Effect of $O_2$/CO ratio

The $O_2$/CO ratio was lowered in order to investigate how the catalyst performs at stoichiometric $O_2$ levels (Figure 5-25).

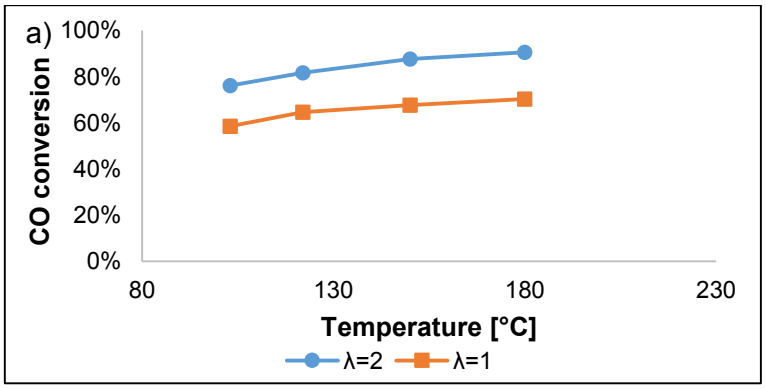

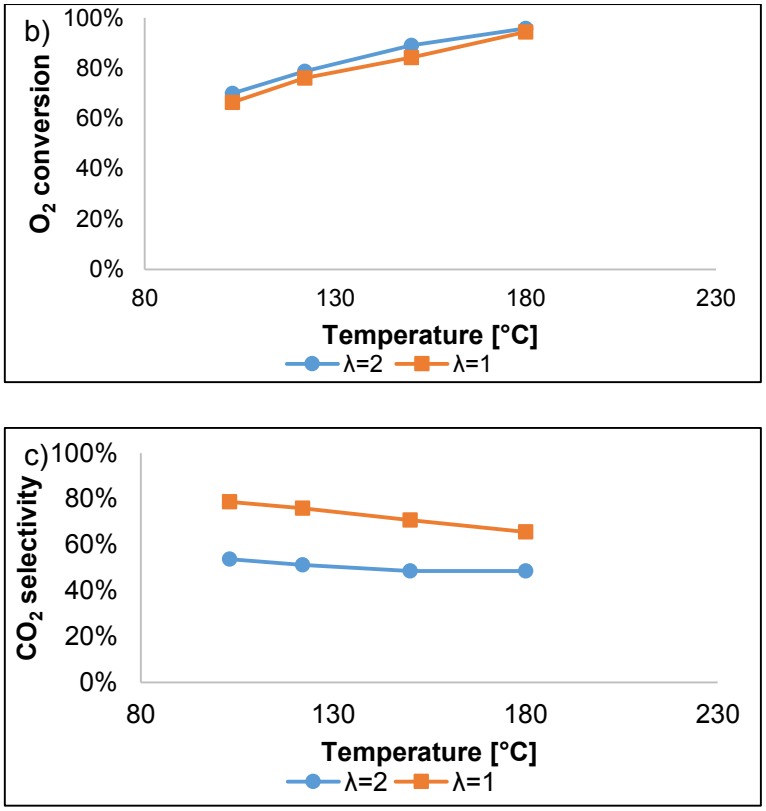


**Figure 5-25: Effect of $O_2$/CO ratio on a) CO conversion b) $O_2$ conversion c) $CO_2$ selectivity on the commercial catalyst Feed conditions: 0.5 % CO, 0.5 % and 0.25 % $O_2$, 45 % $H_2$, 10 % $H_2O$, 15 % $CO_2$, 2 % He, $N_2$ balance at 120 000 ml/(h $g_{cat}$), 597 ml/min. Catalyst mass: 300 mg.**

Higher CO conversions were observed at λ=2, however the $CO_2$ selectivity was higher when λ=1. Thus when there is less $O_2$ in the feed stream, the catalyst is more selective to CO oxidation compared to when there is more $O_2$ in the system.

## 5.7. Comparison of catalysts

The PrOx activity of all the catalysts was compared at the same space velocity, $O_2$/CO ratio and feed composition (Figure 5-26).

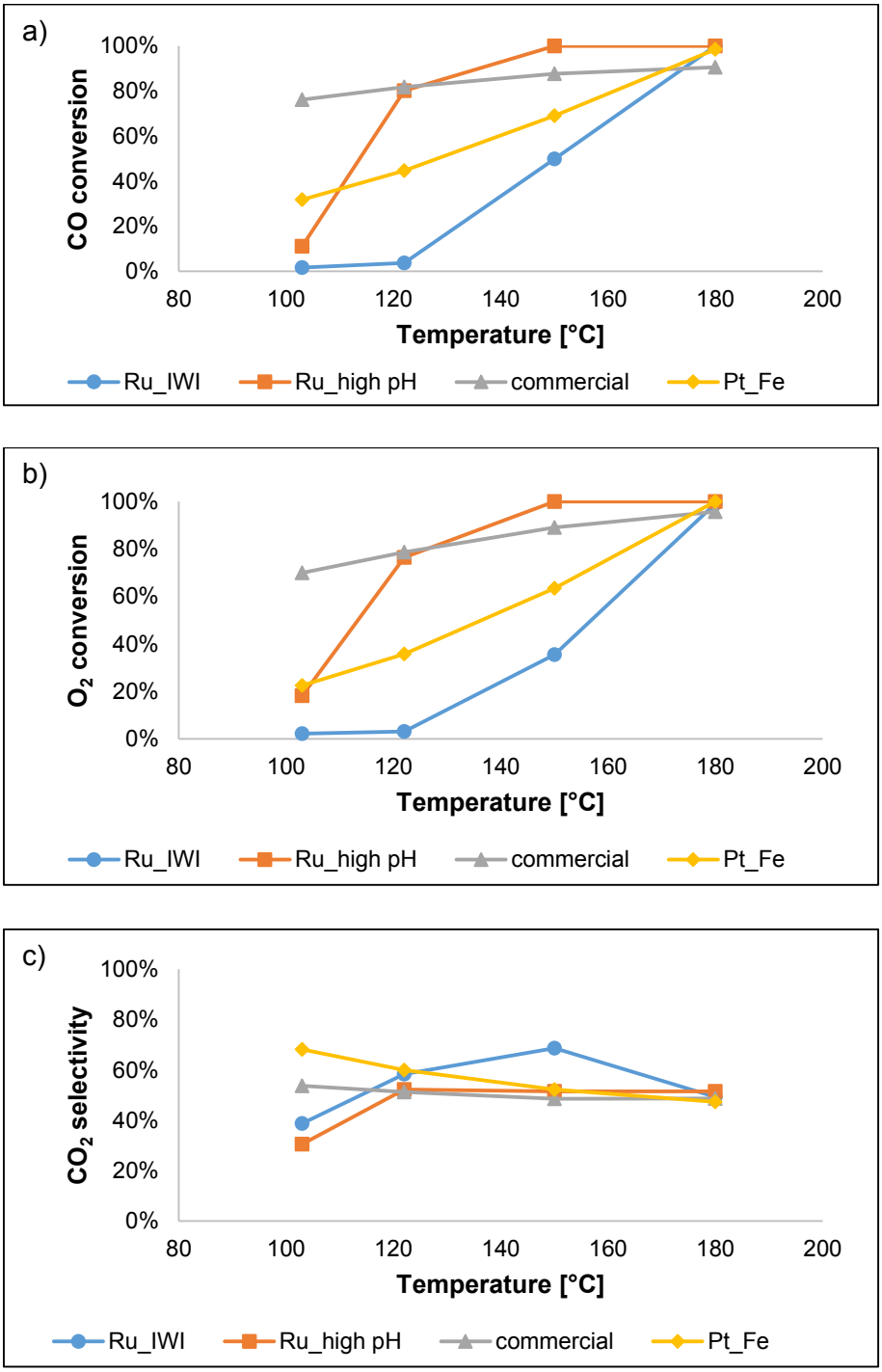


**Figure 5-26: Comparison of a) CO conversion b) $O_2$ conversion c) $CO_2$ selectivity on Ru_IWI, Ru_high pH, commercial and Pt-Fe/M catalysts. Feed conditions: 0.5 % CO, 0.5 % $O_2$, 45 % $H_2$, 10 % $H_2O$, 15 % $CO_2$, 2 % He, $N_2$ balance at SV 120 000 ml/(h $g_{cat}$, 597 ml/min. Catalyst mass: 300 mg.**

The Ru_high pH catalyst shows higher CO conversions at all temperatures when compared to the Ru_IWI catalyst. From the $O_2$ chemisorption results, (Table 5-3) Ru_IWI had a higher dispersion compared to Ru_high pH. This is in contrast to the hypothesis that higher dispersion increases PrOx activity. The increased activity for the Ru_high pH (despite the lower dispersion) catalyst compared to Ru_IWI could be due to the promotion effect from the trace Na (0.06 wt %) detected in ICP-OES (Table 5-1).This translates to a Na:Ru molar ratio of 1:3. It is possible that the activity of the Ru_high pH catalyst could have been improved by using an alumina support with a higher surface area. When compared to the commercial catalyst as well as Pt-Fe, Ru_high pH catalyst shows higher CO conversion only at higher temperature. For all the catalysts the $CO_2$ selectivity at the highest conversion was approximately 50 %.

The catalysts were also compared at a stoichiometric amounts of $O_2$ (λ=1) as shown in Figure 5-27.

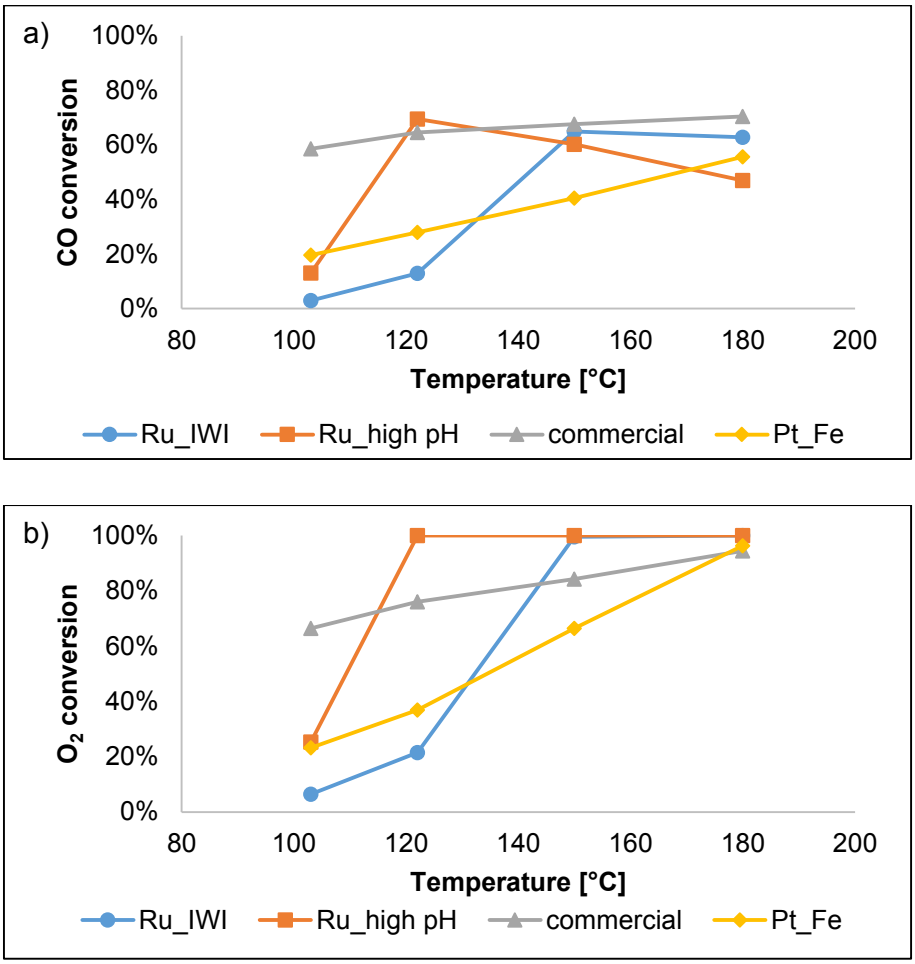

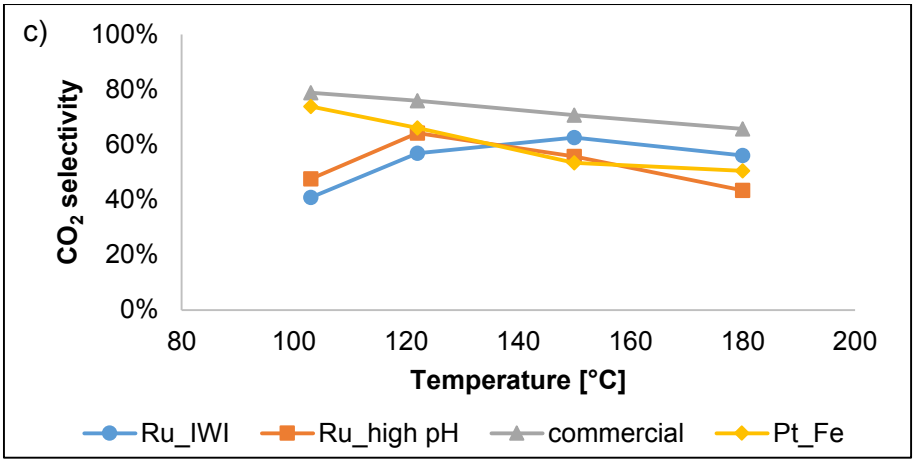


**Figure 5-27: Comparison of a) CO conversion b) $O_2$ conversion c) $CO_2$ selectivity on Ru_IWI, Ru_high pH, commercial and Pt-Fe/M catalysts. Feed conditions: 0.5% CO, 0.25% $O_2$, 45% $H_2$, 10% $H_2O$, 15% $CO_2$, 2%He, $N_2$ balance at SV (dry) 120 000 ml/(h $g_{cat}$), 597 ml/min. Catalyst mass: 80 mg.**

None of the catalyst achieved 100% CO conversion at λ=1. The commercial catalyst showed higher $CO_2$ selectivity at the investigated temperature range.

# 6. Conclusions and recommendations

This study investigated the activity of two Ru catalysts prepared by two different methods (wetness impregnation at high pH and incipient wetness impregnation) as well as a commercial catalyst and a Pt-Fe/Mordenite catalyst. Initially poor results were obtained on the Ru_high pH catalyst and a further hypothesis was proposed that there is $O_2$ present in the system during reduction thus resulting in the sintering of the particles which show poor activity and selectivity. This hypothesis was proved when activity and selectivity improved after flushing out $O_2$ from the system before reducing the catalyst.

Mass transfer limitation effects were found to influence CO oxidation at lower linear velocity. Increasing the linear velocity, thus reducing the boundary layer around the catalyst active sites resulted in higher CO conversions.

Increasing temperature resulted in an increase in CO conversion up to a maximum value after which the conversion began to decrease. This is because at low temperatures $O_2$ adsorption and dissociation is limited because CO strongly adsorbs to the catalyst surface thus blocking catalyst active sites. In order to increase CO conversion at low temperatures the space velocity needs to be lowered. Lowering the space velocity however results in the mass transfer limitations which retard PrOx activity even further. Increasing the reaction temperature weakens the strong adsorption of CO onto the catalyst surface thus more active sites are available for $O_2$ adsorption and dissociation. This leads to increased PrOx activity. However, the pitfalls of increasing temperature are that the rate of the $H_2$ oxidation reaction as well as the methanation reaction are further increased and at high temperatures the rWGS reaction becomes significant. These side reactions can be suppressed by increasing the space velocity.

A stoichiometric amount of $O_2$ could not be used to achieve high CO conversions because the catalysts were not 100 % selective to $CO_2$.

Increasing the water content on the Ru_high pH catalyst resulted in decreased catalyst activity and the activity was not restored after the catalyst was re reduced. This is a concern for a PrOx catalyst since the water content in the feed stream could be higher than 10%. Therefore the effect of a high water content needs to be further investigated and understood.

Similar to literature, the best $CO_2$ selectivity achieved for the in-house synthesised $Ru/Al_2O_3$ catalysts at maximum conversion was ~50 %. In this project however a final CO

concentration of < 10 ppm was not achieved on any of the catalysts. The lowest CO concentration recorded was 35 ppm on the Ru_high pH catalyst.

The original hypothesis which states that, “an improved deposition method for Ru on the $Al_2O_3$ support by modifying the pH, would increase dispersion and hence catalytic activity”, was not conclusively validated or rejected because the surface areas of the two catalysts that were compared were not the same. The Ru_high pH catalyst prepared with the method we hypothesized to give better dispersion actually displayed lower Ru dispersion compared to the Ru_IWI catalyst. The Ru_high pH catalyst dispersion was only about 14 % lower even though the support surface area was an order of magnitude lower. However, despite the lower dispersion, the Ru_high pH catalyst exhibited higher PrOx activity compared to the Ru_IWI catalyst. We therefore suspect that the dispersion can be improved by using a support with higher surface area. Furthermore, the results require an alternative explanation for the high conversion of the Ru_high pH catalyst despite the comparatively lower dispersion. A potential explanation is the possible promotional effect from the trace amounts of Na detected on the Ru_high pH catalyst. This report proposes that the promotion effect of alkali metals on the activity of Ru catalyst for PrOx deserves further investigation.

It is recommended that in order to validate or disprove the original hypothesis, the effect of modifying the pH during impregnation should be investigated making note of the following:

- Using a $Al_2O_3$ support with a higher surface area.
- Using the same $Al_2O_3$ support for both Ru_high pH and Ru_IWI with the same surface area.

The prepared Pt-Fe/M did not achieve 100% CO conversion at λ=1 after the catalyst was prepared using solid state ion exchange to deposit Fe and competitive ion exchange to deposit Pt. More work needs to be done in order to determine if the method used by Watanabe et al., (2003) to synthesise Pt-Fe/Mordenite can be improved.

From the lessons learnt in this study, zeolite supported catalysts are worth pursuing for PrOx application since the $CO_2$ selectivity and maximum CO conversion can be much greater than 50 % which is the best result for Ru catalysts not supported on zeolites.

## References


Amphlett, J.C., Mann, R.F. & Peppley, B.A. 1996. On board hydrogen purification for steam reformation/ PEM fuel cell vehicle power plants. *International Journal of Hydrogen Energy.* 21(8):673-678. DOI:http://dx.doi.org/10.1016/0360-3199(95)00131-X.

Ashraf, M.A., Ercolino, G., Specchia, S. & Specchia, V. 2014. Final step for CO syngas clean-up: Comparison between CO-PROX and CO-SMET processes. *International Journal of Hydrogen Energy.* 39(31):18109-18119. DOI:http://dx.doi.org/10.1016/j.ijhydene.2014.05.164.

Bion, N., Epron, F., Moreno, M., Mariño, F. & Duprez, D. 2008. Preferential oxidation of carbon monoxide in the presence of hydrogen (PROX) over noble metals and transition metal oxides: advantages and drawbacks. *Topics in Catalysis.* 51(1-4):76-88.

Brown, M. & Green, A. 1960. Purifying Hydrogen by Selective Oxidation of Carbon Monoxide. *Industrial & Engineering Chemistry.* 52(-10):841-844. DOI:-10.1021/ie50610a025.

Chin, S.Y., Alexeev, O.S. & Amiridis, M.D. 2005. Preferential oxidation of CO under excess H2 conditions over Ru catalysts. *Applied Catalysis A: General.* 286(2):157-166. DOI:http://dx.doi.org.ezproxy.uct.ac.za/10.1016/j.apcata.2005.02.031.

Choudhary, T.V. & Goodman, D.W. 2002. CO-free fuel processing for fuel cell applications. *Catalysis Today.* 77(1–2):65-78. DOI:http://dx.doi.org.ezproxy.uct.ac.za/10.1016/S0920-5861(02)00233-X.

Dagle, R., Karim, A., Li, G., Su, Y. & King, D. 2011. Syngas conditioning. *Fuel Cells - Technologies for Fuel Processing.* D. Shekhawat, J. Spivey & D. Berry, Eds. 1st ed. Oxford: Elsevier. 361.

de Souza, T.L., Rossi,Carla de Cássia Rodrigues da Silva, Alonso, C.G., Guirardello, R., Cabral, V.F., Fernandes-Machado, N.R.C., Specchia, S., Zabaloy, M.S. et al. 2014. Thermodynamic analysis of autothermal reforming of methane via entropy maximization: Hydrogen production. *International Journal of Hydrogen Energy.* 39(16):8257-8270. DOI:http://dx.doi.org/10.1016/j.ijhydene.2014.03.078.

Denkwitz, Y., Schumacher, B., Kučerová, G. & Behm, R.J. 2009. Activity, stability, and deactivation behavior of supported Au/TiO2 catalysts in the CO oxidation and preferential CO oxidation reaction at elevated temperatures. *Journal of Catalysis.* 267(1):78-88. DOI:http://dx.doi.org/10.1016/j.jcat.2009.07.018.

Echigo, M. & Tabata, T. 2004. Reaction and surface characterization studies of Ru/Al2O3 catalysts for CO preferential oxidation in reformed gas. *Catalysis Letters.* 98(1):-37-42. DOI:- 10.1007/s10562-004-6445-7.

Echigo, M., Shinke, N., Takami, S., Higashiguchi, S., Hirai, K. & Tabata, T. 2003. Development of residential PEFC cogeneration systems: Ru catalyst for CO preferential oxidation in reformed gas. *Catalysis Today.* 84(3–4):209-215. DOI:http://dx.doi.org/10.1016/S0920-5861(03)00276-1.

Echigo, M. & Tabata, T. 2003. A study of CO removal on an activated Ru catalyst for polymer electrolyte fuel cell applications. *Applied Catalysis A: General.* 251(1):157-166. DOI:http://dx.doi.org.ezproxy.uct.ac.za/10.1016/S0926-860X(03)00325-9.

Farrauto, R.J. 2014. New catalysts and reactor designs for the hydrogen economy. *Chemical Engineering Journal.* 238(0):172-177. DOI:http://dx.doi.org.ezproxy.uct.ac.za/10.1016/j.cej.2013.07.004.

Geus, J. & Jos van Dillen, A. 2008. Supported Catalysts. In *Handbook of Heterogeneous Catalysis.* Online: Wiley-VCH. 428-464.

Ghenciu, A.,F. 2002. Review of fuel processing catalysts for hydrogen production in PEM fuel cell systems. *Current Opinion in Solid State and Materials Science.* 6(5):389-399. DOI:http://dx.doi.org.ezproxy.uct.ac.za/10.1016/S1359-0286(02)00108-0.

Gottschalk, D., Hinson, E.A., Baird, A.S., Kitts, H.L. & Layman, K.A. 2010. CO Adsorption on Hydrated $Ru/Al_2O_3$: Influence of Pre-treatment. *Journal of Physical Chemistry C*. 114:4950-4960.

Haber, Block & Delmon 1995. Manual of methods and procedures for catalyst characterization. *International Union of Pure and Applied Chemistry.* 67:1257-1306.

Han, Y., Kahlich, M.J., Kinne, M. & Behm, R.J. 2004a. CO removal from realistic methanol reformate via preferential oxidation—performance of a Rh/MgO catalyst and

comparison to Ru/γ-Al2O3, and Pt/γ-Al2O3. *Applied Catalysis B: Environmental.* 50(4):209-218. DOI:http://dx.doi.org/10.1016/j.apcatb.2003.10.017.

Han, Y., Kinne, M. & Behm, R.J. 2004b. Selective oxidation of CO on Ru/γ-Al2O3 in methanol reformate at low temperatures. *Applied Catalysis B: Environmental.* 52(2):123-134. DOI:http://dx.doi.org/10.1016/j.apcatb.2004.03.017.

Hou, X. & Jones, B. 2000. Inductively Coupled Plasma/Optical Emission Spectrometry. In Encyclopedia of Analytical Chemistry. R. Meyers, Ed. 1st ed. New York: Wiley. 9468-9485.

Huang, C., Chen, Y., Su, C. & Hsu, C. 2007. The cleanup of CO in hydrogen for PEMFC applications using Pt, Ru, Co, and Fe in PROX reaction. *Journal of Power Sources.* 174(1):294-301. DOI:http://dx.doi.org/10.1016/j.jpowsour.2007.09.017.

Igarashi, H., Uchida, H., Suzuki, M., Sasaki, Y. & Watanabe, M. 1997. Removal of carbon monoxide from hydrogen-rich fuels by selective oxidation over platinum catalyst supported on zeolite. *Applied Catalysis A: General*. 159: 159-169.

Jiao, L. & Regalbuto, J.R. 2008. The synthesis of highly dispersed noble and base metals on silica via strong electrostatic adsorption: I. Amorphous silica. *Journal of Catalysis.* 260(2):329-341. DOI:http://dx.doi.org/10.1016/j.jcat.2008.09.022.

Joensen, F. & Rostrup-Nielsen, J.R. 2002. Conversion of hydrocarbons and alcohols for fuel cells. *Journal of Power Sources.* 105(2):195-201. DOI:http://dx.doi.org.ezproxy.uct.ac.za/10.1016/S0378-7753(01)00939-9.

Kawatsu, S. 1998. Advanced PEFC development for fuel cell powered vehicles. *Journal of Power Sources.* 71(1–2):150-155. DOI:http://dx.doi.org/10.1016/S0378-7753(97)02740-7.

Kim, Y.H., Park, J.E., Lee, H.C., Choi, S.H. & Park, E.D. 2012. Active size-controlled Ru catalysts for selective CO oxidation in H2. Applied Catalysis B: Environmental. 127(0): 129-136. DOI:http://dx.doi.org/10.1016/j.apcatb.2012.08.010.

Kim, Y.H. & Park, E.D. 2010. The effect of the crystalline phase of alumina on the selective CO oxidation in a hydrogen-rich stream over Ru/Al2O3. *Applied Catalysis B:*

*Environmental.* 96(1–2):41-50. DOI:http://dx.doi.org.ezproxy.uct.ac.za/10.1016/j.apcatb.2010.02.001.

Kim, Y.H., Park, E.D., Lee, H.C. & Lee, D. 2009a. Selective CO removal in a H2-rich stream over supported Ru catalysts for the polymer electrolyte membrane fuel cell (PEMFC). *Applied Catalysis A: General.* 366(2):363-369. DOI:http://dx.doi.org/10.1016/j.apcata.2009.07.030.

Kim, Y.H., Park, E.D., Lee, H.C., Lee, D. & Lee, K.H. 2009b. Preferential CO oxidation over supported noble metal catalysts. *Catalysis Today.* 146(1–2):253-259. DOI:http://dx.doi.org/10.1016/j.cattod.2009.01.045.

Ko, E., Park, E.D., Seo, K.W., Lee, H.C., Lee, D. & Kim, S. 2006. A comparative study of catalysts for the preferential CO oxidation in excess hydrogen. *Catalysis Today.* 116(3):377-383. DOI:http://dx.doi.org/10.1016/j.cattod.2006.05.072.

Kogel, M., Sandoval, V., Schwieger, W., Tissler, A. & Turek, T. 1998. Simultaneous catalytic reduction of NO and N2O using Fe-MFI prepared by solid-state ion exchange. *Catalysis Letters.* 51(1-2):23-25. DOI:- 10.1023/A:1019049420697.

Korotkikh, O. & Farrauto, R. 2000. Selective catalytic oxidation of CO in H2: fuel cell applications. *Catalysis Today.* 62(2–3):249-254. DOI:http://dx.doi.org.ezproxy.uct.ac.za/10.1016/S0920-5861(00)00426-0.

Kotobuki, M., Watanabe, A., Uchida, H., Yamashita, H. & Watanabe, M. 2005. Reaction mechanism of preferential oxidation of carbon monoxide on Pt, Fe, and Pt–Fe/mordenite catalysts. *Journal of Catalysis.* 236(2):262-269. DOI:http://dx.doi.org/10.1016/j.jcat.2005.09.026.

Liu, K., Wang, A. & Zhang, T. 2012. - Recent Advances in Preferential Oxidation of CO Reaction over Platinum Group Metal Catalysts. - *ACS Catalysis.* 2(6):1165. DOI:-10.1021/cs200418w.

López, I., Valdés-Solís, T. & Marbán, G. 2008. An attempt to rank copper-based catalysts used in the CO-PROX reaction. *International Journal of Hydrogen Energy.* 33(1):197-205. DOI:http://dx.doi.org/10.1016/j.ijhydene.2007.09.011.

Lu, S., Liu, Y. & Wang, Y. 2009. Meso-macro-porous monolithic Pt-Ni/Al2O3 catalysts used for miniaturizing preferential carbon monoxide oxidation reactor. *Chemical Communications.* 46(4):634. DOI:- 10.1039/B912769K.

Miller, J.T., Schreier, M., Kropf, A.J. & Regalbuto, J.R. 2004. A fundamental study of platinum tetraammine impregnation of silica: 2. The effect of method of preparation, loading, and calcination temperature on (reduced) particle size. *Journal of Catalysis.* 225(1):203-212. DOI:http://dx.doi.org/10.1016/j.jcat.2004.04.007.

Mishra, A. & Prasad, R. 2011. A Review on Preferential Oxidation of Carbon Monoxide in Hydrogen Rich Gases. *Bulletin of Chemical Reaction Engineering & Catalysis.* 6(1):1.

Narita, T., Miura, H., Ohira, M., Hondou, H., Sugiyama, K., Matsuda, T. & Gonzalez, R.D. 1987. The effect of reduction temperature on the chemisorptive properties of Ru/Al2O3: Effect of chlorine. *Applied Catalysis.* 32(0):185-190. DOI:http://dx.doi.org/10.1016/S0166-9834(00)80624-7.

Niu, T., Wang, C.X., Zhang, L.H. & Liu, Y. 2013. Potassium promoted Ru/meso-macroporous SiO2 catalyst for the preferential oxidation of CO in H2-rich gases. *International Journal of Hydrogen Energy.* 38(19):7801-7810. DOI:http://dx.doi.org.ezproxy.uct.ac.za/10.1016/j.ijhydene.2013.03.150.

Niu, T., Zhang, L.H. & Liu, Y. 2014. Highly dispersed Ru on K-doped meso–macroporous SiO2 for the preferential oxidation of CO in H2-rich gases. *International Journal of Hydrogen Energy.* 39(25):13800-13807. DOI:http://dx.doi.org/10.1016/j.ijhydene.2014.03.155.

Oh, S.H. & Sinkevitch, R.M. 1993. Carbon Monoxide Removal from Hydrogen-Rich Fuel Cell Feedstreams by Selective Catalytic Oxidation. *Journal of Catalysis.* 142(1):254-262. DOI:http://dx.doi.org/10.1006/jcat.1993.1205.

Opoku-Gyamfi, K., Tafreshi, Z. & Adesina, A. 1998. Activities of δ-Al2O3 supported bimetallic Pt-NiO and Co-NiO catalysts for methane autoreforming: oxidation studies. *Reaction Kinetics, Mechanisms and Catalysis.* 64(2):229-238. DOI:-10.1007/BF02475339.

Park, J.E. & Park, E.D. 2014. Optimal Ru particle size for selective CO oxidation in H2 over Ru/κ-Al2O3. *Korean Journal of Chemical Engineering*. 31(11):1985-1993.

Park, E.D., Lee, D. & Lee, H.C. 2009a. Recent progress in selective CO removal in a H2-rich stream. *Catalysis Today.* 139(4):280-290. DOI:http://dx.doi.org/10.1016/j.cattod.2008.06.027.

Park, E.D., Lee, D. & Lee, H.C. 2009b. Recent progress in selective CO removal in a H2-rich stream. *Catalysis Today.* 139(4):280-290. DOI:http://dx.doi.org/10.1016/j.cattod.2008.06.027.

Perego, C. & Villa, P. 1997. Catalyst preparation methods . *Catalysis Today.* 34:281-305.

Philippaerts, A., Paulussen, S., Turner, S., Lebedev, O., Van Tendeloo, G., Poelman, H., Bulut, M., De Clippel, F. et al. 2010. Selectivity in sorption and hydrogenation of methyl oleate and elaidate on MFI zeolites. *Journal of Catalysis.* 270(1):172-184. DOI:http://dx.doi.org/10.1016/j.jcat.2009.12.022.

Recupero, V., Pino, L., Vita, A., Cipitı`, F., Cordaro, M. & Laganà, M. 2005. Development of a LPG fuel processor for PEFC systems: Laboratory scale evaluation of autothermal reforming and preferential oxidation subunits. *International Journal of Hydrogen Energy.* 30(9):963-971. DOI:http://dx.doi.org/10.1016/j.ijhydene.2004.12.014.

Roberts, G.W., Chin, P., Sun, X. & Spivey, J.J. 2003. Preferential oxidation of carbon monoxide with Pt/Fe monolithic catalysts: interactions between external transport and the reverse water-gas-shift reaction. *Applied Catalysis B: Environmental.* 46(3):601-611. DOI:http://dx.doi.org/10.1016/j.apcatb.2003.07.002.

Ross, J. 2012. Catalyst preparation. In *Heterogeneous Catalysis.* Amsterdam: Elsevier. 65-96.

Rosso, I., Antonini, M., Galletti, C., Saracco, G. & Specchia, V. 2004. Selective CO-oxidation over Ru-based catalysts in H2-rich gas for fuel cell applications. *Topics in Catalysis.* 30(1-4):475-480.

Rozovskii, Y., Kipnis, M., Volnina, E., Samokhin, P. & Lin, G. 2008. Selective CO Oxidation on a Ru/Al2O3 Catalyst in the Surface Ignition Regime: 1. Fine Purification of Hydrogen-Containing Gases. *Kinetics and Catalysis.* 49(1):92-102. DOI:-10.1134/S0023158408010114.

Schwarz, Contescu, C. & Contescu, A. 1995. Methods for Preparation of Catalytic Materials. *Chemical Reviews.* 95(3):477-510. DOI:- 10.1021/cr00035a002.

Shekhawat, D., Spivey, J. & Berry, D. 2011. *Fuel Cells: Technologies for fuel processing.* 1st ed. Oxford: Elsevier.

Shen, L., Zhang, C. & Liu, Y. 2012. Meso-macroporous Al2O3 supported Ru catalysts for CO preferential oxidation in hydrogen-rich gases. *Journal of Natural Gas Chemistry.* 21(6):653-660. DOI:http://dx.doi.org/10.1016/S1003-9953(11)60416-7.

Shen, X., Garces, L., Ding, Y., Laubernds, K., Zerger, R.P., Aindow, M., Neth, E.J. & Suib, S.L. 2008. Behaviour of $H_2$ chemisorption on Ru/TiO2 surface and its application in evaluation of Ru particle sizes compared with TEM and XRD analyses. Applied Catalysis A: General. 335(2):187-195.

Snytnikov, P.V., Popova, M.M., Men, Y., Rebrov, E.V., Kolb, G., Hessel, V., Schouten, J.C. & Sobyanin, V.A. 2008. Preferential CO oxidation over a copper–cerium oxide catalyst in a microchannel reactor. *Applied Catalysis A: General.* 350(1):53-62. DOI:http://dx.doi.org/10.1016/j.apcata.2008.07.036.

Song, C. 2002. Fuel processing for low-temperature and high-temperature fuel cells: Challenges, and opportunities for sustainable development in the 21st century. *Catalysis Today.* 77(1–2):17-49. DOI:http://dx.doi.org/10.1016/S0920-5861(02)00231-6.

Steele, P. & Heinzel, A. 2001. Materials for fuel-cell technologies. *Nature.* 414:345-352.

Trimm, D.L. 1999. Catalysts for the control of coking during steam reforming. *Catalysis Today.* 49(1–3):3-10. DOI:http://dx.doi.org/10.1016/S0920-5861(98)00401-5.

Utaka, T., Takeguchi, T., Kikuchi, R. & Eguchi, K. 2003. CO removal from reformed fuels over Cu and precious metal catalysts. *Applied Catalysis A: General.* 246(1):117-124. DOI:http://dx.doi.org/10.1016/S0926-860X(03)00048-6.

Watanabe, M., Uchida, H., Ohkubo, K. & Igarashi, H. 2003. Hydrogen purification for fuel cells: selective oxidation of carbon monoxide on Pt–Fe/zeolite catalysts. *Applied Catalysis B: Environmental.* 46(3):595-600. DOI:http://dx.doi.org.ezproxy.uct.ac.za/10.1016/S0926-3373(03)00322-9.

Wörner, A., Friedrich, C. & Tamme, R. 2003. Development of a novel Ru-based catalyst system for the selective oxidation of CO in hydrogen rich gas mixtures. *Applied Catalysis A: General.* 245(1):1-14. DOI:http://dx.doi.org/10.1016/S0926-860X(02)00612-9.

Yan, J., Ma, J., Cao, P. & Li, P. 2004. Preferential oxidation of CO in $H_2$-rich gases over Co-promoted Pt-γ-$Al_2O_3$ catalyst. *Catalysis Letters.* 93(1-2):55.

Yopps, J.A. & Fuerstenau, D.W. 1964. The zero point of charge of alpha-alumina. Journal of Colloid Science. 19(1): 61-71. DOI:http://dx.doi.org/10.1016/0095-8522(64)90007-8.

Zhou, S., Yuan, Z. & Wang, S. 2006. Selective CO oxidation with real methanol reformate over monolithic Pt group catalysts: PEMFC applications. *International Journal of Hydrogen Energy.* 31(7):924-933. DOI:http://dx.doi.org.ezproxy.uct.ac.za/10.1016/j.ijhydene.2005.07.014.

# Appendix

## Appendix I – Ru_high pH catalyst preparation calculations

To make 4 g of catalyst with 1wt% Ru loading:

m(Al2O3) = 3.96 g
m(Ru) = 0.04 g

Ru content in $Ru(NO)(NO_3)_3$ = 1.5% (w/v) = 0.015 g/cm$^3$

Therefore to get 0.04 g of Ru from $Ru(NO)(NO_3)_3$:

$$V(Ru(NO)(NO_3)_3 = \frac{m(Ru)}{c(Ru)} = \frac{0.04\ g}{0.015 \frac{g}{cm^3}} = 2.667\ cm^3$$

And :

$$c(Ru) = \frac{0.04\ g}{101.07\ \frac{g}{mol} \cdot 0.002667\ dm^3} = 0.148\ mol/dm^3$$

The dissociation of $Ru(NO)(NO_3)_3$ in dilute nitric acid is as follows:

$Ru(NO)(H_2O)_x \rightarrow Ru(NO)(H_2O)_{x-1}(OH)^- + H^+$

Ka for this reaction then becomes:

$$Ka = \frac{[Ru(NO)(H_2O)_{X-1}(OH)^-][H^+]}{[Ru(NO)(H_2O)_X]}$$

Also $Ka = 10^{-pKa} = 10^{-(-1.4)} = 25.11$

Then:

| | $[Ru(NO)(H_2O)_x]$ | $[Ru(NO)(H_2O)_{x-1}(OH)^-]$ | $[H^+]$ |
|---|---|---|---|
| Initial | 0.148 | 0 | 0 |
| Final | 0.148-x | x | x |

Then:

$$Ka=\frac{x^2}{0.148-x}=25.11$$

Solving for x gives x = $[H^+]$ = 0.147 mol/$dm^3$

Since V = 0.002667 dm3,

$n(H^+)$ = 0.147 mol/$dm^3$ * 0.002667 $dm^3$ = 0.000 392 mol

At pH = 11 the pOH = 3

$[OH]^-$ = $10^{-pOH}$ = $10^{-3}$ = 0.001 mol/$dm^3$ =[NaOH]

In a 1l solution: n(NaOH) = 0.001 mol

m(NaOH) = 0.001 mol * 40 g/mol = 0.04 g

Some of the added will take part in a neutralization reaction with the $H^+$ ions present in solution from the precursor. Therefore more than 0.04 g of NaOH needs to be added in order to keep the pH of the impregnation solution at 11.

The additional amount of NaOH that needs to be added to account for the NaOH lost during neutralization was calculated as follows:

$n(H^+)$ = 0.000 392 mol thus $n(OH^-)$ for neutralization = 0. 000 392 mol

Thus m(NaOH) additional = 40 g/mol * 0.000 392 mol = 0.015 68 g

Therefore total mass of NaOH = 0.04 g + 0.015 68 g = 0.0557 g

## Appendix II - Mass flow controller calibrations

Sample calculation for converting ml/min to sccm (0 °C, 1 atm)

Using the ideal gas law (since P<5 bar)

$$n=\frac{PV}{RT}$$

$$n_1=\frac{P_1V_1}{RT_1} \text{ and } n_1=\frac{P_2V_2}{RT_2}$$

Since $n_1 = n_2$

$$\frac{P_1V_1}{RT_1} = \frac{P_2V_2}{RT_2}$$

Then, $V_2 = \frac{P_1V_1T_2}{T_1P_2}$

Where 1 is the laboratory conditions and 2 is standard conditions (0 °C, 1 atm)

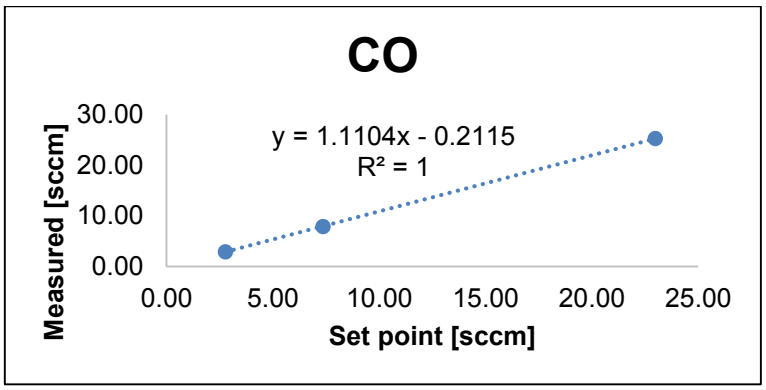


**Figure A-1: CO mass flow controller calibration graph**

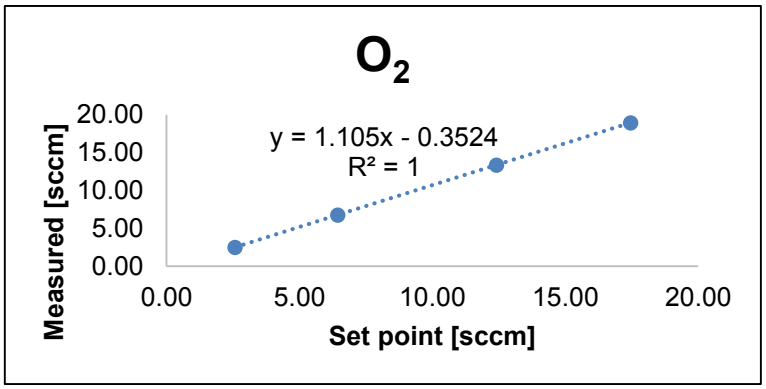


**Figure A-2: $O_2$ mass flow controller calibration graph**

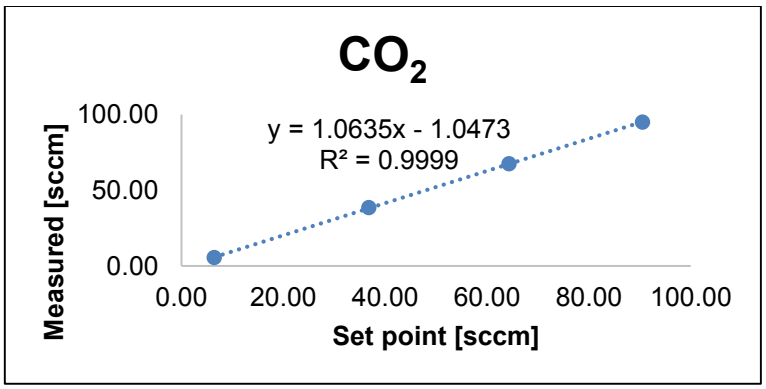


**Figure A-3: $CO_2$ mass flow controller calibration graph**

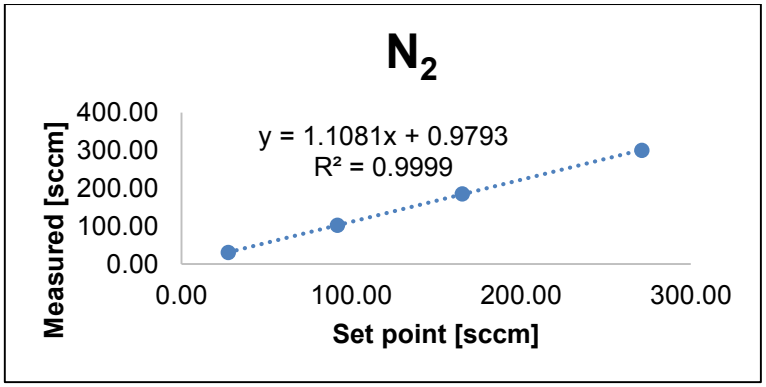


**Figure A-4: $N_2$ mass flow controller calibration graph**

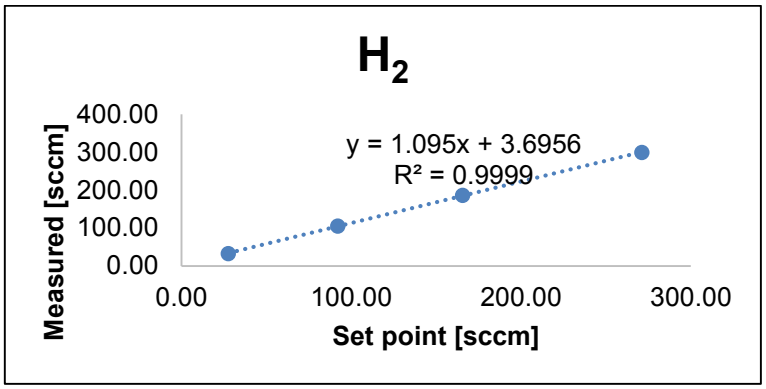


**Figure A-5: $H_2$ mass flow controller calibration graph**

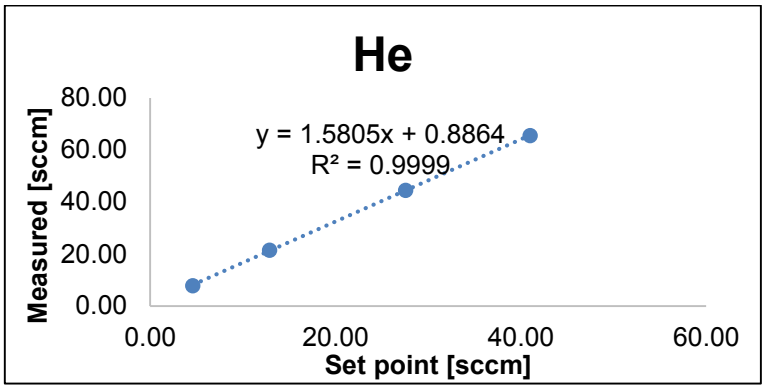


**Figure A-6: He mass flow controller calibration graph**

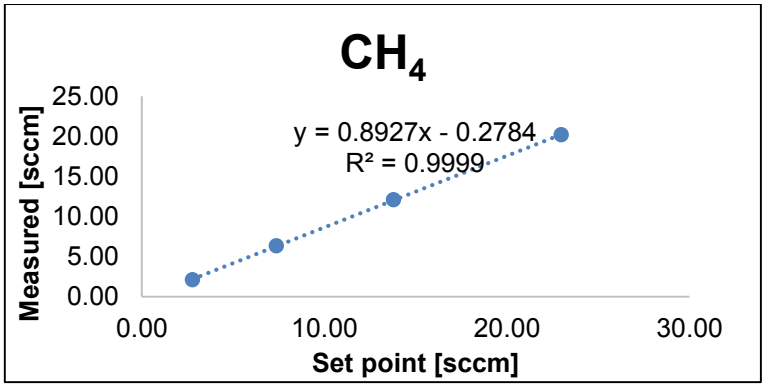


**Figure A-7: $CH_4$ mass flow controller calibration graph**

*calibrated using the CO MFC

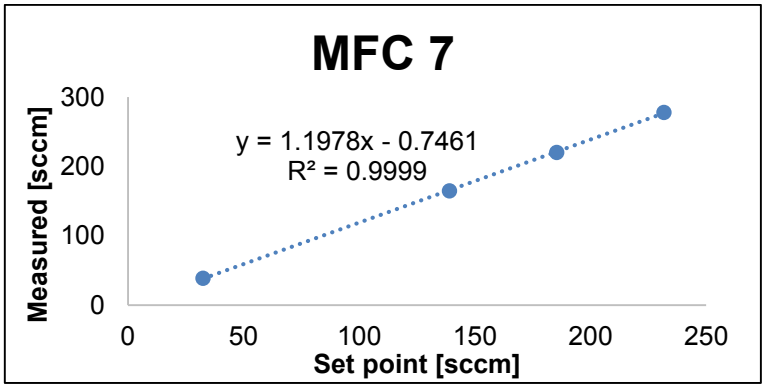


**Figure A-8: MFC 7 mass flow controller calibration graph**

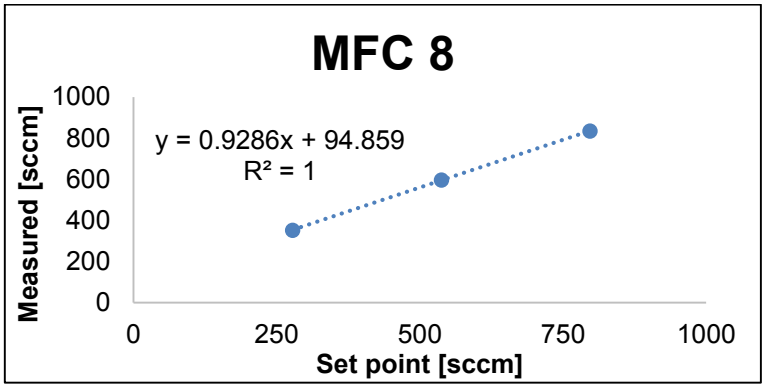


**Figure A-9: MFC 8 mass flow controller calibration graph**

# Appendix III – Pump calibration calculations

**Table A-1: Pump calibration data**

| pump flowrate [ml/min] | Bottle | m(empty bottle) [g] | m(bottle+ water) [g] | m(water ) [ml] | time [min] | flowrate [ml/min | Split | total [ml/min] |
|---|---|---|---|---|---|---|---|---|
| 0.04 | W1 | 65.112 | 67.3421 | 2.2301 | 61 | 0.036559 | 0.906 | 0.040 |
| | R 1 | 64.1328 | 64.3635 | 0.2307 | 61 | 0.003782 | 0.094 | |
| 0.15 | W2 | 67.3421 | 75.7558 | 8.4137 | 62 | 0.135705 | 0.905 | 0.150 |
| | R 2 | 64.3635 | 65.2467 | 0.8832 | 62 | 0.014245 | 0.095 | |
| 0.25 | W3 | 65.487 | 79.5555 | 14.0685 | 63 | 0.22331 | 0.905 | 0.247 |
| | R 3 | 65.2467 | 66.727 | 1.4803 | 63 | 0.023497 | 0.095 | |
| 0.35 | W4 | 65.5943 | 82.652 | 17.0577 | 55 | 0.31014 | 0.905 | 0.343 |
| | R 4 | 66.727 | 68.5099 | 1.7829 | 55 | 0.032416 | 0.095 | |
| 0.5 | W5 | 65.6334 | 94.9603 | 29.3269 | 67 | 0.437715 | 0.906 | 0.483 |
| | R 5 | 68.5099 | 71.5524 | 3.0425 | 67 | 0.04541 | 0.094 | |

**Table A-2: Calculation of theoretical split ratio by determining the flowrate of the waste stream and the flowrate of the reactor feed stream**

| | | |
|---|---|---|
| P pump | 2412 | psi |
| P pump | 166.3074 | bar |
| P beaker | 1 | bar |
| ΔP | 165.3074 | bar |
| r | 0.000025 | m |
| η | 0.000913 | kg/m.s |
| l | 0.45 | m |
| Q | 6.18E-09 | m3/s |
| | 0.370513 | ml/min |

| | | |
|---|---|---|
| P pump | 2412 | psi |
| P pump | 166.3074 | bar |
| P reactor | 1.5 | bar |
| ΔP | 164.8074 | bar |
| r | 0.000025 | m |
| η | 0.000913 | kg/m.s |
| l | 4.508 | m |
| Q | 6.15E-10 | m3/s |
| | 0.036874 | ml/min |

The flowrate was calculated using the Hagen-Poiseuille equation.

**Table A-3: Comparison of the determined experimental split ratio compared to the theoretical split ratio**

| | |
|---|---|
| Experimental split fraction | 0.095 |
| Theoretical split fraction | 0.090513 |
| Difference | 4.42% |

A pump calibration curve was then plotted and used to determine the pump set point for the required flowrate during experiments.

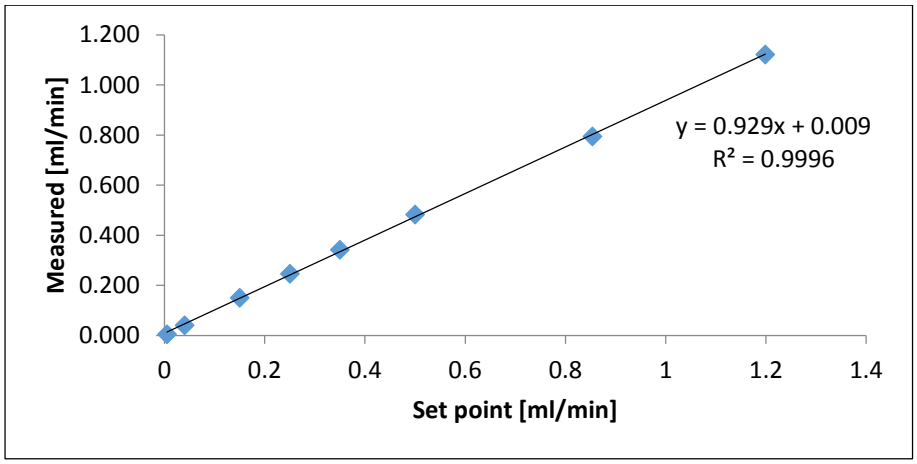


**Figure A-10: Pump calibration curve**

# Appendix IV – GC calibration data

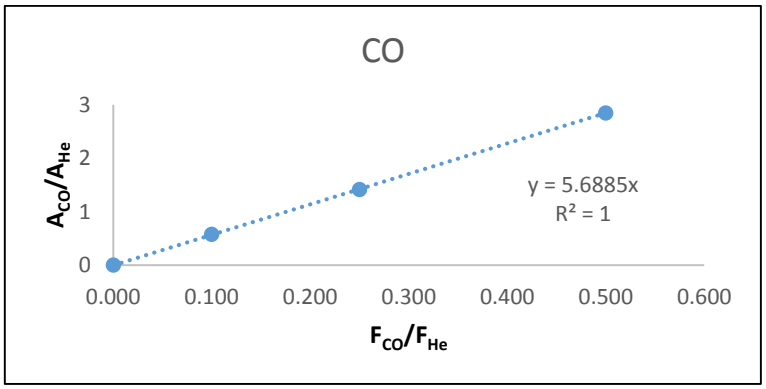


**Figure A-11: CO micro GC calibration graph**

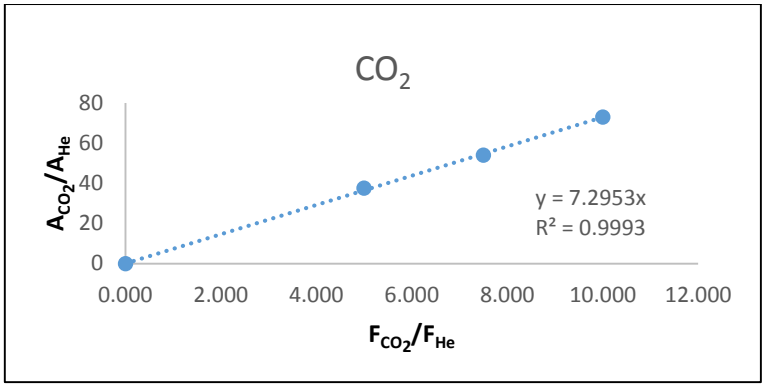


**Figure A-12: $CO_2$ micro GC calibration graph**

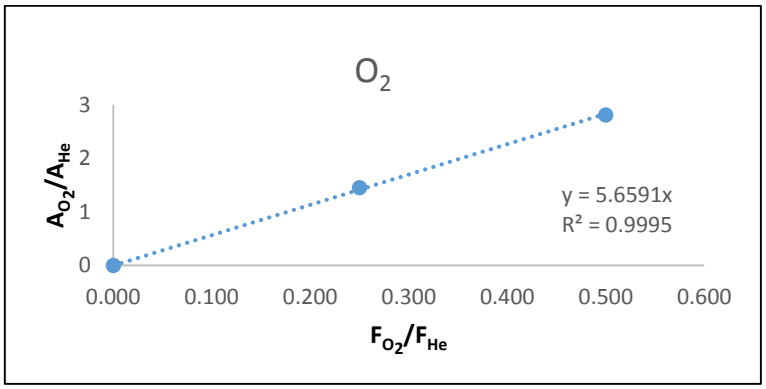


**Figure A-13: $O_2$ micro GC calibration graph**

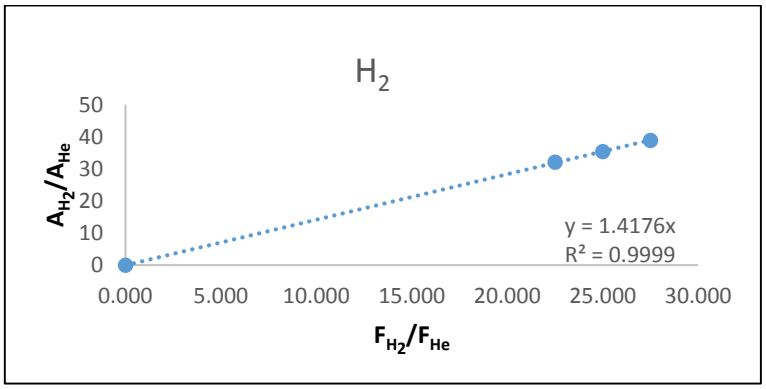


**Figure A-14: $H_2$ micro GC calibration graph**

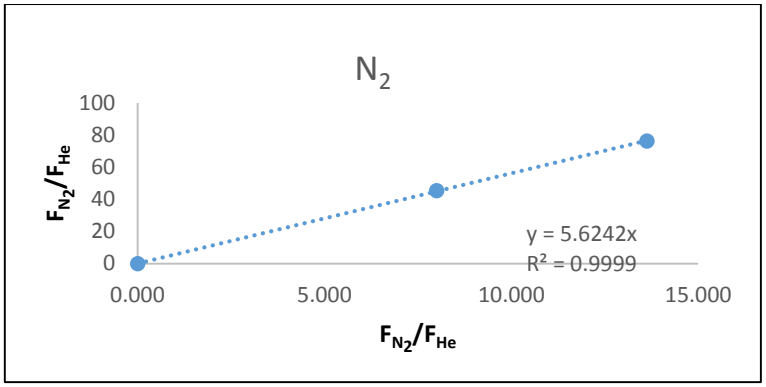


**Figure A-15: $N_2$ micro GC calibration graph**

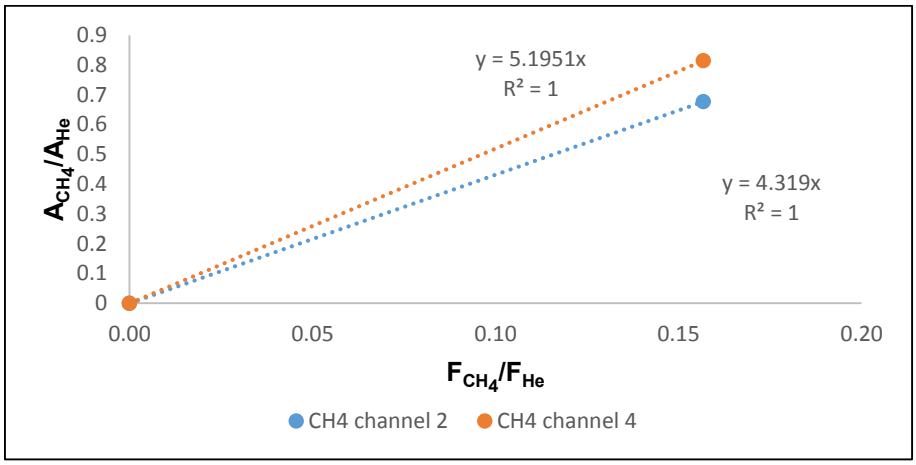


**Figure A-16: $CH_4$ micro GC calibration graph**

# Appendix V – $CO_2$ solubility calculations

$$n(CO_2) = \frac{S_{CO_2} \cdot m_{H_2O}}{M_{CO_2}}$$

$$V(CO_2) = \frac{nRT}{P}$$

Assuming the water in the catch pot is already fully saturated and that any $CO_2$ loss is into the water flowing in and out.

The figure below shows the how the carbon balance would be affected depending on the extent of $CO_2$ saturation in water.

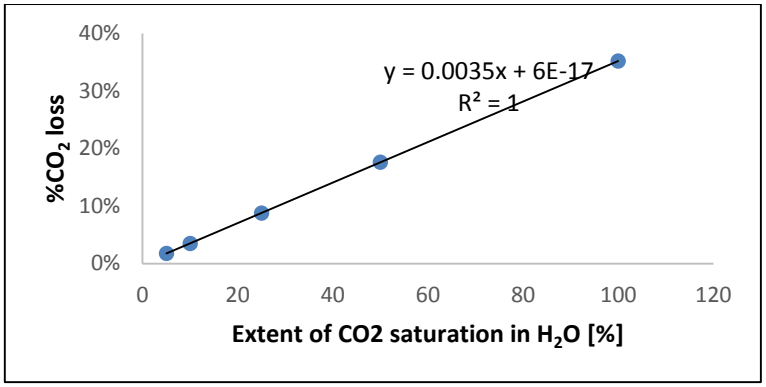


**Figure A-17: Graph showing the percentage $CO_2$ loss depending on the extent of $CO_2$ saturation**

# Appendix VI – Experimental data

## Ru_high pH initial results

The carbon balance is a bit off because the CO MFC was found to be slightly faulty after the runs were done. The water balance was calculated as the difference between the mass of water that was pumped from the source bottle and the sum of the waste water collected and the water into the reactor. The mas of water pumped from the source bottle as well as the mass of waste water collected were determined using a scale. The mass of water to the reactor was determined using the split ratio according to the following equation:

$$m_{water\ to\ reactor} = \frac{m_{waste\ water} \cdot (1\text{-split ratio})}{\text{split ratio}}$$

| Run | conditions | | $X_{CO}$ | $S_{CO2}$ | $X_{O2}$ | Carbon balance | $H_2O$ balance |
|---|---|---|---|---|---|---|---|
| 1 | T [°C] | 103 | 17.7% | 45.0% | 22.9% | 100.3% | |
| | SV [ml/(h $g_{cat}$) | 30400 | | | | | |
| | λ | 2 | | | | | |
| 2 | T [°C] | 103 | 24.6% | 37.4% | 38.4% | 99.5% | 6.3% |
| | SV [ml/(h $g_{cat}$) | 16900 | | | | | |
| | λ | 2 | | | | | |
| 3 | T [°C] | 122 | 34.9% | 25.7% | 76.5% | 99.6% | 2.1% |
| | SV [ml/(h $g_{cat}$) | 16900 | | | | | |

| | | | | | | | |
|---|---|---|---|---|---|---|---|
| | λ | 2 | | | | | |
| 4 | T [°C] | 122 | 39.7% | 26.2% | 85.5% | 98.4% | 1.4% |
| | SV [ml/(h $g_{cat}$) | 9 100 | | | | | |
| | λ | 2 | | | | | |
| 5 | T [°C] | 150 | 42.0% | 23.7% | 100.0% | 98.3% | 6.4% |
| | SV [ml/(h $g_{cat}$) | 9 100 | | | | | |
| | λ | 2 | | | | | |
| 6 | T [°C] | 150 | 36.2% | 20.5% | 98.8% | 97.7% | 3.1% |
| | SV [ml/(h $g_{cat}$) | 16 900 | | | | | |
| | λ | 2 | | | | | |

## Ru_high pH

With 80 mg of catalyst

| **Run** | **conditions** | | **$X_{CO}$** | **$S_{CO2}$** | **$X_{O2}$** | **Carbon balance** | **$H_2O$ balance** | |
|---|---|---|---|---|---|---|---|---|
| 1 | T [°C] | 150 | 84.6% | 38.9% | 100.0% | 100.6% | 90.8% | Feed 2 |
| | SV [ml/(h $g_{cat}$)] | 120 000 | | | | | | |
| | λ | 2 | | | | | | |
| 2 | T [°C] | 122 | 99.0% | 45.6% | 100.0% | 100.8% | 99.5% | |
| | SV [ml/(h $g_{cat}$)] | 120 000 | | | | | | |
| | λ | 2 | | | | | | |
| 3 | T [°C] | 103 | 19.2% | 52.6% | 16.9% | 100.0% | 100.9% | |
| | SV [ml/(h $g_{cat}$)] | 120 000 | | | | | | |
| | λ | 2 | | | | | | |
| 4 | T [°C] | 180 | 63.7% | 29.4% | 100.0% | 100.1% | 98.9% | |
| | flow [ml/min] | 120 000 | | | | | | |

| | | | | | | | | |
|---|---|---|---|---|---|---|---|---|
| | λ | 2 | | | | | | |
| | T [°C] | 180 | | | | | | |
| | SV [ml/(h $g_{cat}$)] | 120 000 | 62.1% | 30.3% | 100.0% | 100.3% | 100.6% | |
| 5 | λ | 2 | | | | | | |
| | T [°C] | 150 | | | | | | |
| | SV [ml/(h $g_{cat}$)] | 120 000 | 82.3% | 42.1% | 99.6% | 99.4% | 99.6% | |
| 6 | λ | 2 | | | | | | |
| | T [°C] | 122 | | | | | | |
| | SV [ml/(h $g_{cat}$)] | 120 000 | 25.2% | 52.4% | 24.2% | 101.7% | 99.8% | |
| 7 | λ | 2 | | | | | | |
| | T [°C] | 103 | | | | | | |
| | SV [ml/(h $g_{cat}$)] | 120 000 | 0% | 0% | 0% | 99.3% | 101.7% | |
| 8 | λ | 2 | | | | | | |
| | T [°C] | 122 | | | | | | |
| | SV [ml/(h $g_{cat}$)] | 42 000 | 57.7% | 44.5% | 64.1% | 97.5% | 100.0% | |
| 9 | λ | 2 | | | | | | |
| | T [°C] | 122 | | | | | | |
| | SV [ml/(h $g_{cat}$)] | 23 000 | 62.2% | 41.8% | 73.6% | 97.9% | 99.8% | |
| 10 | λ | 2 | | | | | | |
| | T [°C] | 103 | | | | | | |
| | SV [ml/(h $g_{cat}$)] | 42 000 | 11.8% | 38.0% | 15.4% | 100.6% | 97.9% | |
| 11 | λ | 2 | | | | | | |
| | T [°C] | 150 | | | | | | |
| | SV [ml/(h $g_{cat}$)] | 42 000 | 64.4% | 34.5% | 92.3% | 101.3% | 100.5% | |
| 12 | λ | 2 | | | | | | |
| | T [°C] | 180 | | | | | | |
| | SV [ml/(h $g_{cat}$)] | 42 000 | 54.6% | 28.6% | 94.6% | 101.8% | 100.4% | |
| 13 | λ | 2 | | | | | | |
| | T [°C] | 150 | | | | | | |
| | SV [ml/(h $g_{cat}$)] | 23 000 | 48.1% | 31.1% | 76.4% | 98.7% | 100.0% | |
| 14 | | | | | | | | |

1%CO Feed 2

Feed 1

| | | | | | | | | |
|---|---|---|---|---|---|---|---|---|
| | λ | 2 | | | | | | |
| | T [°C] | 150 | | | | | | |
| | SV [ml/(h $g_{cat}$)] | 120 000 | 69.1% | 34.3% | 99.6% | 100.0% | 92.8% | |
| 15 | λ | 2 | | | | | | |
| | T [°C] | 150 | | | | | | |
| | SV [ml/(h $g_{cat}$)] | 250 000 | 76.4% | 37.7% | 99.6% | 99.8% | 102.6% | |
| 16 | λ | 2 | | | | | | |
| | T [°C] | 150 | | | | | | |
| | SV [ml/(h $g_{cat}$)] | 340 000 | 79.8% | 39.7% | 99.0% | 100.2% | 99.9% | |
| 17 | λ | 2 | | | | | | |
| | T [°C] | 122 | | | | | | |
| | SV [ml/(h $g_{cat}$)] | 250 000 | 16.8% | 40.0% | 20.7% | 100.4% | 100.2% | |
| 18 | λ | 2 | | | | | | |
| | T [°C] | 122 | | | | | | |
| | SV [ml/(h $g_{cat}$)] | 120 000 | 31.0% | 39.7% | 38.6% | 99.7% | 99.2% | |
| 19 | λ | 2 | | | | | | |
| | T [°C] | 103 | | | | | | |
| | SV [ml/(h $g_{cat}$)] | 120 000 | 4.9% | 31.6% | 7.6% | 98.8% | 99.4% | |
| 20 | λ | 2 | | | | | | |
| | T [°C] | 180 | | | | | | |
| | SV [ml/(h $g_{cat}$)] | 120 000 | 72.0% | 36.1% | 99.3% | 99.2% | 99.9% | |
| 21 | λ | 2 | | | | | | |
| | T [°C] | 150 | | | | | | |
| | SV [ml/(h $g_{cat}$)] | 250 000 | 97.0% | 51.5% | 64.1% | 100.7% | 99.7% | |
| 22 | λ | 3 | | | | | | |
| | T [°C] | 122 | | | | | | |
| | SV [ml/(h $g_{cat}$)] | 42 000 | | | | | | |
| 23 | λ | 2 | 53.6% | 31.7% | 88.5% | 101.5% | 100.4% | Feed 2 |

With 300 mg catalyst

| Run | conditions | | $X_{CO}$ | $S_{CO2}$ | $X_{O2}$ | Carbon balance | $H_2O$ balance | |
|---|---|---|---|---|---|---|---|---|
| 1 | T [°C] | 180 | 100.0% | 51.5% | 100.0% | 99.7% | 99.6% | FEED 1 |
| | SV [ml/(h $g_{cat}$)] | 120 000 | | | | | | |
| | λ | 2 | | | | | | |
| 2 | T [°C] | 180 | 85.0% *589 ppm $CH_4$ | 45.4% | 94.5% | 98.7% | 98.9% | |
| | SV [ml/(h $g_{cat}$)] | 10 000 | | | | | | |
| | λ | 2 | | | | | | |
| 3 | T [°C] | 150 | 72.3% | 38.9% | 92.7% | 99.3% | 99.0% | |
| | SV [ml/(h $g_{cat}$)] | 10 000 | | | | | | |
| | λ | 2 | | | | | | |
| 4 | T [°C] | 150 | 100.0% | 51.5% | 100.0% | 99.7% | 99.6% | |
| | SV [ml/(h $g_{cat}$)] | 120 000 | | | | | | |
| | λ | 2 | | | | | | |
| 5 | T [°C] | 122 | 84.8% | 44.6% | 94.8% | 99.6% | 99.4% | |
| | SV [ml/(h $g_{cat}$)] | 10 000 | | | | | | |
| | λ | 2 | | | | | | |
| 6 | T [°C] | 122 | 80.2% | 52.3% | 76.5% | 100.1% | 99.7% | |
| | SV [ml/(h $g_{cat}$)] | 120 000 | | | | | | |
| | λ | 2 | | | | | | |
| 7 | T [°C] | 103 | 90.3% | 48.1% | 93.6% | 99.7% | 100.3% | |
| | SV [ml/(h $g_{cat}$)] | 10 000 | | | | | | |
| | λ | 2 | | | | | | |
| 8 | T [°C] | 103 | 40.7% | 60.0% | 33.8% | 100.0% | 99.6% | |
| | SV [ml/(h $g_{cat}$)] | 120 000 | | | | | | |
| | λ | 2 | | | | | | |
| 9 | T [°C] | 180 | 46.9% | 43.4% | 100.0% | 99.8% | 99.2% | |
| | SV [ml/(h $g_{cat}$)] | 120 000 | | | | | | |
| | λ | 1 | | | | | | |
| 10 | T [°C] | 150 | 60.2% | 55.7% | 100.0% | 100.0% | 99.4% | |
| | SV [ml/(h $g_{cat}$)] | 120 000 | | | | | | |

| | | | | | | | | |
|---|---|---|---|---|---|---|---|---|
| | λ | 1 | | | | | | |
| | T [°C] | 150 | | | | | | |
| | SV [ml/(h $g_{cat}$)] | 20 250 | 51.8% | 47.9% | 100.0% | 99.9% | 97.2% | |
| 11 | λ | 1 | | | | | | |
| | T [°C] | 122 | | | | | | |
| | SV [ml/(h $g_{cat}$)] | 20 250 | 63.7% | 58.9% | 100.0% | 99.5% | 98.2% | |
| 12 | λ | 1 | | | | | | |
| | T [°C] | 122 | | | | | | |
| | SV [ml/(h $g_{cat}$)] | 120 000 | 69.5% | 64.2% | 100.0% | 99.1% | 99.8% | |
| 13 | λ | 1 | | | | | | |
| | T [°C] | 103 | | | | | | |
| | SV [ml/(h $g_{cat}$)] | 120 000 | 13.0% | 47.5% | 25.3% | 99.2% | 99.7% | |
| 14 | λ | 1 | | | | | | |
| | T [°C] | 103 | | | | | | |
| | SV [ml/(h $g_{cat}$)] | 20 250 | 32.2% | 44.9% | 66.2% | 99.6% | 91.6% | |
| 15 | λ | 1 | | | | | | |
| | T [°C] | 180 | | | | | | |
| | SV [ml/(h $g_{cat}$)] | 10 000 | 80.7% | 43.6% | 92.3% | 99.2% | 91.9% | |
| 16 | λ | 2 | | | | | | |
| | T [°C] | 180 | | | | | | |
| | SV [ml/(h $g_{cat}$)] | 6 000 | 72.9% | 47.9% | 77.1% | 99.1% | 81.9% | |
| 17 | λ | 2 | *1 754 ppm $CH_4$ | | | | | |
| | T [°C] | 180 | | | | | | |
| | SV [ml/(h $g_{cat}$)] | 50 000 | 75.9% | 38.4% | 100.0% | 99.9% | 98.8% | |
| 18 | λ | 2 | *315 ppm $CH_4$ | | | | | |
| | T [°C] | 150 | | | | | | |
| | SV [ml/(h $g_{cat}$)] | 50 000 | 80.1% | 40.6% | 100.0% | 99.8% | 99.3% | |
| 19 | λ | 2 | | | | | | |
| | T [°C] | 150 | | | | | | |
| 20 | SV [ml/(h $g_{cat}$)] | 6 000 | 55.6% | 36.5% | 77.3% | 98.9% | 95.4% | |

| | | | | | | | | |
|---|---|---|---|---|---|---|---|---|
| | λ | 2 | | | | | | |
| | T [°C] | 122 | | | | | | |
| | SV [ml/(h $g_{cat}$)] | 50 000 | 65.8% | 35.1% | 95.1% | 100.3% | 99.4% | |
| 21 | λ | 2 | | | | | | |
| | T [°C] | 122 | | | | | | |
| | SV [ml/(h $g_{cat}$)] | 6 000 | 47.3% | 32.6% | 73.6% | 99.1% | 107.1% | |
| 22 | λ | 2 | | | | | | |
| | T [°C] | 103 | | | | | | |
| | SV [ml/(h $g_{cat}$)] | 6 000 | 49.7% | 38.3% | 65.9% | 99.1% | 104.3% | |
| 23 | λ | 2 | | | | | | |
| | T [°C] | 103 | | | | | | |
| | SV [ml/(h $g_{cat}$)] | 50 000 | 23.5% | 29.6% | 40.4% | 100.9% | 99.7% | |
| 24 | λ | 2 | | | | | | |
| | T [°C] | 103 | | | | | | |
| | SV [ml/(h $g_{cat}$)] | 10 000 | 42.8% | 30.0% | 72.3% | 100.2% | 102.7% | |
| 25 | λ | 2 | | | | | | |
| | T [°C] | 103 | | | | | | |
| | SV [ml/(h $g_{cat}$)] | 120 000 | 11.1% | 30.6% | 18.2% | 100.7% | 98.8% | |
| 26 | λ | 2 | | | | | | |
| | T [°C] | 122 | | | | | | |
| | SV [ml/(h $g_{cat}$)] | 120 000 | 75.6% | 41.2% | 93.0% | 100.8% | 96.7% | |
| 27 | λ | 2 | | | | | | |
| | T [°C] | 122 | | | | | | |
| | SV [ml/(h $g_{cat}$)] | 10 000 | 59.6% | 35.0% | 86.3% | 99.3% | 101.6% | |
| 28 | λ | 2 | | | | | | |
| | T [°C] | 180 | | | | | | |
| | SV [ml/(h $g_{cat}$)] | 120 000 | 68.7% | 33.6% | 100.0% | 99.8% | 102.3% | **15% H2O** |
| 29 | λ | 2 | | | | | | |
| | T [°C] | 150 | 68.3% | 33.4% | 100.0% | 100.2% | 100.5% | |
| 30 | SV [ml/(h $g_{cat}$)] | 120 000 | | | | | | |

| | | | | | | | | |
|---|---|---|---|---|---|---|---|---|
| | λ | 2 | | | | | | |
| 31 | T [°C] | 150 | 67.9% | 33.8% | 100.0% | 100.0% | 99.7% | 20% H2O |
| | SV [ml/(h $g_{cat}$)] | 120 000 | | | | | | |
| | λ | 2 | | | | | | |
| 32 | T [°C] | 180 | 68.0% | 33.8% | 100.0% | 100.1% | 99.2% | |
| | SV [ml/(h $g_{cat}$)] | 120000 | | | | | | |
| | λ | 2 | | | | | | |
| 33 | T [°C] | 150 | 65.5% | 31.6% | 100.0% | 100.3% | 99.6% | FEED 1 |
| | SV [ml/(h $g_{cat}$)] | 120 000 | | | | | | |
| | λ | 2 | | | | | | |

## Ru_IWI catalyst

| Run | conditions | | $X_{CO}$ | $S_{CO2}$ | $X_{O2}$ | Carbon balance | $H_2O$ balance |
|---|---|---|---|---|---|---|---|
| Feed 2 | | | | | | | |
| 1 | T [°C] | 103 | 1.7% | 38.8% | 2.2% | 99.6% | 98.5% |
| | SV [ml/(h $g_{cat}$) | 120 000 | | | | | |
| | λ | 2 | | | | | |
| 2 | T [°C] | 122 | 3.7% | 58.9% | 3.1% | 99.9% | 98.3% |
| | SV [ml/(h $g_{cat}$) | 120 000 | | | | | |
| | λ | 2 | | | | | |
| 3 | T [°C] | 122 | 24.9% | 49.0% | 25.1% | 98.9% | 103.4% |
| | SV [ml/(h $g_{cat}$) | 10 100 | | | | | |
| | λ | 2 | | | | | |
| 4 | T [°C] | 150 | 84.5% | 49.3% | 84.5% | 99.6% | 101.0% |
| | SV [ml/(h $g_{cat}$) | 10 100 | | | | | |
| | λ | 2 | | | | | |

| | | | | | | | |
|---|---|---|---|---|---|---|---|
| 5 | T [°C] | 150 | 49.8% | 69.3% | 35.5% | 100.3% | 99.9% |
| | SV [ml/(h $g_{cat}$) | 120 000 | | | | | |
| | λ | 2 | | | | | |
| 6 | T [°C] | 180 | 72.7% * 145 ppm $CH_4$ | 43.6% | 82.2% | 99.3% | 99.2% |
| | SV [ml/(h $g_{cat}$) | 10 100 | | | | | |
| | λ | 2 | | | | | |
| 7 | T [°C] | 180 | 100.0% | 49.8% | 99.1% | 100.5% | 99.4% |
| | SV [ml/(h $g_{cat}$) | 120 000 | | | | | |
| | λ | 2 | | | | | |
| 8 | T [°C] | 150 | 65.0% | 62.5% | 99.6% | 100.8% | 99.5% |
| | SV [ml/(h $g_{cat}$) | 120 000 | | | | | |
| | λ | 1 | | | | | |
| 9 | T [°C] | 122 | 13.0% | 56.9% | 21.4% | 99.8% | 99.6% |
| | SV [ml/(h $g_{cat}$) | 120 000 | | | | | |
| | λ | 1 | | | | | |
| 10 | T [°C] | 103 | 2.9% | 40.9% | 6.4% | 100.1% | 99.5% |
| | SV [ml/(h $g_{cat}$) | 120 000 | | | | | |
| | λ | 1 | | | | | |
| 11 | T [°C] | 180 | 62.8% | 56.0% | 100.0% | 100.0% | 99.7% |
| | SV [ml/(h $g_{cat}$) | 120 000 | | | | | |
| | λ | 1 | | | | | |

## Commercial catalyst

| Run | conditions | | $X_{CO}$ | $S_{CO2}$ | $X_{O2}$ | Carbon balance | $H_2O$ balance |
|---|---|---|---|---|---|---|---|
| Feed 2 | | | | | | | |
| 1 | T [°C] | 180 | 90.5% | 48.6% | 95.7% | 99.9% | 101.3% |
| | SV [ml/(h $g_{cat}$) | 120 000 | | | | | |
| | λ | 2 | | | | | |
| 2 | T [°C] | 150 | 87.7% | 48.5% | 89.0% | 100.2% | 97.2% |
| | SV [ml/(h $g_{cat}$) | 120 000 | | | | | |
| | λ | 2 | | | | | |
| 3 | T [°C] | 122 | 81.8% | 51.2% | 78.7% | 100.0% | 100.6% |
| | SV [ml/(h $g_{cat}$) | 120 000 | | | | | |
| | λ | 2 | | | | | |
| 4 | T [°C] | 103 | 76.2% | 53.7% | 69.9% | 100.0% | 84.0% |
| | SV [ml/(h $g_{cat}$) | 120000 | | | | | |
| | λ | 2 | | | | | |
| 5 | T [°C] | 103 | 58.6% | 78.8% | 66.4% | 99.6% | 101.8% |
| | SV [ml/(h $g_{cat}$) | 120000 | | | | | |
| | λ | 1 | | | | | |
| 6 | T [°C] | 122 | 64.6% | 76.0% | 76.0% | 99.7% | 99.3% |
| | SV [ml/(h $g_{cat}$) | 120000 | | | | | |
| | λ | 1 | | | | | |
| 7 | T [°C] | 150 | 67.7% | 70.7% | 84.2% | 99.9% | 99.5% |
| | SV [ml/(h $g_{cat}$) | 120000 | | | | | |
| | λ | 1 | | | | | |
| 8 | T [°C] | 180 | 70.4% | 65.7% | 94.4% | 99.8% | 99.5% |
| | SV [ml/(h $g_{cat}$) | 120000 | | | | | |
| | λ | 1 | | | | | |

## Pt-Fe/M catalyst

| Run | conditions | | $X_{CO}$ | $S_{CO2}$ | $X_{O2}$ | Carbon balance | $H_2O$ balance |
|---|---|---|---|---|---|---|---|
| Feed 2 | | | | | | | |
| 1 | T [°C] | 180 | 55.6% | 50.5% | 96.3% | 99.6% | 100.0% |
| | SV [ml/(h gcat) | 120000 | | | | | |
| | λ | 1 | | | | | |
| 2 | T [°C] | 150 | 40.5% | 53.4% | 66.4% | 99.7% | 98.9% |
| | SV [ml/(h gcat) | 120000 | | | | | |
| | λ | 1 | | | | | |
| 3 | T [°C] | 122 | 27.9% | 66.0% | 36.9% | 100.0% | 97.9% |
| | SV [ml/(h gcat) | 120000 | | | | | |
| | λ | 1 | | | | | |
| 4 | T [°C] | 103 | 19.6% | 73.9% | 23.2% | 99.8% | 98.6% |
| | SV [ml/(h gcat) | 120000 | | | | | |
| | λ | 1 | | | | | |
| 5 | T [°C] | 180 | 98.5% | 47.3% | 100.0% | 100.4% | 98.8% |
| | SV [ml/(h gcat) | 120000 | | | | | |
| | λ | 2 | | | | | |
| 6 | T [°C] | 150 | 69.0% | 52.2% | 63.5% | 100.3% | 98.8% |
| | SV [ml/(h gcat) | 120000 | | | | | |
| | λ | 2 | | | | | |
| 7 | T [°C] | 122 | 44.7% | 60.0% | 35.8% | 100.1% | 98.7% |
| | SV [ml/(h gcat) | 120000 | | | | | |
| | λ | 2 | | | | | |
| 8 | T [°C] | 103 | 32.4% | 68.1% | 22.8% | 100.3% | 98.1% |
| | SV [ml/(h gcat) | 120000 | | | | | |
| | λ | 2 | | | | | |